DNV

THEORY & VALIDATION

# UDM MODEL FOR PRESSURISED INSTANTANEOUS RELEASES

DATE: December 2023

This report documents an improved formulation in the Phast Unified Dispersion Model UDM for pressurised instantaneous releases. This includes both the initial INEX phase of pressurised instantaneous expansion, and the subsequent post-INEX stage.

Contract 984B0008 for RIVM

Reference to part of this report which may lead to misinterpretation is not permissible.

| No. | Date | Reason for Issue | Prepared by | Verified by | Approved by |
|-----|------|------------------|-------------|-------------|-------------|
| 1 | July 2012 | First draft | Witlox | Webber&Harper | |
| 2 | Jan 2015 | Reformatted and minor updates | Witlox | Harper | |
| 3 | August 2015 | Add verification and validation | Witlox | | |
| 4 | December2015 | Further complete/update validation and refinements theory, add abstract, etc. | Witlox | | |
| 5 | Sep 2017 | 8.0 version | Witlox | Harper | |
| 6 | Mar 2017 | 8.1 version | Witlox | | |
| 7 | May 2021 | Apply new template | D. Vatier | | |

Date: December 2023

**Prepared by:  Digital Solutions at DNV**

# ABSTRACT

This report documents an improved formulation in the Phast Unified Dispersion Model UDM for pressurised instantaneous releases. This includes both the initial INEX phase of pressurised instantaneous expansion, and the subsequent post-INEX stage. This complements the description in the UDM theory manual on the new generalised UDM model accounting of along-wind diffusion for time-varying dispersion (including potential rainout. The report includes a description of the theory, solution algorithm, model verificaton against analytical solutions, and model validation against experimental data.

The old INEX model did not take into account gravity effects and assumed a single droplet size moving along a fixed upward angle resulting in too little rainout. The new INEX model is based on sounder phyisical principles. It includes gravity effects, and assumes the liquid to move radially away from the cloud centre. In case of a INEX cloud touching down the ground, this results in time-varying rainout.

The correctness of the new INEX numerical predictions has been verified against analytical solutions for ground-level vapor or two-phase releases and elevated non-evaporating liquid releases.

The new INEX model has been validated against experiments for ground-level presurised releases for nitrogen vapour and flashing liquid propylene, and elevated flashing liquid releases for Freon 11, Freon 12, propane and butane. Overall the new INEX model tends to underpredict the cloud radius and cloud speed versus time, while the new model provides larger predictions and more closely agrees against experimental data. In addition, the new model predicts a larger amount of rainout which is again more in line with the experimental data. Therefore the new model produces smaller concentrations and doses, and is less conservative. For two-phase releases the new model predicts an increased amount of rainout, which again is more in line with the experimental data.

Experiments identified so far derive the cloud radius and cloud speed from the visible cloud front. This results in added uncertainty since the visible cloud expansion velocity depends amongst others on humidity, and this may e.g. explain some of the discrepancy in results shown in this paper between the experiments by Schmidli and Pettitt for the measured fraction fkinetic of total energy converted to kinetic energy. Therefore additional experimental work to measure concentrations is strongly recommended to provide a sounder basis for model validation. In addition experimental data including additional measurements of droplet sizes and rainout would be useful. This may assist in developing improved droplet size correlations applicable for instantaneous releases.

# Table of contents

## Table of figures

## List of tables

# 1 INTRODUCTION

Background

The Phast model DISC includes a sub-model for modelling catastrophic vessel ruptures (instantaneous release from a vessel). This model describes the expansion of the pollutant from the initial stagnation pressure to the atmospheric pressure. During this phase it is assumed that no air is entrained. The Phast dispersion module UDM (Unified Dispersion Model) calculates the subsequent dispersion of the instantaneous cloud, which includes the initial INEX stage of instantaneous energetic expansion (where entrainment due to radial expansion is dominant). When the source is no longer dominated by radial momentum, the output from the 'INEX' stage provides input to the subsequent calculations (post-INEX stage) in the UDM dispersion model.

The theory governing the Phast atmospheric dispersion model UDM (Unified Dispersion Model) is described by the UDM theory manual[i], for continuous, finite-duration, time-varying and instantaneous releases. The UDM invokes for its thermodynamic calculations (mixing of air with released pollutant) the sub-module THRM and for the pool spreading/evaporating calculations the sub-module PVAP; see the THRM and PVAP theory manuals[ii,iii].

The UDM theory was extended by Witlox and Harper[iv], to account for rigorous inclusion of along-wind diffusion including rainout as part of work sponsored by RIVM and TOTAL. This work was formulated using the so-called observer concept. For instantaneous releases, this involved an 'instantaneous observer'. After rainout this instantaneous observer was also accounting for added vapour from the pool, until the upwind edge of the instantaneous cloud had passed the upwind edge of the pool, i.e. $x_{cld} - W_{gnd} > x_{pool} - R_{pool}$. Here $x_{cld}$ is the downwind distance of the centre-line of the instantaneous cloud, $x_{pool}$ the downwind distance of the pool centre, $R_{pool}$ the pool radius and $W_{gnd}$ the cloud footprint radius. Afterwards, additional non-instantaneous observers are released from the upwind edge of the pool, to account for pool evaporation after the cloud has left the pool behind.

The Phase I report by Witlox[v] did include a literature survey and some suggestions for INEX model development. The INEX model is currently based on an empirical formula for the cloud radius R(t) versus time t, from which the air entrainment is derived. The INEX stage currently simplistically assumes the cloud to move horizontally and the droplets to move under a positive fixed angle often leading to insufficient rainout.

Partly based on recommendations from the Phase I work, the Phase II report by David Webber[vi] includes a modified method to resolve the above issues in the original INEX model. This report proposed a different method for determining the cloud radius R(t) and associated air entrainment, and allows the droplets to move radially in all directions effectively resulting in time-varying rainout while the cloud is touching down the ground. Furthermore the cloud no longer moves horizontally during the INEX stage, but the UDM momentum equation is applied for both horizontal and vertical directions. This report also discusses possible future validation against experimental data.

New INEX model – theory, solution algorithm, model verification and validation

As part of the Phase II work, the current document describes a further integration (and partial modification/extension) of the new INEX model to allow a more seamless integration within the overall UDM. This includes extending the new INEX model developed by David Webber where necessary. This includes a modification of the immediate rainout formulation, and an extension of the cloud thermodynamics adopted by David Webber to account for multi-component mixtures and non-equilibrium effects (as for the UDM). It includes addition of linking between the cloud and the pool (as for the overall UDM), to account for pool vapour added back to the cloud, and the inclusion of heat transfer and water-vapour transfer from the substrate.

The current document includes an overall description of the overall instantaneous model (INEX and post-INEX stages), where only the modelling of the instantaneous observer is described. No changes have been applied to modelling for the subsequent non-instantaneous observers.

The adopted formulation and notation is chosen to be as close as possible to the new UDM AWD formulation as described in the UDM theory manual[iv], to facilitate UDM model implementation, to minimise code changes, and to ensure maximum consistency between INEX and the remaining UDM model. This includes a formulation of the theory in terms of mass (e.g. pollutant mass, mass-specific enthalpies) rather than moles (e.g. number of pollutant moles, molar-specific enthalpies). The current report could be considered to be further embedded in the future in the overall UDM theory manual (to ensure remaining consistency between INEX/UDM models etc.).

Phase III work included implementation of the new INEX model into the UDM. This phase also included verification and validation of the new model against the dataset identified in Phase II. Results of this work are also included in the current report.

Plan of report

The plan of this report is as follows.

Chapter 2 describes the cloud geometry, which is adopted for the overall UDM model (unchanged), and the new UDM sub-model INEX.

Chapter 3 describes the key equations underlying the modelling of INEX energetic cloud expansion. It also includes a description of the UDM THRM thermodynamics equations (unchanged) for mixing of the air with the pollution.

Chapter 4 includes a description of the top-level algorithm, including both the previous (now out-of-date) algorithm including the AWD extension as well as the new modified algorithm based on the new improved INEX methodology.

Chapter 5 includes a detailed algorithm for the solution of the equations for the instantaneous observer (INEX and post-INEX stage). First a list of primary variables is presented, including a description of the initialisation of these variables. Subsequently modelling of rainout is described, and finally the equations for the primary variables are presented.

Chapter 6 describes the model verification and model validation. This includes verification of the numerical INEX model against an analytical solution applicable for a ground-level hemispheric cloud for both cases of vapour or two-phase releases. Furthermore, it includes model validation for ground-level pressurised instantaneous releases against experiments by Landis (nitrogen vapour) and Maurer (flashing propylene liquid). Finally, it includes validation for elevated releases against experiments by Pettitt (Freon-11 without rainout) and Schmidli (Freon 12, propane and butane with rainout).

# 2 CLOUD GEOMETRY

## 2.1 UDM cloud geometry (unchanged)

This section summarises the UDM cloud geometry as depicted by Figure 1. For full details see Section 3.1.2 of the UDM theory manual.

Concentration profile
The concentration profile c (kg/m$^3$) is expressed as function of Cartesian coordinates x (downwind distance), y (cross-wind distance) and z (vertical height above the ground), in terms of cloud horizontal radius $R_y = R_x$, a cloud vertical radius $R_z$, concentration profile exponents n,m, cloud centre-line position (downwind distance $x_{cld}$ and cloud elevation height $z_{cld}$):

$$c(x, y, \zeta; t) = c_o(t) F_v(\zeta) F_h(x, y) \tag{1}$$

with $\zeta = z - z_{cld}$ and

$$F_v(\zeta) = \exp\left\{-\left|\frac{\zeta}{R_z(x)}\right|^{n(x)}\right\}, \quad F_h(x, y) = \exp\left\{-\left[\left(\frac{x - x_{cld}(t)}{R_x(t)}\right)^2 + \left(\frac{y}{R_y(t)}\right)^2\right]^{m/2}\right\} \tag{2}$$

Effective cloud
The instantaneous cloud is modelled as an equivalent effective cloud with effective circular cross-section $A_{eff} = \pi W_{eff}^2$ and height $H_{eff}(1+h_d)$. Here $W_{eff}$ is the effective radius, $H_{eff}$ the effective height; $h_d = 0$ for ground-level plume ($z_{cld}=0$) and $h_d=1$ for an aloft plume. Thus the cloud volume $V_{cld}$ is defined by

$$V_{cld} = \pi W_{eff}^2 \, H_{eff}(1 + h_d) \tag{3}$$

with

$$H_{eff} = \frac{1}{c(x, y, 0)} \int_0^\infty c(x, y, \zeta) d\zeta = \int_0^\infty F_v(\zeta) d\zeta = \Gamma\left(1 + \frac{1}{n}\right) R_z \tag{4}$$

$$A_{eff} = \frac{1}{c(x_{cld}, 0, \zeta)} \int_{-\infty}^\infty \int_{-\infty}^\infty c(x, y, \zeta) \, dx \, dy = 2\pi \int_0^\infty \exp\left(-\left[\frac{r}{R_y}\right]^m\right) r \, dr = \pi R_y^2 \Gamma\left(1 + \frac{2}{m}\right) \tag{5}$$

$$W_{eff} = \frac{1}{\pi}\sqrt{A_{eff}} = \sqrt{\Gamma\left(1 + \frac{2}{m}\right)} \, R_y$$

$$h_d = P\left[\frac{1}{n}, \left(\frac{z_{cld}}{R_z}\right)^n\right] \tag{6}$$

Cloud touchdown
An elevated cloud is modelled in the UDM as a sphere of radius $R_y = R_z$. Onset of touching down is defined by $z_{cld} = R_z$ and final touchdown $z_{cld}=0$. $R_y = R_z$ presumed before the regimes of heavy and passive dispersion; $R_x = R_y$ is always assumed, i.e. circular horizontal cross-section. Thus after touchdown a capped ellipsoid, and after full touchdown we have a semi-ellipsoid.

Consider the ellipsoid $(r/R_y)^m + (\zeta/R_z)^n = 1$ with ellipsoid semi-axes $R_y, R_z$ corresponding to the contour level $e^{-1}c_o(t)$ and with the radius $r = [(x-x_{cld})^2+y^2]^{1/2}$. The surface area $S_{above}$ (m$^2$) of this ellipsoid above the ground is set approximately as function of $R_y$ and $R_z$ [Equation (34) in UDM theory manual], while the area of cloud touching down the ground [Equation (35)], is set as $S_{gnd} = \pi W_{gnd}^2$ with

$$W_{gnd} = R_y \left\{1 - \left(\frac{z_{cld}}{R_z}\right)^n\right\}^{1/m} \quad , \quad for \ 0 \leq z_{cld} < R_z \tag{7}$$

$$= 0 \quad , \quad \quad\quad\quad for \ z_{cld} \geq R_z$$
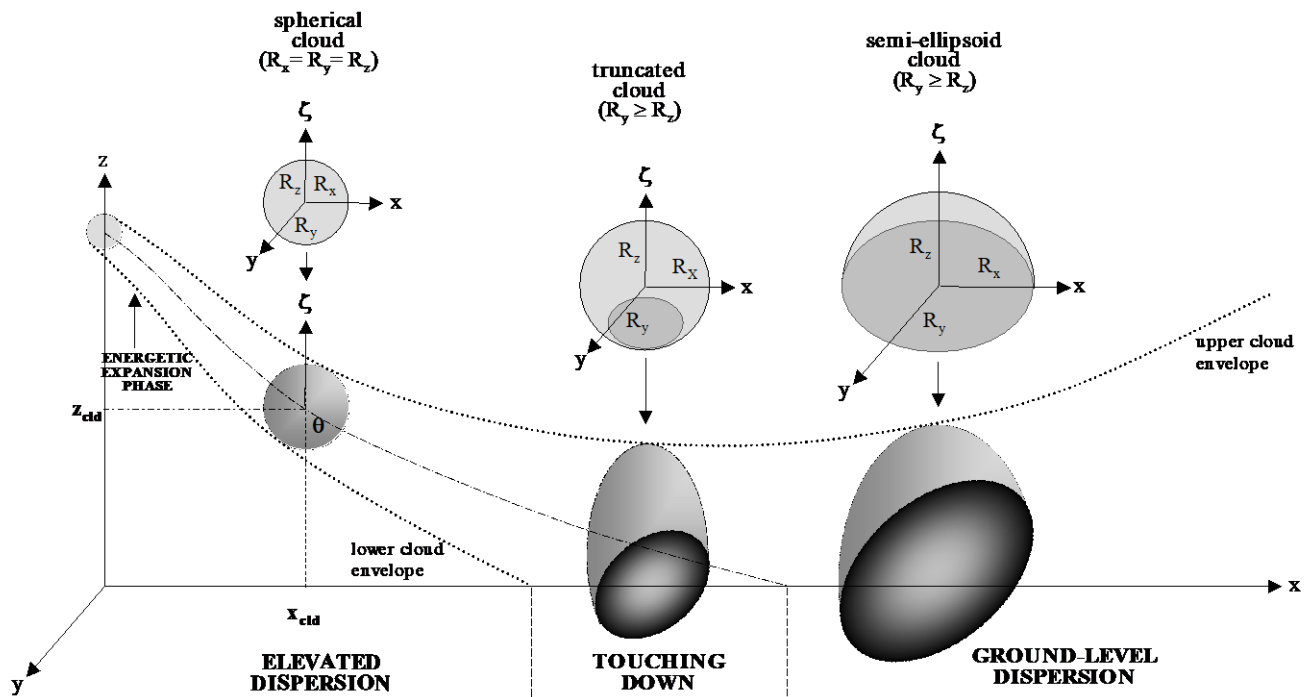
**Figure 1.** **UDM instantaneous cloud geometry (notation, stages of dispersion)**
Cartesian co-ordinates: horizontal, cross-wind, vertical distances x,y,z
Plume co-ordinates: plume arc-length s, vertical distance $\zeta$ to cloud centre-line
Cloud position: centre-line height $z_{cld}= z_{cld}(s)$, angle $\theta=\theta(s)$ to horizontal plane [$z = z_{cld} +\zeta$]
Cloud profile: $[(x/R_x)^2+(y/R_y)^2]^{m/2} +(\zeta/R_z)^n=1$, with radii $R_x=R_y(s)$, $R_y=R_y(s)$ and $R_z=R_z(s)$
Cloud shape at core averaging time $t_{av}^{core}$ ($R_x=R_y$ is assumed):
- spherical during jet dispersion
- truncation by ground during touching down
- semi-ellipsoid during ground-level dense and passive dispersion. After onset of touching down, the cloud ground surface area is circular.

Increasing averaging time increases effects of wind meander. This leads to increasing $R_y$ downwind of passive transition [more wide (elliptic) cloud].

## 2.2 INEX cloud geometry

The old INEX uses $V_{cld} = (4/3) \pi R^3$, i.e. presuming a elevated spherical cloud of radius R (regardless whether the cloud is touching down the ground or not), where an empirical formula is derived for the cloud radius R(t), and from this the added mass of wet air $m_{wa}$ is derived. Note that R differs from $R_x = R_y = R_z$.



<div align="center">

(a) Elevated cloud       (b) cloud in contact with ground
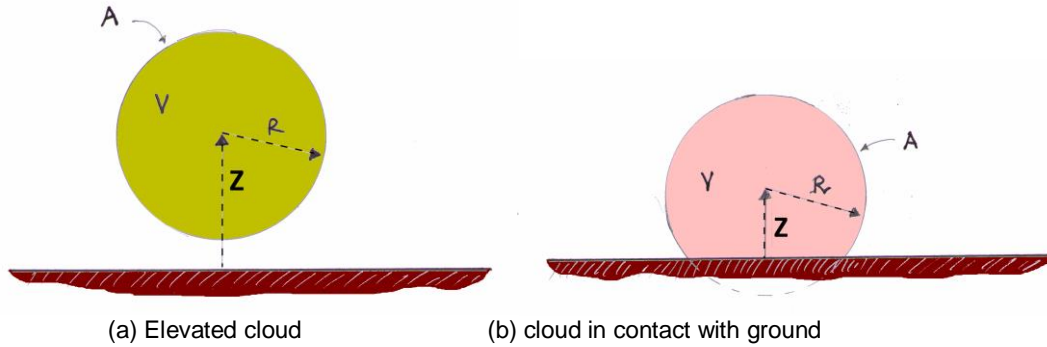
**Figure 2.**      **INEX cloud geometry**

</div>

Figure 2 depicts the geometry proposed for the new INEX model by David Webber (see Section 3.1 of INEX Phase II report[vi] for details), with the cloud being modelled by a sphere while elevated, by a capped sphere while touching down, and by a hemisphere after full touchdown. In this figure $V = V_{cld}$ and $Z = z_{cld}$, R is the cloud radius, and A is the cloud area above the ground. Furthermore David denotes the footprint area by $A_{footprint} = \pi L^2$, where L is the footprint radius. Relevant equations are as follows:

$$V_{cld} = \frac{4}{3}\pi R^3 \ , \ A = 4\pi R^2 \ , \ L = 0 \quad , \quad if \ \ z_{cld} \geq R \ (cloud \ elevated)$$

$$V_{cld} = \frac{1}{3}\pi (R + z_{cld})^2 (2R - z_{cld}), \ A = 2\pi R(R + z_{cld}), \ L = \sqrt{R^2 - z_{cld}^2} \ , \ if \ 0 < z_{cld} < R$$

$$V_{cld} = \frac{2}{3}\pi R^3 \ , \ A = 2\pi R^2, \ L = R \quad , \quad if \ \ z_{cld} = 0 \ (cloud \ grounded)$$

**( 8 )**

The radius R can be derived as a secondary variable from $z_{cld}$ and $V_{cld}$ from Equation ( 8 ). This involves solution of a cubic equation for R during touching down, with solution as given in the report by David Webber[vi].

Although both the INEX cloud (Figure 2) and UDM cloud (Figure 1) are spherical, it is noted that the definition of the INEX radius R differs from the definition of the UDM radius $R_x = R_y = R_z$. Likewise, A differs from the UDM area $S_{above}$ above the ground, $A_{footprint}$ differs from the UDM footprint area $S_{gnd,}$ and L differs from the UDM footprint radius $W_{gnd}$.[1]

---

[1] For UDM transitions (such as touchdown) not the INEX cloud geometry but the UDM geometry is applied as explained in Section 2.1. This further guarantees continuity between INEX and post-INEX phases.

# 3 CLOUD THERMODYNAMICS OF MIXING AIR WITH POLLUTANT

## 3.1 UDM THRM thermodynamics (unchanged)

Full details of this are given in the UDM thermodynamics theory manual[ii]. This section includes a brief summary only. THRM includes isenthalpic mixing of the released pollutant (mass $m_c$, at post-expansion temperature $T_f$ and post-expansion liquid fraction $\eta_{cLf}$), entrained air (wet-air mass $m_{wa}$ at ambient temperature $T_a$ and relative humidity $r_h$), and water-vapour pick-up from water substrate (mass $m_{wv}{}^{gnd}$ at ground temperature $T_{gnd}$). The model also accounts for heat $q_{gnd}$ (J) added from the substrate to the cloud.

From the above it follows that the total cloud mass $m_{cld}$ is given by

$$m_{cld} \;=\; m_a + m_w + m_c \;\;,\;\; m_w = m_{wv}{}^{a} + m_{wv}{}^{gnd} \tag{9}$$

Here $m_a$ is the mass of dry air, $m_w$ the total mass of water, and $m_{wv}{}^a$ the mass for water from the entrained wet air.

The enthalpy of the total cloud $H_{cld}$ is the sum of the enthalpies of the component before mixing and the heat transferred from the substrate,

$$H_{cld} \;=\; H_c + H_{wa} + H_{gnd} + q_{gnd} \tag{10}$$

where the pollutant enthalpy $H_c$, the wet-air enthalpy $H_{wa}$, and the enthalpy $H_{gnd}$ of the water-vapour added from the ground are given by

$$H_c \;=\; [1-\eta_{cLf}]\, m_c\, h_{cv}(T_f) + \eta_{cLf}\, m_{pol}\, h_{cL}(T_o) \tag{11}$$
$$H_{wa} \;=\; m_a\, h_a(T_a) + m_{wv}{}^{a} h_{wv}(T_a)$$
$$H_{gnd} \;=\; m_{wv}{}^{gnd} h_{wv}(T_{gnd})$$

Here $h_{cv}, h_{cL}, h_a, h_{wa}$ are the specific enthalpies (J/kg) for pollutant vapour, pollutant liquid, dry air and water vapour, respectively. The temperature $T$ is set using conservation of enthalpy,

$$H_{cld} = m_a h_a(T) + m_{wv} h_{wv}(T) + m_{wn} h_{wn}(T) + m_{cv} h_{cv}(T) + m_{cL} h_{cL}(T_d) \tag{12}$$

Where the droplet temperature $T_d = T$ in case of HEM, and $T_d$ is set from the droplet energy balance in case of the non-equilibrium model. THRM also accounts for solid effects (water ice, and $CO_2$ pollutant currently only), and multi-component releases (assuming Raoult's law). In the above equation $m_{wv}$ is the mass of water vapour, $m_{wn}$ the mass of water non-vapour (either liquid or ice).

The thermodynamics model is invoked while incrementally solving the dispersion equations in the downwind direction. In case of the non-equilibrium model, input data supplied by the dispersion model include the liquid pollutant mass and the liquid pollutant (droplet) temperature. After each incremental step, the UDM uses the thermodynamic model to calculate the cloud temperature $T$, the cloud density $\rho_{cld}$, and the cloud volume $V_{cld}$. These calculations are done as follows by the thermodynamics model:

1. Set total cloud enthalpy $H_{cld}$ (sum of enthalpies of individual components before mixing) from Equation ( 10 )

2. Set mass and mole fractions of dry air, water and pollutant

3. Use Brent root solver to solve enthalpy equation ( 12 ) for temperature $T$, and determine phase distribution

4. Set specific volumes (m³/kg) for liquid $v_{liq}$, vapour $v_{vap}$ and cloud $v_{cld}$:

$$v_{liq} = \eta_{ws}/\rho_{ice} + \eta_{wL}/\rho_{wL} + \eta_{cL}/\rho_{cL}(T_d) \tag{13}$$
$$v_{vap} = [(\eta_a + \eta_{wv})/(\rho_a T_a/T_{vap})] + [\eta_{cv}/\rho_{pol,v}(T_{vap})]$$
$$v_{cld} = v_{vap} + v_{liq}$$

5. Set cloud density (kg/m³): $\rho_{cld} = 1/v_{cld}$

6. Set cloud volume $V_{cld} = v_{cld} * m_{cld}$

## 3.2 INEX energetic cloud expansion

By means of differentiating Equation ( 8 ) for $V_{cld}$, the following differential equation can be derived for the total INEX cloud expansion velocity $U = dR/dt$,

$$\frac{dV_{cld}}{dt} = AU \ , \qquad\qquad if \ z_{cld} \geq R(cloud\ elevated) \ or \ if \ z_{cld} = 0 \ (cloud\ grounded) \tag{14}$$

$$= AU + A_{footprint}\frac{dz_{cld}}{dt} \ , \quad if \ 0 < z_{cld} < R \ (cloud\ touching\ down)$$

Here A is the surface area of the cloud above the ground (UDM equivalent $S_{above}$), and $A_{footprint} = \pi \ (R^2 - z_{cld}^2)$ the cloud footprint area; see Equation ( 8 ).

### 3.2.1 Formulation excluding air-displacement velocity ($U_d=0$)

This option is currently available in the product only. It assumes that the INEX cloud expansion velocity U equals the air entrainment velocity $U_E$, and the air displacement velocity $U_D$ is ignored.  and the following equations apply:

$$\frac{dm_{wa}}{dt} = \rho_a \frac{dV_{cld}}{dt} \tag{15}$$

$$U = \frac{dR}{dt} = U_E \ , \ U_D = 0 \tag{16}$$

### 3.2.2 Formulation including air-displacement velocity ($U_d>0$)

This option is currently available via the UDM spreadsheet only. Based on a proposed formulation by David Webber[vi], it assumes that the INEX cloud expansion velocity U equals the sum of the air entrainment velocity $U_E$ and the air displacement velocity $U_D$ with which the air is displaced by the cloud:

$$\frac{dm_{wa}}{dt} = \rho_a A \, U_E \ , if \ z_{cld} \geq R(cloud\ elevated) \ or \ if \ z_{cld} = 0 \ (cloud\ grounded) \tag{17}$$

$$= \rho_a \left\{ AU_E + A_{footprint}\frac{dz_{cld}}{dt} \right\} \ , \quad if \ 0 < z_{cld} < R \ (cloud\ touching\ down)$$

$$U = \frac{dR}{dt} = U_E + U_D \tag{18}$$

The cloud volume $V_{cld}$ as determined by THRM (see Section 3.1) can be considered to be a function of the following primary variables: pollutant mass $m_c$, wet-air mass $m_{wa}$, water pick-up $m_{wv}^{gnd}$, substrate heat pickup $q^{gnd}$, pollutant enthalpy $H_c$, and (in case of non-equilibrium model) droplet temperature $T_d$ and droplet mass $m_d$:

$$\frac{dV_{cld}}{dt} = \frac{\partial V_{cld}}{\partial m_{wa}} \frac{dm_{wa}}{dt} + \frac{\partial V_{cld}}{\partial m_c} \frac{dm_c}{dt} + \frac{\partial V_{cld}}{\partial m_{wv}^{gnd}} \frac{dm_{wv}^{gnd}}{dt} + \frac{\partial V_{cld}}{\partial q^{gnd}} \frac{dq^{gnd}}{dt} \tag{19}$$

$$+ \frac{\partial V_{cld}}{\partial H_c} \frac{dH_c}{dt} + \frac{\partial V_{cld}}{\partial T_d} \frac{dT_d}{dt} + \frac{\partial V_{cld}}{\partial m_d} \frac{dm_d}{dt}$$

Using Equation ( 17 ) into Equation ( 19 ), $U_E$ can be derived as a secondary variable by,

$$U_E = \frac{\dfrac{dV_{cld}}{dt} - \dfrac{\partial V_{cld}}{\partial m_c}\dfrac{dm_c}{dt} - \dfrac{\partial V_{cld}}{\partial m_{wv}{}^{gnd}}\dfrac{dm_{wv}{}^{gnd}}{dt} - \dfrac{\partial V_{cld}}{\partial q^{gnd}}\dfrac{dq^{gnd}}{dt} - \dfrac{\partial V_{cld}}{\partial H_c}\dfrac{dH_c}{dt} - \dfrac{\partial V_{cld}}{\partial T_d}\dfrac{dT_d}{dt} - \dfrac{\partial V_{cld}}{\partial m_d}\dfrac{dm_d}{dt}}{A\,\rho_a\,\dfrac{\partial V_{cld}}{\partial m_{wa}}} \qquad (20)$$

$$- (A_{footprint}/A)\,\frac{dz_{cld}}{dt}$$

where $dV_{cld}/dt$ is determined from Equation ( 14 ). Ignoring rainout and effects of heat and water vapour transfer from the substrate and using HEM, this reduces to [2, 3]

$$U_E = \frac{U}{\rho_a \dfrac{\partial V_{cld}}{\partial m_{wa}}} \quad,\quad for\ \ z_{cld} > R\,(elevated)\ or\ z_{cld} = 0\ (grounded) \qquad (21)$$

$$= \frac{U + (A_{footprint}/A)\dfrac{dz_{cld}}{dt}}{\rho_a \dfrac{\partial V_{cld}}{\partial m_{wa}}} - (A_{footprint}/A)\frac{dz_{cld}}{dt}, \quad for\ \ 0 < z_{cld} < R\ (touching\,down)$$

Subsequently the displacement velocity is set as

$$U_D = U - U_E \qquad (22)$$

Equations will be formulated in Section 5.3 for the time derivatives of the primary variables $m_{wa}$, $m_c$, $m_{wv}{}^{gnd}$, $q^{gnd}$, $H_c$, $T_d$, $m_d$ and thus these results are available without the need of substantial additional code. Running THRM at values $m_{wa}$ and at an incremental larger mass $m_{wa}+dm_{wa}$ (while keeping all other input data constant) leads to an approximation of the partial derivative $\partial V_{cld}/\partial m_{wa}$, and likewise all other partial derivatives in Equation ( 19 ) can be determined[4].

The above implies a generalisation of the theory developed by David Webber[vi] to multi-component non-equilibrium thermodynamics, and it also facilitates the implementation maximising use of existing THRM logic.

---

[2] JUSTIFY. CODE currently applies Equation ( 21 ) instead of ( 20 ). In case a large amount of liquid is present, this may not be appropriate, since $dm_c/dt$ is very large.

[3] ERROR. The code currently erroneously omits the term $(A_{footprint}/A)\ dz_{cld}/dt$ in Equation ( 21 ) (relevant during touching down only). This has not been corrected, since the option $U_d>0$ has not been made available in the product.

[4] IMPROVE. The partial derivative $\partial V_{cld}/\partial m_{wa}$ is currently approximately determined via differencing [from values of cloud volume $V_{cld}$ at $m_{wa} - 10^{-3}\min(m_{wa},m_{wc})$ and $m_{wa} + 10^{-3}\min(m_{wa},m_{wc})$. Alternatively, $V_{cld}$ can be made into an additional primary variable (INEX stage only), with equation $dV_{cld}/dt = A\ U$, and its partial derivatives to the primary variables could then be derived more precisely from the Jacobian as provided by the UDM numerical solver.

# 4 TOP-LEVEL ALGORITHM

## 4.1 Previous algorithm including AWD extension

The phases in the dispersion for an instantaneous release for the current model (old UDM model including AWD) are depicted by Figure 3.

1. <u>Set observer release location and observer release times</u>

   The initial observer moves with the instantaneous cloud. Pools and instantaneous clouds can only co-exist after rainout. Following rainout, the instantaneous cloud will pick up vapour from the pool until the upwind edge of the instantaneous cloud has left the downwind edge of the pool behind. After the upwind edge of the instantaneous cloud has left the upwind edge of the pool behind (this may happen almost immediately if the cloud moves faster than the pool spreads), additional observers will be released from the upwind edge of the pool with equal PVAP mass evaporation segments as for non-instantaneous releases.

2. <u>Carry out UDM dispersion calculations for each observer</u> (instantaneous calculations for initial observer for instantaneous release; steady-state calculations for all observers released from upwind edge of the pool). As part of the above equations, observer droplet rainout is applied at the time at which the observer droplet hits the ground or the bund wall.

3. Inclusion of <u>gravity spreading correction and along-wind diffusion</u> as before. For an instantaneous release gravity spreading and along-wind diffusion has already been applied to the initial instantaneous observer, and therefore downwind gravity spreading and along-wind diffusion are only applied to the 'non-instantaneous' observers released from the upwind edge of the pool. Afterwards the instantaneous concentration is added to obtain the overall concentration.

For purpose of calculating the correct pool data, the calculations for all observers are carried out simultaneously with the pool calculations.
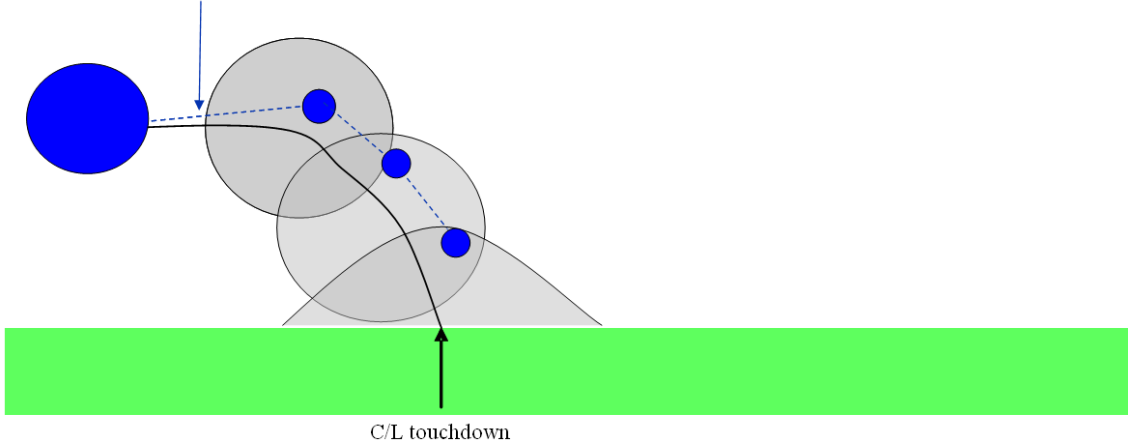
(a)  Dispersion before rainout (single instantaneous observer 1 only)
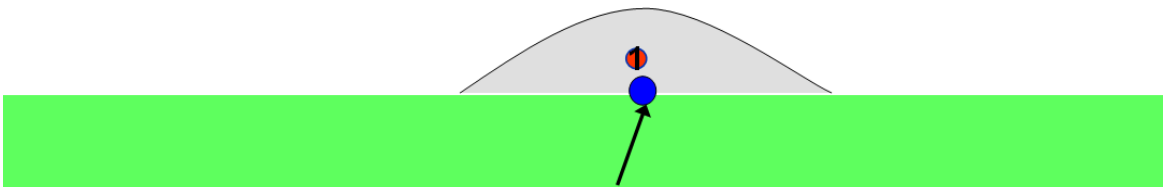
(b)  Rainout (adjust observer variables at rainout location; solve pool equations afterwards)
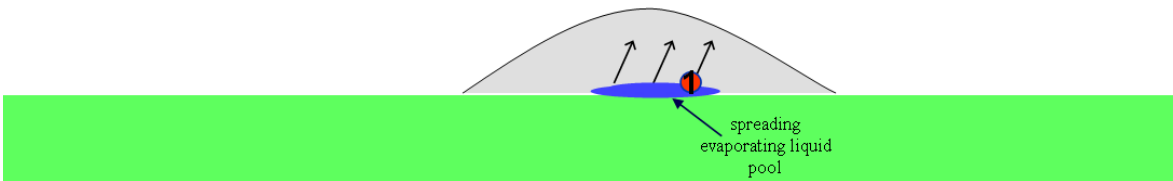
(c)  Dispersion after rainout (account for pool vapour pick-up by instantaneous observer)

(c) Release 'pool observers' after upwind edge of  instantaneous observer passes upwind pool edge
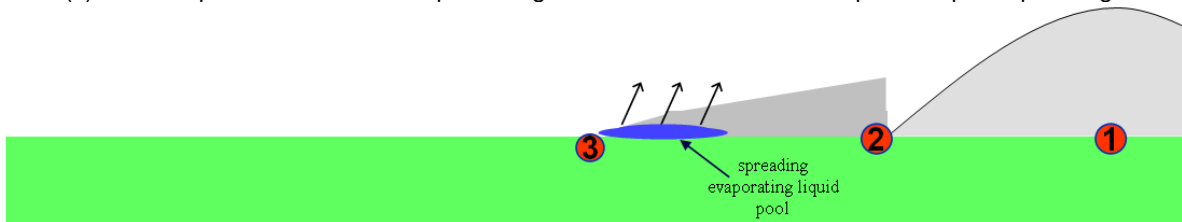
(d) Dispersion directly from pool, with original instantaneous cloud moving away from pool

**Figure 3.**          **Phases in dispersion for two-phase instantaneous release (old UDM AWD model INEX)**

## 4.2 Modifications using new improved INEX methodology

The phases in the dispersion for an instantaneous release for the new INEX are depicted by Figure 4. The following key differences apply between the new and old INEX sub-models for the initial dispersion stage of energetic expansion in the UDM AWD model:

1. Radial expansion and air entrainment

   o Old INEX: empirical formula for cloud radius R versus time, from which (using THRM) the amount of air entrainment is derived
   o New INEX: added differential equations are derived for added primary variables, i.e. wet-air mass $m_{wa}$, rained out mass $m_{ro}$ and radial momentum $I_r = m_{cld} \, dR/dt$, where the cloud expansion speed $dR/dt$ is set from an added differential equation for cloud volume $V_{cld}$.

2. Momentum equations:

   o Horizontal: both models apply standard UDM horizontal momentum equation; $u_x = dx_{cld}/dt$
   o Vertical:
     ▪ Old INEX: simplistically assumed cloud to move horizontally, $u_z = 0$, $z_{cld} = z_R$
     ▪ New INEX: include UDM standard vertical momentum (added primary variable $I_z$); $u_z = dz_{cld}/dt$.

3. Droplet equations and rainout

   o Old INEX:
     ▪ One single droplet is modelled only, with the starting position assumed at the edge of the instantaneous cloud, i.e. $x_d(t=0) = x_{cld}(t=0) + W_{eff}$. The droplet is moving with a known fixed angle. The droplet position and speed was thus provided by an analytical expression, and the standard UDM differential equations are solved to determine the droplet temperature and the droplet mass (non-equilibrium model to allow the cloud vapour temperature to be different to the droplet temperature).
     ▪ Rainout
       (a) no rainout occurs during the INEX stage
       (b) possible instantaneous rainout during the post-INEX stage.
   o New INEX:
     ▪ The droplets are assumed to move in all directions.
     ▪ Rainout
       (a) The INEX rainout rate is calculated analytically with time-varying rainout presumed because of radial expansion only for $0<z_{cld}<R$. No momentum equations are solved numerically for droplet trajectories. In case of non-equilibrium, droplet equations are solved for droplet mass and droplet temperature.
       (b) Thus no INEX rainout occurs after full touchdown. In case of liquid remaining at the end of the INEX stage, immediate instantaneous rainout occurs in case the cloud is grounded at the end of the INEX stage, and otherwise instantaneous rainout may occur later on during the post-INEX stage in case the droplets hit the ground.
     ▪ Two repeated calculations are carried out for the instantaneous observer, the first set to determine the rainout (without linking with the pool) and the second set to include linking with the pool.
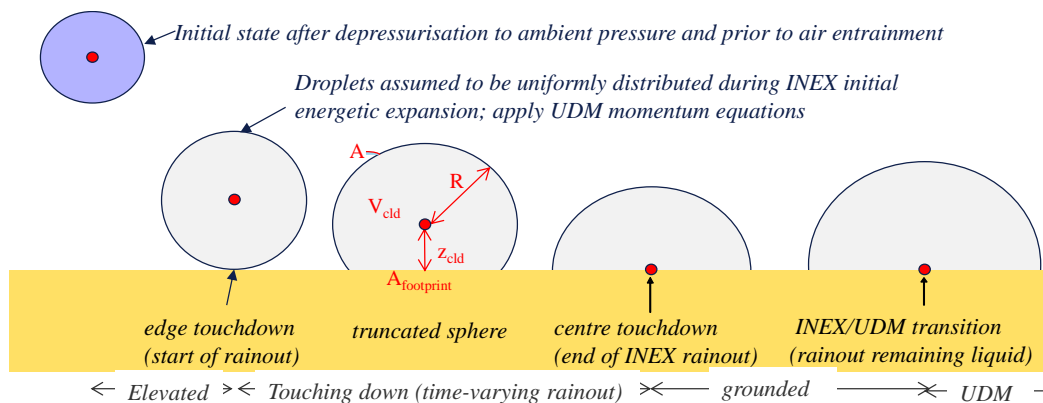


**Figure 4.** **Phases in dispersion for two-phase instantaneous release (new UDM AWD model INEX)**

# 5 DETAILED ALGORITHM

For instantaneous releases, the initial 'instantaneous' observer corresponds with the original instantaneous cloud. In case of rainout and after the upwind edge of the original instantaneous cloud has left behind the upwind edge of the pool, 'steady-state' observers are released from the upwind edge of the pool. This section only deals with the instantaneous observer, since the formulation for the subsequent pool observers has not been modified. In this section a single droplet size (SMD) is presumed.

## 5.1 Primary variables and initialisation of variables

For the instantaneous observer, differential equations are formulated for the unknown primary variables listed in Table 1. Variables listed in italic are added primary variables compared to the original 6.54 UDM formulation.

| UDM PRIMARY VARIABLE | SYMBOL | UNIT | INITIAL VALUE (f = post-exp. data) | When? (TD = touchdown) |
|---|---|---|---|---|
| *downwind distance of pool centre[5]* | $x_{pool}$ | m | 0 | after initial rainout |
| PVAP POOL PRIMARY VARIABLES | various; see PVAP theory manual | - | | after initial rainout |
| UDM PRIMARY VARIABLES[6] | | | | |
| *component mass rained out* | $m_{ro}$ | kg | $\eta_{immediate\_rainout}\, m_{cR}$ | during rainout |
| *compon. mass evaporated from pool* | $m_c^{vap}$ | kg | 0 | cloud above pool |
| *component enthalpy rained out* | $H_c^{ro}$ | J | $m_{ro}\, h_{cL}(P_a, T_f)$ | during rainout |
| *comp. enth. evaporated from pool* | $H_c^{vap}$ | J | 0 | cloud above pool |
| mass of wet air in the cloud | $m_{wa}$ | kg | 0 | always |
| *radial momentum* | $I_r = m_{cld}U = (m_c + m_{wa} + m_{wv}^{gnd})dR/dt$ | kg m/s | $m_c\,(2E_{exp}/m_{cR})^{0.5}$ | INEX |
| excess downwind momentum | $I_{x2} = I_x - m_{cld}u_a(z_c) = m_{cld}u_x - m_{cld}u_a(z_c) = I_x - m_{cld}u_w = m_{cld}u_x - m_{cld}u_w$ | kg m/s | $-m_c u_a(z_R)$ | always |
| vertical momentum | $I_z = m_{cld}\,u_z \qquad = m_{cld}\,u_z$ | kg m/s | 0 | before full TD |
| downwind position | $x_{cld}$ | m | 0 | always |
| vertical position | $z_{cld}$ | m | release height $z_R$ | before full TD |
| heat conduction from substrate | $q_{gnd}$ | J | 0 | after start TD |
| water evaporated from substrate | $m_{wv}^{gnd}$ | Kg | 0 | after start TD if above water |
| cross-wind dispersion coefficient[7] | $R_y = 2^{1/2}\sigma_y \qquad = 2^{1/2}\sigma_y$ | m | - | post-INEX, heavy & passive regime |
| DROPLET PRIMARY VARIABLES | | | | Before droplets evaporated |
| droplet downwind position | $x_d$ | m | 0 | post-INEX |
| droplet vertical position | $z_d$ | m | $z_R$ | post-INEX |
| droplet horizontal velocity | $u_{dx}$ | m/s | 0 | post-INEX |
| droplet vertical velocity | $u_{dz}$ | m/s | 0 | post-INEX |
| droplet mass | $m_d$ | kg/drop | $4\rho_L(P_a, T_f)\pi(SMD_f)^3/3$ | if non-equilibrium |
| droplet temperature | $T_d$ | K | $T_f$ | if non-equilibrium |

**Table 1.** **List of UDM primary plume variables for instantaneous observer**

In addition to the above differential equations for the UDM primary variables, a number of expressions are formulated for a range of UDM secondary variables.[8]

The differential equations for the above primary variables are solved while stepping forward in the time t. Thus the PVAP pool equations and the observer UDM equations are all solved simultaneously enabling a rigorous solution while the instantaneous observer moves over the pool.

Initialisation of primary variables
Table 1 also indicates the initial values of the primary variables and at which stages of the dispersion differential equation are solved for each of the primary variables. The initialisation of the variables at time t=0 is carried out by means of the following successive steps:

---

[5] FUTURE CODE. This is not currently implemented. Instead first instantaneous observer calculations are carried out until rainout is finished (without pool/cloud linking). These observer results are then used to find the time $t_{ro}$ at which 50% of final rainout has occurred. This time is then used to set the rainout temperature $T_d(t_{ro})$ and the downwind rainout distance $x(t_{ro})$. Subsequently instantaneous PVAP calculations are carried out presuming that the UDM total overall rainout occurs instantaneously at time $t_{ro}$ and downwind distance $x(t_{ro})$ with a rainout temperature $T_d(t_{ro})$ with pool evaporation commencing at time $t_{ro}$. Subsequently the instantaneous observer calculations are rerun to account for the pool vapour added back to the instantaneous cloud. Actual implementation of time-varying rainout, would also require extension of PVAP to allow time-varying spill rates simultaneously with instantaneous rainout; also note inconsistency of PVAP results between short-duration spills and instantaneous spills.

[6] Component mass $m_c = m_{cR} - m_{ro} + m_c^{vap}$ and component enthalpy $H_c = m_{cR}\,h_c(T_f;\eta_{cLf}) - H_c^{ro} + H_c^{vap}$ are secondary variables, with $m_{ro}$, $m_c^{vap}$, $H_c^{ro}$, $H_c^{vap}$ treated as primary variables

[7] A differential equation is not used for the INEX phase and jet phase (circular jet assumed), but for the heavy and passive phase only.

[8] Primary variables may be added for variables currently involving iterations for nonlinear equations (e.g. for cloud thermodynamics and cloud geometry).

- The initial centre-line of the cloud corresponds to the location of the centre of the vessel, i.e. $x_{cld}=0$ and $z_{cld} = z_R$.

- The post-expansion data (liquid mass fraction $\eta_{cLf}$, liquid temperature $T_f$, Sauter Mean Diameter $SMD_f$, expansion energy[9] $E_{exp} = f_{kinetic} \{h_c(P_{st},T_{st}; \eta_{cLst}) - h_c(P_a,T_f; \eta_{cLf})\}$ are derived as UDM input from output of the Phast discharge model DISC using isentropic expansion. Here $f_{kinetic}$ is the fraction of total energy converted to kinetic energy, and the specific pollutant enthalpy $h_c$ is determined in DISC using the property system. The initial value of the radial expansion speed $U = dR/dt$ is derived from $E_{exp} = \frac{1}{2} (dR/dt)^2$.

- No rainout occurs during the DISC expansion, and it is assumed that the substrate does not affect the DISC expansion, even if the vessel is at ground-level. In case $\eta_{cLf}>0$, an initial provisional value of cloud radius $R_{pr}$ is calculated presuming a spherical cloud regardless whether the initial cloud (at time t=0) touches the ground or not, i.e. from

$$\frac{4}{3}\pi R_{pr}{}^3 = m_{cR}\ \rho_c(P_a,T_f;\eta_{cLf}) \qquad (23)$$

If $R_{pr} \leq z_{cld}$, the cloud is indeed elevated, $R=R_{pr}$, and no immediate rainout occurs. If $R_{pr}>z_{cld}$, the cloud is not elevated after the DISC expansion and prior to the INEX expansion, and immediate rainout is presumed to occur. The initial pool mass and the mass of pollutant in the cloud are set as follows,

$$M_{pool}(t=0) = \eta_{immediate\_rainout} m_{cR} \qquad (24)$$
$$m_c(t=0) = m_{cR} - M_{pool}(t=0)$$

Here $m_{cR}$ is the entire vessel inventory (kg) and the immediate-rainout mass fraction[10] is defined by[11]

$$\eta_{immediate\_rainout} = \frac{\frac{4}{3}\pi R_{pr}{}^3 - V_{cld}(z_{cld},R_{pr})}{\frac{4}{3}\pi R_{pr}{}^3}\ \eta_{cLf} \qquad (25)$$

and with the centre of the pool initialised as $x_{pool}=0$. Here $V_{cld}(z_{cld},R_{pr})$ is set from Equation ( 8 ). The above implies that in case the cloud is 'elevated' ($z_{cld}>R_{pr}$) at time t=0 no rainout occurs, while in case of a grounded plume ($z_{cld}=0$) at t=0, 50% of the liquid rains out.

The initial liquid fraction is reset accordingly:

$$\eta_{cL}(t=0) = \frac{\eta_{cLf} - \eta_{immediate\_rainout}}{1 - \eta_{immediate\_rainout}} \qquad (26)$$

- The pollutant enthalpy equals

$$H_c = m_c\ h_c(P_a,T_f;\eta_{cL}) = m_c\left\{[1-\eta_{cL}]h_{cv}(P_a,T_f)+\eta_{cL}h_{cL}(P_a,T_f)\right\} \qquad (27)$$

with the vapour and liquid specific enthalpies $h_{cv}$ and $h_{cL}$ set from the Phast property system.

- The initial droplet temperature equals the post-expansion temperature $T_f$. The droplet mass is derived from the product of the initial liquid density $\rho_L(P_a,T_f)$ and the droplet volume of droplet with droplet diameter equal to the post-expansion droplet size (Sauter Mean Diameter) $SMD_f$. Here $P_a$ is the ambient pressure.

- The "cloud geometry" section in the UDM theory manual (see also Section 2.1 in current report) includes a formula for the exponent m as function of $\rho_{cld}$, an expression for n as function of $H_{eff}$, $H_{eff}$ as function of n and $R_z$, and $h_d$ as function of $z_{cld}$, $R_z$, θ and n. By insertion of these expressions into the formula for $V_{cld}$, a non-linear equation for $R_z$ can be formulated, which is solved iteratively for $R_z$.

- Set centroid height $z_c$ from the thus found values for $R_z$, $h_d$, $H_{eff}$, and n, and subsequently set excess downwind momentum $I_{x2}$ from the Equation included in Table 1

- The radial momentum is set as $I_r = m_c (dR/dt)$

---

[9] This is a modification of original formula (used prior to 8.0) for expansion energy (J/kg) in DISC; see report by David Webber[vi] for a detailed discussion. In case of input $f_{kinetic}>0$, DISC calculates the total expansion energy using the formala: $E_{exp} = f_{kinetic}\ \{h_c(P_{st},T_{st}; \eta_{cLst}) - h_c(P_a,T_f; \eta_{cLf})\}$; $E_{exp}$ is input to the UDM.

[10] Equation ( 24 ) could also be used to apply the Purple Book formula (and Flanders method), where a modified definition of $\eta_{immediate\_rainout}$ is used.

[11] Equation ( 25 ) is applicable in case of the absence of bunds. See Equation ( 102 ) in case of presence of bunds.

- All remaining primary variables are initialised as indicated in Table 1.

## 5.2 Rainout

### 5.2.1 Time-varying rainout (INEX stage)

A. EVALUATE RAINOUT RATE AND DOWNWIND DISTANCE OF POOL CENTRE (INEX stage)[12]

For the purpose of pool spill and pool vapour pick-up calculations, the time-varying rainout mass $dm_{ro}/dt$ (PVAP spill rate; kg/s) and downwind distance $x_{pool}$ of pool centre are evaluated.

During the INEX stage, the ('averaged') droplet position is taken equal to the cloud centre-line position, i.e. $x_d = x_{cld}$, $z_d = z_{cld}$, $u_{dx} = u_x$, $u_{dz} = dz_{cld}/dt$, and rainout is assumed to occur for the radially expanding cloud assuming droplets moving in all directions, and assuming those droplets to rain out which either touch the ground or who hit the bund wall (if bund present)[13]. During the INEX stage, rainout will start to occur when the cloud starts touching down and will stop when the cloud has become fully grounded (or cloud lifts off again). Droplet mass and droplet temperature are determined using the existing THRM model and droplet mass and droplet temperature equations.

Following possibly initial immediate instantaneous rainout according to Equation ( 24 ), subsequent time-varying rainout is set during the INEX stage as follows[14,15]:

$$
\begin{aligned}
&implemented: \\
&\frac{dm_{ro}(t)}{dt} = 0 \quad, \; z_{cld} > R \; ('elevated' \; plume) \; or \; z_{cld} = 0 \; ('grounded' \; plume) \\
&\qquad = \max\left\{ K_D \frac{m_{cL}}{V_{cld}} A_{footprint}\left[ \frac{z_{cld}}{R}\frac{dR}{dt} - \frac{dz_{cld}}{dt} \right], 0 \right\}, \quad else \\
&alternative \; (more \; consistent \; with \; UDM \quad geometry - not \, recommended) \\
&\frac{dm_{ro}(t)}{dt} = 0 \quad, \; z_{cld} > R_z \; ('elevated' \; plume) \; or \; z_{cld} = 0 \; ('grounded' \; plume) \\
&\qquad = K_D \; \frac{m_{cL}}{V_{cld}} \; S_{gnd}\left[ \frac{z_{cld}}{R} \; \frac{dR}{dt} - \frac{dz_{cld}}{dt} \right] \quad (during \; TD)
\end{aligned}
\tag{28}
$$

In the derivation of the above equation it is presumed that the radial cloud velocity $u(r)$ linearly increases, $u(r) = (r/R)(dR/dt)$, and thus the vertical downward component at the footprint equals $(z_{cld}/R) \, dR/dt$; the maximum value of the parameter $K_D=1$, which presumes that all liquid hitting the ground will rainout. The first term in the right-hand side of the equation represents the rainout due to the cloud expansion and this term is proportional to the INEX cloud expansion speed $dR/dt$. The second term represents the rainout due to the cloud centre-line height $z_{cld}$ reducing and this term is proportional to the vertical cloud centre-line speed $dz_{cld}/dt$.

In the case of the presence of a bund and as long rainout occurs inside the bund, $x_{pool}$ is subject to the additional condition

$$
x_{pool}(t) = \min\left[ x_{pool}(t), R_{bund} - R_{pool}(t) \right]
\tag{29}
$$

However as soon as rainout occurs outside the bund, bund effects from that time on will be ignored for the pool calculations and consequently the above condition is no longer applied. Accounting for a rainout rate $m_{ro}(t)$ and applying conservation of mass centroid, this leads to the differential equation (now using new INEX model, similar logic as continuous releases):

$$\tag{30}$$

---

[12] Steps A, B, C, D have also been referred to in the description of the UDM algorithm in Section 5.3.2 of the UDM theory manual; step B is not applicable for instantaneous releases.

[13] IMPROVE. In the presence of a cylindrical bund (bund radius $R_{bund}$), it is currently simplistically assumed that immediate instantaneous rainout occurs of all remaining liquid when the cloud centre-line ($x_{cld}$, $z_{cld}$) hits the bund. See Appendix D for potential further improvement of this logic.

[14] An alternative not-implemented formulation is proposed, which may be more in line with the remaining UDM formulation. E.g. UDM uses a different criterion for touchdown as well as a modified definition for the cloud footprint and the cloud area above the ground.

[15] For instantaneous releases during INEX stage (driven by radial momentum), the minimum droplet size criterion (default UDM parameter 10μm is applied i.e. droplets do not rainout below the minimum droplet size.

## 5.2.2 Instantaneous rainout (post-INEX stage)

C.        APPLY OBSERVER RAINOUT AT RAINOUT TIME (POST-INEX STAGE)

After the INEX stage, rainout is assumed to occur using existing UDM droplet equations. This means that instantaneous cloud rainout will occur immediately if the cloud is grounded at INEX transition[16], and possibly at a later stage if the cloud is elevated at INEX transition.[17] This is only applicable for the instantaneous observer for the post-INEX stage, if the droplets have not yet been fully evaporated after the end of the INEX stage.

Instantaneous rainout is applied at the time $t=t_{ro}^i$ at which the observer vertical droplet coordinate reduces to zero [$y_d^i(t)=0$] or when the observer hits the bund wall. The liquid component is removed from the cloud [only droplets above critical droplet size; mass $m_{ro}(t)$] to obtain primary and secondary variables for the "residual" cloud:

1. Reset centre of pool to maintain conversation of mass centroid

$$x_{pool}^i(t_{ro}^i) = \frac{M_{pool}^i(t_{ro}^i)\, x_{pool}^i(t_{ro}^i)\, + m_{ro}(t_{ro}^i)\, x_d}{M_{pool}^i(t_{ro}^i)\, + m_{ro}(t_{ro}^i)} \tag{31}$$

2. Reset residual component mass $m_c$ and residual enthalpy $H_c$ by removing rained-out liquid

$$m_c^i(t_{ro}^i) = m_c^i(t_{ro}^i) - m_{ro}(t_{ro}^i),\ \ H_c^i(t_{ro}^i) = H_c^i(t_{ro}^i) - m_{ro}(t_{ro}^i) h_{cL}\left(T_{d,ro}^i\right) \tag{32}$$

3. The following primary variables are presumed to be unchanged: $m_{wa}$, $x_{cld}$, $z_{cld}$, $q_{gnd}$, $m_{wv}^{gnd}$. Also the cloud speed ($u_x$, $u_z$) is assumed to be unchanged. The remaining primary variables are set as follows:

   3.1. Set residual total cloud mass (secondary variable)

$$m_{cld}^i\ \ =\ \ m_{wa}^i + m_c^i + m_{wv}^{gnd^i} \tag{33}$$

   3.2. Set cloud geometry

      3.2.1. Carry out THRM calculations to set residual cloud density $\rho_{cld}$; set residual cloud volume $V_{cld} = m_{cld}/\rho_{cld}$. Set exponent m from new $\rho_{cld}$.

      3.2.2. In case at time of rainout the transition from jet to heavy phase has taken place, $R_y$ is a primary variable[18] and it is presumed that $W_{eff}$ is not changed during rainout: set $C_m$ from m and set cloud radius $R_y = W_{eff} / C_m$.

      3.2.3. The "cloud geometry" section in the UDM theory manual includes an expression for n as function of $H_{eff}$, $H_{eff}$ as function of n and $R_z$, and $h_d$ as function of $z_{cld}$, $R_z$, $\theta$ and n. By insertion of these expressions into formulas for $V_{cld}$ (instantaneous) or $A_{cld}$ (continuous), a non-linear equation for $R_z$ can be formulated, which is solved iteratively for $R_z$.

      3.2.4. Set centroid height $z_c$ from the thus found values for $R_z$, $h_d$, $H_{eff}$, and n.

   3.3. Residual cloud momentum (assuming $u_x$ and $u_z$ remain unchanged at rainout as indicated above):

$$I_{x2} = m_{cld}[u_x - u_a],\ I_z = m_{cld} u_z, \tag{34}$$

4. Reset other secondary variables accordingly

---

[16] IMPROVE CODE. This may be un-conservative resulting in too much rainout. More conservative is to presume the UDM droplet height at the end of the INEX phase to be equal to the INEX cloud centroid height $z_c^{INEX}$. Using Equation ( 115 ) and presuming that INEX liquid is uniformly distributed along the INEX cloud, it can be derived that $z_c^{INEX} = z_{cld} + 0.75\ (R - z_{cld})^2/(2R - z_{cld})$, if $0 \le z_{cld} \le R$ (ground-level or touching down) and $z_c^{INEX} = z_{cld}$, if $z_{cld} > R$ (elevated).

[17] This discontinuity in rainout is not entirely satisfactory. However after radial expansion usually a significant entrainment has already taken place, and for superheated liquids most liquid will have already been evaporated. For sub-cooled releases with virtually no evaporation, almost immediate 100% rainout will occur anyway, and therefore this may be the best approach. The discontinuity could be removed (or reduced) using an approach similar to the droplet parcel approach, i.e. assuming a range of droplets at different heights but this would make things more complex. In the UDM code, the above time-varying rainout rate is currently calculated by the UDM. However the UDM PVAP pool calculations simplistically presume instantaneous rainout modelled at the 50% rainout fraction; see footnote 5 for details.

[18] CHECK. Perhaps it would be more convenient to apply $W_{eff}$ as a primary variable instead of $R_y$

## 5.3 UDM equations for primary variables

The equations for the initial instantaneous observer distinguish between the initial INEX stage (entrainment dominated by cloud radial expansion, with possibly time-varying rainout as described in above step A) and the post-INEX stage (standard UDM equations, with possibly instantaneous rainout as described in above step C if observer droplet hits the ground or the bund wall).

Two repeated calculations are carried out for the instantaneous observer:

- The first set of calculations serves to determine the rainout. The calculations are carried until rainout is finished, and these calculations do not include linking with the pool. These observer results are then used to find the time $t_{ro}$ at which 50% of final rainout has occurred. This time is then used to set the rainout temperature $T_d(t_{ro})$ and the downwind rainout distance $x(t_{ro})$. Subsequently instantaneous PVAP calculations are carried out presuming that the UDM total overall rainout occurs instantaneously at time $t_{ro}$ and downwind distance $x(t_{ro})$ with a rainout temperature $T_d(t_{ro})$ with pool evaporation commencing at time $t_{ro}$.
- Finally the instantaneous observer calculations are rerun to account for the pool vapour added back to the instantaneous cloud.
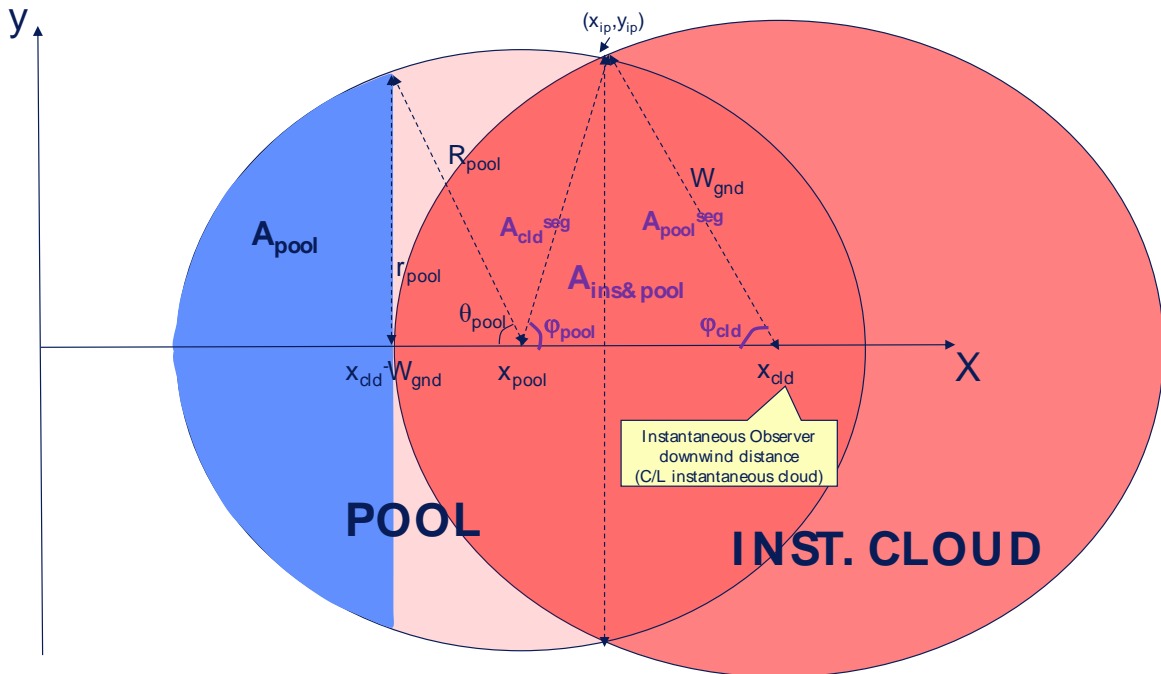


**Figure 5.** **Vapour pick-up from pool while observer is moving over the pool**
Vapour from pool area $\pi R_{pool}^2 - A_{pool}$ is added back to instantaneous cloud; $W_{gnd}$ is radius of instantaneous cloud touching the ground; area of cross-section of pool and instantaneous cloud ground area is $A_{ins\&pool} = A_{cld}^{seg} + A_{pool}^{seg}$]

As soon as the upwind edge of the original instantaneous cloud reaches the upwind edge of the pool, i.e. as soon as $x_{cld}(t) - W_{gnd}(t) \geq x_{pool} - R_{pool}(t)$, non-instantaneous observers will be released from the upwind edge of the pool. Before this time, the entire pool vapour will be added back to the instantaneous cloud. The instantaneous cloud is considered to have left the pool behind if the 'upwind edge' of the instantaneous cloud reaches the downwind edge of the evaporating pool, i.e. when $x_{cld}(t) - W_{gnd}(t) = x_{pool} + R_{pool}(t)$. After this time, the original instantaneous plume moves away from the pool and no vapour is picked up from the pool[19,20].

The UDM observer dispersion equations are as follows:

---

[19]In 6.54 it was assumed that the instantaneous cloud picks up vapour from the entire pool before it leaves the pool behind, while no vapour pick up is assumed after the pool leaves the pool behind. Furthermore the instantaneous cloud was considered to have left the pool behind if the 'upwind edge' $x = x_{cld}(t) - W_{eff}(t)$ of the instantaneous cloud reaches the downwind edge of the evaporating pool, i.e. when $x_{cld}(t) - W_{eff}(t) = x_d^{ro} + R_{pool}(t)$. This results in a discontinuity. After this time, the original instantaneous plume moves away from the pool, and a new finite-duration continuous plume emanates from the pool. At this transition time, the downwind edge of the PCLP plume is located at the downwind edge of the pool (=upwind edge of instantaneous plume).

[20] If $z_{cld} - R_z > 1$ (i.e. as the residual cloud appears to lift off) while vapour is being added back to the plume, then the model issues a warning (UDM 1017). In future $W_{gnd}$ = 0 might be adopted as another criterion for leaving the pool behind.

- *Conservation of pool mass centroid for downwind distance of pool centre, $x_{pool}$*

Equation ( 30 ) is solved during the time-varying rainout during the initial INEX stage. Following this stage $x_{pool}$ is constant, and is reset according to Equation ( 31 ) in case instantaneous rainout occurs during the post-INEX stage.

- *Mass balance for observer component mass $m_c$; enthalpy balance for observer component enthalpy $H_c$*

Prior to rainout and after the instantaneous observer has left the pool behind, the secondary variables $m_c^i$ and $H_c^i$ remain constant. When the instantaneous observer moves over the pool, it is assumed to pick up vapour from that part of the pool which lies downwind of $x = x_{cld}-W_{gnd}$. The vapour upwind of this part will be added back to subsequent non-instantaneous observers. Also during the INEX stage, there may be time-varying rainout causing spillage into the pool. Thus the following equations are applied for the primary varable $m_c^{vap}$ (component mass evaporated from the pool, kg), and the secondary variable $m_c$ (component mass in cloud, kg)

$$\frac{dm_c^{vap}}{dt}(t) = \frac{\pi\left[R_{pool}(t)\right]^2 - A^{pool}(t)}{\pi\left[R_{pool}(t)\right]^2} m_c^{pool}(t) \; , \; m_c = m_{cR} - m_{ro} + m_c^{vap}$$

( 35 )

Here $A^{pool}(t)$ is the area of that part of the pool for which vapour is not added back to the instantaneous cloud[21], and $m_c^{pool}(t)$ is the pool evaporation rate (kg/s).

For $x_{cld}-W_{gnd} \le x_{pool}-R_{pool}$, the upwind edge of the instantaneous cloud is upwind of the upwind edge of the pool and $A_{pool} = 0$. For $x_{cld}-W_{gnd} \ge x_{pool}+R_{pool}$, the upwind edge of the instantaneous cloud is downwind of the downwind edge of the pool and $A_{pool} = \pi R_{pool}^2$. Otherwise, for $x_{pool}-R_{pool} \le x_{cld}-W_{gnd} \le x_{pool}+R_{pool}$, we define (see Figure 5), $r_{pool} = R_{pool}\sin(\theta_{pool})$, $x_{pool} - (x_{cld}-W_{gnd}) = R_{pool}\cos(\theta_{pool})$ with the angle $\theta_{pool}$ $(0 \le \theta_{pool} \le \pi)$,

$$\theta_{pool} = \arccos\left(\frac{x_{pool} - \left(x_{cld} - W_{gnd}\right)}{R_{pool}}\right)$$

( 36 )

It can be derived that $A^{pool}(t)$ is given by

$$\begin{aligned} A_{pool}(t) &= R_{pool}^2 \, \vartheta_{pool} - \left[x_{pool} - (x_{cld} - W_{gnd})\right] r^{pool}(t) \\ &= R_{pool}^2 \left[\vartheta_{pool} - \cos(\vartheta_{pool})\sin(\vartheta_{pool})\right] \\ &= \frac{R_{pool}^2}{2}\left[2\vartheta_{pool} - \sin(2\vartheta_{pool})\right] \end{aligned}$$

( 37 )

Conservation of instantaneous observer enthalpy yields the following equations for primary variables $H_c^{vap}, H_c^{ro}$ and secondary variable $H_c^i$:

$$\frac{dH_c^{vap,i}}{dt}(t) = \left[\frac{dm_c^{vap,i}}{dt}(t)\right] h_{cv}(T_{pool}, P_a) \; , \; \frac{dH_c^{ro,i}}{dt}(t) = \frac{dm_{ro}^i}{dt}(t) \; h_{cL}(T_d, P_a) \; ,$$

$$H_c^i = m_{cR} \, h_f(T_f, \eta_{cLf}) - H_c^{ro,i} + H_c^{vap,i}$$

( 38 )

- *Conservation of observer mass of wet-air in cloud, $m_{wa}^i$ (kg)*

$$\begin{aligned} \frac{dm_{wa}^i}{dt} &= \rho_a A U_E \quad , \text{if } z_{cld} \ge R \, (cloud\, elevated) \text{ or if } z_{cld} = 0 \, (cloud\, grounded) \; [INEX] \\ &= \rho_a \left\{ A U_E + A_{footprint}\frac{dz_{cld}}{dt} \right\} \, , \quad \text{if } 0 < z_{cld} < R \, (cloud\, touching\, down) \qquad [INEX] \\ &= E_{tot}^i \qquad\qquad\qquad\qquad\qquad\qquad\qquad\qquad\qquad\qquad\qquad\qquad [post-INEX] \end{aligned}$$

( 39 )

---

[21] This is slightly inconsistent with the formulation previously adopted for Phase III of the Droplet Modelling JIP (Report C2). Here the instantaneous cloud was assumed to leave the pool behind, when the upwind instantaneous-cloud $x_{cld}(t)-W_{eff}(t)$ reaches the downwind edge of the evaporating pool. In the current formulation we have used the more appropriate choice of $W_{gnd}$ instead of $W_{eff}(t)$, since pool vapour pick-up should be affected by the ground.

Here $U_E$ is evaluation from either equation ( 16 ) or ( 21 ), and $E_{tot}^i$ is the total wet air entrainment rate as defined in 01.1.1Appendix A Appendix A (kg/s).

- *Conservation of radial momentum $I_r$ (kg m/s) – INEX stage only*

$$\frac{dI_r^i}{dt} = -K \rho_a A U_D^2 - \frac{dm_{ro}}{dt} U$$

$$= -K \rho_a S_{above} U_D^2 - \frac{dm_{ro}}{dt} U \text{ , more UDM consistent?}$$

(40)

Here A (INEX geometry) and $S_{above}$ (UDM geometry), is the surface area of the cloud above the ground.

The first term in the above equation represents a drag term, where K is the drag coefficient. The second term in the above equation represents the loss of radial momentum due to rainout and this term is proportional to the rainout rate $dm_{ro}/dt$.

- *Conservation of observer excess horizontal and vertical component of momentum*

The horizontal momentum equation for excess downwind momentum $I_{x2} = I_x - m_{cld}u_a(z_c) = m_{cld}u_x - m_{cld}u_a(z_c)$, and the vertical momentum equation for vertical momentum $I_z = m_{cld}u_z$ are modified at observer rainout as described above. They are further modified to account for added momentum of pool vapour.

For an instantaneous observer[22], [cloud volume $V_{cld} = m_{cld} / \rho_{cld}$],

$$\begin{bmatrix} \dfrac{dI_{x2}}{dt} \\ \dfrac{dI_z}{dt} \end{bmatrix} = F_{drag}^{air} \begin{bmatrix} |\sin\theta| \\ -\cos\theta \dfrac{\sin\theta}{|\sin\theta|} \end{bmatrix} + F_{impact}^{ground} \begin{bmatrix} -\sin\theta \\ \cos\theta \end{bmatrix} +$$

$$F_{drag}^{ground} \begin{bmatrix} 1 \\ 0 \end{bmatrix} + V_{cld}(\rho_{cld} - \rho_a)g \begin{bmatrix} 0 \\ -1 \end{bmatrix} +$$

$$\left\{ \frac{dm_c^i}{dt}(t) - \frac{dm_{ro}^i}{dt}(t) \right\} \begin{bmatrix} -u_a(z_c) \\ u_z^{pool} \end{bmatrix} + \frac{dm_{ro}^i}{dt}(t) \begin{bmatrix} u_x - u_a(z_c) \\ u_z \end{bmatrix}$$

(41)

- *Observer horizontal and vertical position:*

The equation for horizontal position is unchanged,

$$\frac{dx_{cld}}{dt} = u_x = u_{cld} \cos\theta$$

(42)

The equation for vertical position is modified to account for addition of evaporated pool mass at ground level z=0 instead at the C/L height $z_{cld}$ (conservation of mass centroid height)[23],

$$\frac{dz_{cld}}{dt} = u_z - \frac{z_{cld}}{m_{cld}} \frac{dm_c^{vap}}{dt} = u_{cld} \sin\theta - \frac{z_{cld}}{m_{cld}} \frac{dm_c^{vap}}{dt}$$

(43)

---

[22] CHECK. Following discussions with David Webber, the ground impact force may be considered to be modified to point vertically upwards [0,1] instead of perpendicular to the cloud [-sin$\theta$, cos$\theta$].

[23] This equation is appropriate for continuous observer logic as well as instantaneous post-INEX observer logic, for which it is associated with conservation of mass centroid height (loosing or gaining mass at z=0 because of evaporation). This equation adopts the term $dm_c^{vap}/dt$ instead of $dm_c/dt$. In case the latter term would have been used, rainout would increase the C/L height while evaporation reduces the C/L height. However, during the INEX phase significant rainout may occur, which may result in an erroneous upward movement of the cloud; therefore, the term $dm_c^{vap}/dt$ has been used instead of $dm_c/dt$ with $dm_c^{vap}/dt$, in order to avoid erroneous plume rise because of rainout.

- *Rate of heat convection from the substrate*

Heat transfer will take place from the pool to the cloud, but the amount of heat transfer will be different in case the cloud is not above the pool since the pool is at temperature $T_{pool}$ and not at the substrate temperature $T_{gnd}$. Moreover, part of the cloud could be above the pool and part above the substrate. Thus the following is assumed for the heat transfer from the substrate:

$$\frac{d\,q^{gnd^i}}{dt} = \frac{d\,q^{gnd,pool^i}}{dt} + \frac{d\,q^{gnd,gnd^i}}{dt} \tag{44}$$

Here the first term represents the heat transfer from the pool to the cloud and the second term represents the heat transfer from the substrate to the cloud:

$$\frac{dq^{gnd,pool^i}}{dt} = Q_{gnd,T_{pool}} A_{ins\&pool}$$
$$\frac{dq^{gnd,gnd^i}}{dt} = Q_{gnd,T_{gnd}} \left\{ S_{gnd}^{\ i} - A_{ins\&pool} \right\} \tag{45}$$

in W, instantaneous

Here $A_{ins\&pool}$ is that part of the ground surface area of the instantaneous cloud which covers the pool (red-coloured area in Figure 5).

The point $(x_{ip}, y_{ip})$ as depicted in Figure 5 is given by

$$x_{ip} = x_{pool} + \frac{\left(x_{cld} - x_{pool}\right)^2 + R_{pool}^{\ 2} - W_{gnd}^{\ 2}}{2\left(x_{cld} - x_{pool}\right)}$$
$$y_{ip} = \sqrt{R_{pool}^{\ 2} - \left(x_{pool} - x_{ip}\right)^2} \tag{46}$$

Equation ( 37 ) includes a formula for the pool-circle area segment $A_{pool}$ defined by the angle $\theta_{pool}$ ($x_{pool}-R_{pool} \leq x \leq x_{cld}-W_{gnd}$). In case the instantaneous cloud partly covers the pool, one can similarly calculate the area $A_{ins\&pool}$ as the sum of area $A_{pool}^{seg}$ for the pool-circle area segment define by angle $\varphi_{pool}$ ($x_{ip} \leq x \leq x_{pool}+R_{pool}$) in Figure 5 and the area $A_{cld}^{seg}$ for the cloud-circle area segment defined by angle $\varphi_{cld}$ ($x_{cld}-W_{gnd} \leq x \leq x_{ip}$) in Figure 5, where

$$A_{pool}^{\ seg} = \frac{R_{pool}^2}{2}\left[2\varphi_{pool} - \sin\left(2\varphi_{pool}\right)\right] \ , \ A_{cld}^{\ seg} = \frac{W_{gnd}^2}{2}\left[2\varphi_{cld} - \sin\left(2\varphi_{cld}\right)\right] \tag{47}$$

Thus:

$$A_{ins\&pool} = 0, \qquad\qquad (no\ \mathrm{int}\,er\,section)$$
$$= \pi R_{pool}^{\ 2}, \qquad\qquad (entire\ pool\ co\mathit{vered})$$
$$= \pi W_{gnd}^{\ 2}, \qquad\qquad (entire\ cloud\ above\ pool)$$
$$= A_{pool}^{\ seg} + A_{cld}^{\ seg}, \qquad\qquad (else) \tag{48}$$

The angles $\varphi_{pool}$ and $\varphi_{cld}$ in Figure 5b can be calculated as follows with the use of Equation ( 46 )

$$\varphi_{pool} = \cos^{-1}\left(\frac{x_{ip} - x_{pool}}{R_{pool}}\right) = \cos^{-1}\left(\frac{R_{pool}^2 + \left(x_{cld} - x_{pool}\right)^2 - W_{gnd}^2}{2R_{pool}\left(x_{cld} - x_{pool}\right)}\right)$$
$$\varphi_{cld} = \cos^{-1}\left(\frac{x_{cld} - x_{ip}}{W_{gnd}}\right) = 2\cos^{-1}\left(\frac{W_{gnd}^2 + \left(x_{cld} - x_{pool}\right)^2 - R_{pool}^2}{2W_{gnd}\left(x_{cld} - x_{pool}\right)}\right) \tag{49}$$

- *Water-vapour transfer from the substrate*

Water vapour transfer from the substrate to the cloud will only take place for that part of the cloud above the water. As a result, the water vapour transfer from the substrate is now set identical as previously, however now using $dq^{gnd,gnd}/dt$ instead $dq^{gnd}/dt$, i.e.

$$\frac{dm_{wv}^{gnd}}{dt} = \frac{5\left[P_v^w(T_{gnd}) - P_v^w(T_{vap})\right]\dfrac{dq_{gnd,gnd}}{dt}}{C_p^{cld}\,T_{gnd}\,P_a}\;,\quad T_{gnd} > T_{vap} \tag{50}$$

where $P_v^w$ is the saturated vapour pressure of the water. If $T_{gnd} < T_{vap}$ or $T_{gnd} < 0^oC$ (substrate is ice) or if the cloud is passing over dry ground, $dm_{wv}^{gnd}/dt = 0$.

- *Crosswind spreading*

    In general, cross-wind spreading consists of the following three subsequent phases.

    1.  Near-field ('jet') spreading *(unmodified)*. The cloud is assumed to remain circular until the passive transition or (after onset of touching down) until the spread rate reduces to the heavy-gas spread rate, i.e. $R_y = R_z$

    2.  Heavy-gas spreading *(modified to account for added pool vapour).*
        The heavy-gas spread rate is applied until the passive transition ($C_E = 1.15$). In case of the absence of a pool, the heavy gas spread rate can be written as

        $$\frac{dR_y}{dt} = \frac{F_{CE}}{C_m}\;,\quad with\; F_{CE} = C_E\sqrt{\frac{g\left\{\max\left[0, \rho_{cld} - \rho_a(z = z_{cld})\right]\right\}H_{eff}(1 + h_d)}{\rho_{cld}}} \tag{51}$$

        For an incremental step $\Delta t$ of an instantaneous observer with the presence of a pool, the incremental spread is calculated based on mass averaging of the component mass $m_c$ in the cloud (kg) and the mass component added from the pool $\Delta m_c$ (kg),

        $$C_m\Delta R_y = \frac{m_c F_{CE}\Delta t + \Delta m_c C_m \max\left[0, r_{pool}^{uw} - W_{gnd}\right]}{m_c + \Delta m_c}\; with\; r_{pool}^{uw} = \sqrt{\frac{\pi R_{pool}^2 - A_{pool}}{\pi}} \tag{52}$$

        Here $r_{pool}^{uw}(t)$ is equivalent radius for the area of the part of the pool of which the vapour is added back to the instantaneous cloud (i.e. downwind of the upwind edge of the instantaneous cloud), while $W_{gnd}$ is the radius of the instantaneous cloud area at the ground (Figure 5). The above equation reduces in differential form to:

        $$\frac{dR_y}{dt} = \frac{F_{CE}}{C_m} + \frac{1}{m_c}\frac{dm_c}{dt}\max\left[0, r_{pool}^{uw} - W_{gnd}\right] \tag{53}$$

        Thus in case the equivalent 'pool' radius $r_{pool}^{uw}(t)$ is larger than $W_{gnd}$, the above equation applies mass averaging over the cloud mass $m_{cld}$ (kg) and the mass flow added from the pool $dm_c/dt$ (kg/s).

    3.  Passive spreading *(modified to account for added pool vapour – however unlikely passive when observer still moving over the pool; possibly ignore this).* After the passive transition the passive spread rate is applied [$\sigma_{ya}(x)$ = ambient passive dispersion coefficient; $x_0 = 0$ presently]

        $$\frac{dR_y}{dt}[at\; x] = \frac{1}{C_m}\left\{[r_{pool}(s) - W_{eff}]\frac{1}{m_c}\frac{dm_c}{dt}\right\} + u_x 2^{0.5}\frac{d\sigma_{ya}}{dx}[at\; x - x_o] \tag{54}$$

## 5.4    Transition between INEX and post-INEX stages

The old INEX model carried out a transition from INEX to the UDM if the cloud expansion speed $U = dR/dt$ reduced to the rather arbitrary value of 1 m/s.

In the new model it is proposed to carry out the transition if the INEX entrainment rate $\rho_a A U_E$ reduces to the UDM entrainment rate $E_{tot}^i$; see Equation ( 39 ). This will avoid a discontinuity in the air entrainment at the transition, and is

expected to provide a smoothest transition. This transition criterion is applied for both elevated, partially elevated and grounded plumes.

For a grounded plume an earlier transition is made if the spread rate reduces to the gravity-spreading rate defined by either Equation ( 51 ) or ( 53 )[24]. For further details of the evaluation of the spread rate during the INEX stage, see Appendix B.

During the INEX stage the averaged droplet position is assumed to be identical to the cloud centre-line, and the droplet vertical velocity or droplet momentum equal to that of the cloud. In case liquid is still present at the INEX transition, droplet trajectory equations will be solved in the post-INEX stage in addition to the conservation equations for droplet mass and droplet energy. This also implies that immediate rainout occurs of all remaining liquid (above critical droplet size) if the cloud is fully ground at the INEX transition.

## 5.5   Selection of model parameters

A selection of these values has also been discussed by David Webber and is partly repeated here:

The model has one or two of free constants – unknown coefficients of order 1 – which must be determined by fits to data. The new model parameters are as follows:

- K   *a resistance coefficient determining air resistance to radial expansion [Eq.( 40 )].*
    This value is only relevant in case the air-displacement velocity $U_D$ is included in evaluating the overall air entrainment (option available in UDM spreadsheet only). However, this term was found to have minimal effect for the validation against the Landis/Maurer experiments.  Suggest to use default value of K=1.

- $K_D$   *a coefficient in the rainout equation ( 28 ) .*
    The maximum value $K_D$=1 (all droplets raining out as soon as they reach the ground) was shown to result in the best overall agreement against the rainout data of Schmidli et al.[xxi] (see Table 10). Thus the default value $K_D$=1 is selected.

- $f_{kinetic}$ *fraction of the available enthalpy which transforms into radial kinetic energy*.
    This will affect the initial expansion rate compared with the data of Landis et al (1994), Maurer et al (1977) and Pettitt (1990).   A default value of 0.04 is selected following the recommendation of Pattison[vii], and this value was also found to result in good agreement against the experimental data as shown in Chapter 6.

In addition, the following model parameters have been retained with unchanged default values; see UDM theory manual for details and default values). This for example includes the drag coefficient $C_{Da}$ of plume in air (momentum equation; always to be set equal to zero), the jet-entrainment parameters $\alpha_1, \alpha_2$, and the heavy-gas side entrainment parameter $\gamma$; see Appendix A for details.

---

[24] Check for partially grounded plumes

# 6  MODEL VERIFICATION AND VALIDATION

This chapter first describes an approximate analytical solution of the INEX cloud radius R and INEX cloud speed U to the numerical INEX equations, which is applicable for a ground-level hemispheric cloud.

Subsequently the INEX model is applied for validation against experiments involving ground-level pressurised instantaneous releases by Landis (nitrogen vapour) and Maurer (flashing propylene liquid). This validation was carried out previously by David Webber[viii] using the old INEX model. The current chapter provides an updated description and reports results from the latest UDM INEX model. For both sets of experiments, the correctness of the numerical INEX equations has been verified against the above analytical solution.

Finally, the INEX model is applied for validation against experiments involving elevated pressurised instantaneous two-phase releases by Pettitt (Freon 11 without rainout) and Schmidli (Freon 12, propane and butane with rainout).

## 6.1  Ground-level releases

### 6.1.1  Analytical solution to INEX equations for ground-level release ($U_D<<U_E$)

An analytical solution is derived below for the new INEX model in the case of a ground-level cloud. Here the following is assumed:

- The displacement velocity $U_D$ is much smaller than the entrainment velocity $U_E$, i.e. it is assumed that the cloud expansion speed $U = dR/dt = U_E + U_D \approx U_E$.
- $U_D$ is sufficiently small such that it can be assumed that the radial momentum $I_r = m_{cld} U = m_{cld} \, dR/dt$ is constant [see Eq. ( 40 )] .
- In case of a two-phase or liquid release, it is assumed that during the INEX stage the mass evaporating from the pool $m_c^{vap}$ can be ignored, i.e. $m_c^{vap} << m_o$. Here $m_o = m_{cR}-m_{ro}(t=0)$ is the released vessel mass after immediate rainout. Thus $m_{cld} = m_o + m_c^{vap} + m_{wa} \approx m_o + m_{wa}$.

According to Eq. ( 8 ) the following applies for the geometry of a ground-level hemispherical cloud: cloud centre-line $z_{cld}=0$, cloud volume $V_{cld}=(2/3)\pi R^3$, cloud surface area $A=2\pi R^2$.

It follows from Equations ( 14 ) and ( 17 ) that

$$\frac{dm_{wa}}{dt} = \rho_a \, A \, U_E \approx \rho_a \, A \, U = \rho_a \frac{dV_{cld}}{dt} \quad \Rightarrow \quad m_{wa} = \rho_a \left(V_{cld} - V_0\right) = \rho_a \frac{2\pi}{3}\left(R^3 - r_o^{\,3}\right) \tag{55}$$

where $m_{wa}$ is the added air entrained into the cloud (kg), $\rho_a$ is the ambient density (kg/m³), and $V_o = V_{cld}(t=0)$ and $r_o=R(t=0)$ are the initial volume and initial radius after expansion to atmospheric pressure, after immediate rainout (if applicable) and prior to air entrainment.

By presuming constant radial momentum and ignoring mass evaporating from the pool (if applicable) it can now be derived that [$m_o$ = released vessel mass after immediate rainout (if applicable)]:

$$I_r = m_o u_o \approx m_{cld} U \approx \left[m_0 + m_{wa}\right]\frac{dR}{dt} = \left[m_0 + \rho_a \frac{2\pi}{3}\left(R^3 - r_o^{\,3}\right)\right]\frac{dR}{dt} \tag{56}$$

Here $u_o=U(t=0)$ the initial velocity after expansion to atmospheric pressure and prior to air entrainment. Furthermore, $m_o = (2/3)\pi R^3 \rho_o$, where $\rho_o$ is the initial cloud density after expansion to ambient pressure and after immediate rainout (if applicable). Separation of variables R and t in Equation ( 68 ), and subsequent integration leads to

$$u_o t = \int_{r_o}^{R} \left\{1 + \frac{\rho_a}{m_0}\frac{2\pi}{3}\left(r^3 - r_o^{\,3}\right)\right\} dr = R - r_0 + \left(\frac{\rho_a}{\rho_o r_o^{\,3}}\right)\left(\frac{1}{4}R^4 - r_o^{\,3}R + \frac{3}{4}r_o^{\,4}\right) \tag{57}$$

Thus the time t can be expressed as function of the radius R as

$$t = \frac{R}{u_o}\left\{1+\left[\frac{\rho_a}{\rho_o}\right]\left[\frac{1}{4}\left(\frac{R}{r_o}\right)^3-1\right]\right\} - \frac{r_0}{u_o}\left\{1-\frac{3}{4}\left[\frac{\rho_a}{\rho_o}\right]\right\}$$

( 58 )

which for large values of $R/r_o$ simplifies to

$$R \approx \left\{4\left(\frac{\rho_o}{\rho_a}\right)r_o^3 u_o t\right\}^{1/4}$$

( 59 )

By means of differentiation of Equation ( 58 ), the following expression can be derived for the cloud expansion speed U as function of the cloud radius R:

$$U = \frac{u_o}{1+\left[\frac{\rho_a}{\rho_o}\right]\left[\left(\frac{R}{r_o}\right)^3-1\right]}$$

( 60 )

Thus the cloud radius U can be analytically evaluated as function of time t by first evaluating radius R as function of time t using Equation ( 58 ) and subsequently evaluating U as function of R using Equation ( 60 ).

Using Equations ( 59 ) and ( 60 ), it can be derived that for R>>$r_o$, the expansion speed varies as follows with time

$$U = \frac{u_o}{\left[\frac{\rho_a}{\rho_o}\right]\left(\frac{R}{r_o}\right)^3} = \left[\frac{\rho_o}{\rho_a}u_o\right]^{1/4}\left[\frac{r_o}{4t}\right]^{3/4}$$

( 61 )

Thus presuming $U_D$ is sufficiently small, it follows from the above equations that the cloud radius R and the cloud speed U for a ground-level cloud are independent of the parameters K, $K_D$. The expansion energy $E_{exp}$ is defined to be linearly proportional to the parameter $f_{kinetic}$, which equals the fraction of overall released energy converted to kinetic energy. Since $u_o = [2E_{exp}]^{1/2}$ is proportional to $f_{kin}^{1/2}$, it follows from Equations ( 59 ) and ( 61 ) that both the cloud radius R and the cloud expansion speed U are proportional to $f_{kin}^{1/8}$.

## 6.1.2   Experiments by Landis et al. (nitrogen vapour)

Description of experiments

Landis et al[ix] released various quantities of mixtures of nitrogen and fumed silica from a container. The experiments considered two initial stagnation temperatures (273 or 303K) and four different initial stagnation pressures (4.2, 8.2, 21.5 or 71.7 bara). The container was a cylinder of length L=12" and radius r=2" with a hemispherical end cap.  Accordingly, its volume is $V_{vessel} = \pi r^2 L + 2\pi r^3/3 = 0.00275$ m$^3$.

Landis et al are not clear about the precise nature of the fumed silica, which they refer to as a "tracer".   Following the discussions in the previous report by David Webber[viii], the silica is indeed presumed to be just a tracer, and therefore for modelling purposes the mixture of nitrogen and silica is approximated by pure nitrogen.

Evaluation and verification of vessel mass, expansion energy and initial expansion velocity

In his original calculations David Webber derived the released mass M using the ideal-gas law for the nitrogen vapour density ρ, i.e. $\rho = M_W P_{st}/(RT_{st})$ where $M_w$ = 28.01 kg/kmol is the nitrogen molecular weight, $P_{st}$ equals the absolute stagnation pressure, $T_{st}$ the stagnation temperature and R = 8314 J/K/kmol the gas constant. In the current new calculations Phast has been used to derive the density ρ.

Table 2 includes a comparison between the ideal-gas calculations and the new calculations:

- yellow cells indicate spreadsheet input data: stagnation temperature $T_{st}$, stagnation pressure $P_{st}$, ambient pressure $P_a$
- orange cells indicate results from Phast property calculations: stagnation vapour density $\rho(P_{st},T_{st})$, specific stagnation vapour enthalpy $h(P_{st},T_{st})$, final post-expansion enthalpy $h(P_a,T_f)$
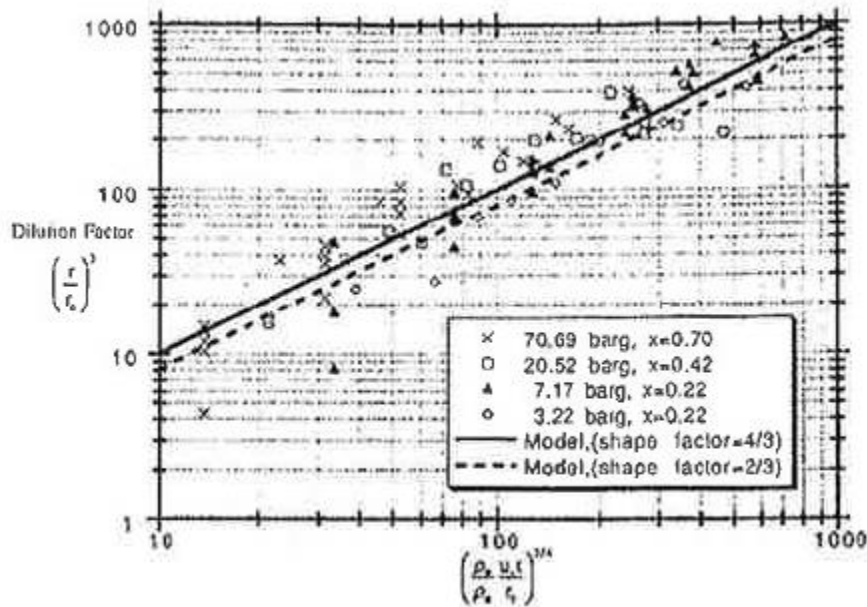
- blue cells indicate results from the Phast discharge model DISC based on Phast property calculations: post-expansion temperature $T_f$, old value of expansion energy $E_{exp}^{old} = h(P_{st},T_{st}) - h(P_a,T_f) - (P_{st}-P_a)/ \rho(P_{st},T_{st})$
- white cells indicate results from the Excel spreadsheet. These include the vessel mass $M = \rho(P_{st},T_{st}) V_{vessel}$ and the old value of expansion energy, J/kg.

The following can be concluded from the table:

- As expected, difference in results between ideal-gas and Phast 'real' gas calculations are seen to be very small for the lower pressures with increasing difference in results with increasing pressure.
- The value of the 'old' expansion energy $E_{exp}^{old}$ calculated by the spreadsheet (based on Phast property calculations) was confirmed to match identically those calculated by the old DISC spreadsheet.
- The calculated values based on Phast property calculations of new expansion energy $E_{exp}^{new} = f_{kinetic} [h(P_{st},T_{st}) - h(P_a,T_f)]$ and initial INEX velocity $u_o = U(t=0) = (2 E_{exp})^{0.5}$, were confirmed to match identically those calculated by the new DISC and new UDM INEX code. Note that the value of uo_old is the value of the initial velocity as reported by the current Phast 6.7/7.1 version of the discharge model DISC. This value however differs from the actual velocity $U(t=0)$ presumed by the old INEX model, which is in fact significantly smaller.

| Vessel radius = | 2 | inches | = | | 0.0508 | m | | | Yellow cell - input data (user) | | | | | |
| Vessel length : | 12 | inches | = | | 0.3048 | m | | | Orange cell - from PROP spreadsheet | | | | | |
| Vessel volume | 167.55 | inch**3 | = | | 0.00275 | m**3 | | | Blue cell - from DISC spreadsheet | | | | | |
| f_kinetic | 0.04 | | = (vessel volume) * ρ | | | | | | | | | | | |

| Stagnation data | | | | Final Data | | Vapour enthalpies | | | Old UDM - expansion energy | | | New exp.en. | Initial velocity | |
|---|---|---|---|---|---|---|---|---|---|---|---|---|---|---|
| T_st (K) | P_st (bara) | ρ_st (kg/m³) | Mass M (kg) | T_f (K) | P_a (bara) | h(P_st,T_st) (J/kg) | h(P_a,T_f) (J/kg) | h_st-h_f (J/kg) | (Pst-Pa) /ρst | EexpUD M old | From DISC (UDMold) | fkin (hst-hf) | old DISC uo_old (m/s) | new INEX uo_new (m/s) |
| Ideal gas law for densities: Mw p/(RT) | | | | | | | | | | | | | | |
| 273 | 4.2 | 5.18 | 0.014 | 181.64 | 1.01325 | -27297 | -121733 | 94435.3 | 61483 | 32952 | 32991 | 3777 | 257 | 87 |
| 273 | 8.2 | 10.12 | 0.028 | 149.69 | 1.01325 | -28374 | -155152 | 126778 | 71020 | 55758 | 55835 | 5071 | 334 | 101 |
| 273 | 21.5 | 26.53 | 0.073 | 112.70 | 1.01325 | -31867 | -194043 | 162176 | 77214 | 84962 | 85108 | 6487 | 413 | 114 |
| 273 | 71.7 | 88.48 | 0.243 | 77.41 | 1.01325 | -43722 | -231669 | 187947 | 79887 | 108059 | 107704 | 7518 | 464 | 123 |
| 303 | 4.2 | 4.67 | 0.013 | 201.69 | 1.01325 | 4179 | -100785 | 104964 | 68240 | 36724 | 36685 | 4199 | 271 | 92 |
| 303 | 8.2 | 9.12 | 0.025 | 166.33 | 1.01325 | 3377 | -137732 | 141108 | 78824 | 62284 | 62186 | 5644 | 353 | 106 |
| 303 | 21.5 | 23.91 | 0.066 | 125.51 | 1.01325 | 789 | -180538 | 181327 | 85699 | 95628 | 95287 | 7253 | 437 | 120 |
| 303 | 71.7 | 79.72 | 0.219 | 86.92 | 1.01325 | -7860 | -221438 | 213577 | 88666 | 124911 | 123089 | 8543 | 496 | 131 |
| Phast density from PROP DIPPR spreadsheet | | | | | | | | | | | | | | |
| 273 | 4.2 | 5.19 | 0.014 | 181.64 | 1.01325 | -27297 | -121733 | 94435.3 | 61444 | 32991 | 32991 | 3777 | 257 | 87 |
| 273 | 8.2 | 10.13 | 0.028 | 149.69 | 1.01325 | -28374 | -155152 | 126778 | 70943 | 55835 | 55835 | 5071 | 334 | 101 |
| 273 | 21.5 | 26.58 | 0.073 | 112.70 | 1.01325 | -31867 | -194043 | 162176 | 77068 | 85108 | 85108 | 6487 | 413 | 114 |
| 273 | 71.7 | 88.09 | 0.242 | 77.41 | 1.01325 | -43722 | -231669 | 187947 | 80242 | 107704 | 107704 | 7518 | 464 | 123 |
| 303 | 4.2 | 4.67 | 0.013 | 201.69 | 1.01325 | 4179 | -100785 | 104964 | 68279 | 36685 | 36685 | 4199 | 271 | 92 |
| 303 | 8.2 | 9.11 | 0.025 | 166.33 | 1.01325 | 3377 | -137732 | 141108 | 78923 | 62186 | 62186 | 5644 | 353 | 106 |
| 303 | 21.5 | 23.81 | 0.065 | 125.51 | 1.01325 | 789 | -180538 | 181327 | 86040 | 95287 | 95287 | 7253 | 437 | 120 |
| 303 | 71.7 | 78.12 | 0.214 | 86.92 | 1.01325 | -7860 | -221438 | 213577 | 90488 | 123089 | 123089 | 8543 | 496 | 131 |

**Table 2.**          **Landis experiments – evaluation of released mass and expansion energy**

**Figure 6.** **Landis N$_2$ experiments - Validation of Landis model of cloud volume versus time**
The figure is taken from Figure 5 in paper by Landis et al.[ix]. It plots dimensionless volume versus dimensionless time.

Cloud radius versus time - analytical solution of equations (Landis model)

The analytical solution to the INEX equations described in Section 6.1 presumes a hemispheric cloud. However, the release for the Landis experiments is from a cylindrically shaped vessel with 'frontal capture'. For a ground-level cloud Landis et al. set $V_{cld} = a\pi R^3$ with the shape factor $a=2/3$ (consistent with a hemispherical cloud and not a cylindrical vessel volume!). Furthermore, they assume frontal capture, i.e. air entrainment only at the frontal part with area $\pi R^2$: $dV_{cld}/dt = \pi R^2 U$. This assumption differs from the INEX assumption $dV_{cld}/dt = 3a\pi R^2 U = 2\pi R^2 U$. Thus they derive the following equation for the radius [(Eq. (14) in Landis paper]

$$R = \left\{ \frac{4}{3a}\left(\frac{\rho_o}{\rho_a}\right)r_o^3 u_o t \right\}^{1/4} = \left\{ 2\left(\frac{\rho_o}{\rho_a}\right)r_o^3 u_o t \right\}^{1/4} \quad \text{, Landis paper - hemisphere} \qquad (\,62\,)$$

Or equivalently (for $R \gg r_o$):

$$\left(\frac{R}{r_o}\right)^3 = \left\{ \frac{4}{3a}\left(\frac{\rho_o}{\rho_a}\right)\frac{u_o t}{r_o} \right\}^{3/4} = \left\{ 2\left(\frac{\rho_o}{\rho_a}\right)\frac{u_o t}{r_o} \right\}^{3/4} \quad \text{, Landis(frontal capture; hemisphere)} \qquad (\,63\,)$$

$$\left(\frac{R}{r_o}\right)^3 = \left\{ 4\left(\frac{\rho_o}{\rho_a}\right)\frac{u_o t}{r_o} \right\}^{3/4} \quad \text{UDM new INEX (hemisphere)}$$

The ratio of the above predictions equals: $(2/4)^{3/4}=0.595$. Figure 6 is taken from Landis paper and shows a smaller value for $a=2/3$ than $a=4/3$, which seems to be incorrect.

Cloud radius versus time – verification of INEX numerical against INEX analytical predictions; validation against experimental data

In line with Figure 6 (from Landis), Figure 7 plots the dimensionless volume $(R/r_o)^3$ versus the dimensionless time $[(\rho_o u_o t)/(\rho_a r_o)]^{3/4}$ for two selected tests ($T_{st}=273K$, $P_{st}= 4.2$ or $71.7$ bara). The figure includes the following curves[25]:

- Experimental data (given by markers; data at 4.2, 8.2, 21.5 and 71.7 bara)
- Red curves: predictions by Landis model [see Eq. ( 62 )] for shape factors $a = 2/3$ (hemisphere) and $a = 4/3$ (sphere). The experimental data are seen to agree fairly well with the Landis curves.
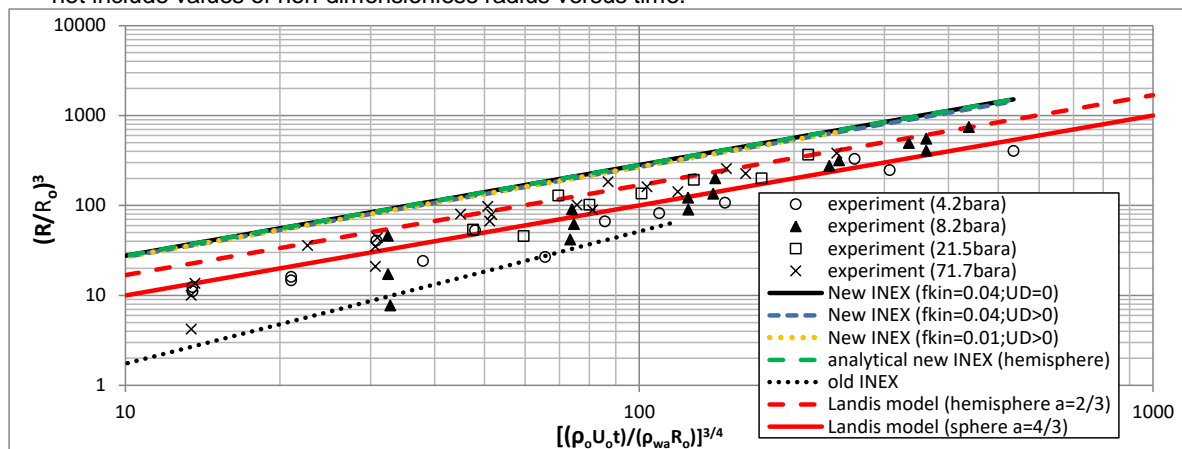- Predictions of old INEX model; this model is seen to under-predict the experimental data.

---

[25] DOC. Consider extending Figure 7 to include all 8 tests.

- Analytical predictions of the new INEX model ($U_D$=0) [see Eq. ( 58 )]
- Numerical INEX predictions
  - Figure 7b includes numerical results for $f_{kinetic}$ =0.04 only ($U_D$=0 or $U_D$>0), while Figure 7a includes also numerical results for $f_{kinetic}$ = 0.01 ($U_D$>0). Since the radius R is proportional to $f_{kin}^{1/8}$, the dimensionless volume is proportional to $f_{kin}^{3/8}$ and the numerical new INEX results in Figure 7b reconfirm that indeed the dimensionless volume increases with $f_{kin}$.
  - It is confirmed that the analytical predictions are very close to the numerical predictions. This is with the exception of the very near-field for the large pressure $P_{st}$=71.7bar, where there are very limited effects of $U_D$ (which are included by the numerical INEX model, but have been ignored by the above analytical approximation).
  - The numerically predicted cloud radius versus time was also confirmed to be independent of the other parameters $K_D$ and K (as long as $KU_D^2$ is sufficiently small, i.e. radial momentum can assumed to remain to be constant; and presuming an INEX ground-level cloud). Thus it it seen that there is very little difference between the $U_D$=0 and $U_D$>0 formulations.
  - The new INEX model is seen to slightly over-predict the experimental data.

The above results are also expected to apply for the other experiments, as along as radial momentum can presumed to be constant. Thus overall the old INEX considerably under-predicts the dimensionless cloud radius versus dimensionless time, and the new INEX slightly over-predicts. Thus the new INEX predicts a slightly too rapid air entrainment and therefore slightly under-predicts concentrations (slightly un-conservative), while the old INEX produces considerable conservative concentrations. This is subject to an accurate prediction of the initial velocity U(t=0), which will depend on the appropriate selection of $f_{kinetic}$.

In summary, there are the following issues with Landis experiments[26]:

- Not pure nitrogen, also includes silica
- Not hemispherical vessel, but cylindrically shaped
- Landis model assumes isentropic expansion to evaluate $u_o$; this differs from new INEX approach (with term $f_{kinetic}$ < 1).
- Landis paper does not seem to give actually adopted values for $u_o$, $r_o$, $\rho_o$, $\rho_a$ for deriving Figure 5. It also does not include values of non-dimonsionless radius versus time.



(a)  $T_{st}$ = 273K, $P_{st}$ = 4.2 bara



---
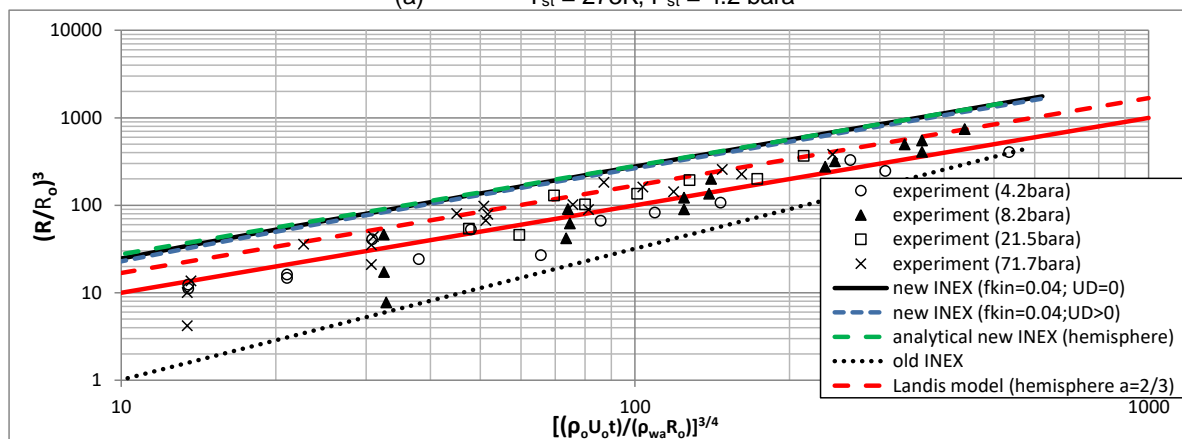
[26] DISCUSS. Suggest to discuss these conclusions possibly also with Air Products e.g. on availability of data for $u_o$, $r_o$, $\rho_o$, $\rho_a$ and non-dimensionless radius versus time.

(b) $T_{st}$ = 273K, $P_{st}$ = 71.7 bara

**Figure 7. Landis N$_2$ experiments - INEX validation of cloud volume versus time**
The figure plots dimensionless volume versus dimensionless time.

Old UDM model[27]

For the new INEX model R$^3$~t$^{3/4}$ applies, while for the old INEX model R$^3$~t$^{9/8}$. Figure 8 plots the scaled volume (R/r$_o$)$^3$ versus scaled time (u$_o$t/r$_o$)$^{3/4}$ for the pure nitrogen releases at the four pressures and the two temperatures, where the blue curves correspond to the UDM results and the pink curves with the 3/8 UDM power law. In is seen that the UDM power law applies after a very short time.

The power laws to which the UDM results are asymptotic are of the form

$$\left(\frac{r}{r_0}\right)^3 = k\left[\left(\frac{\rho_0 u_0 t}{\rho_a r_0}\right)^{3/4}\right]^{3/2}$$

with the extracted constant k varying between 0.0235 and 0.037; k tends to decrease with increasing temperature and pressure.

Figure 9 includes the (dimensionless) volume versus time plot of Landis et al with the region of UDM power law predictions for pure nitrogen superimposed. It is seen that the UDM results do not follow the trend of the data, but do come into agreement with it at larger times.

---

[27] DOC. Description of old UDM model retained for now, to demonstrate improvement for new INEX model. Consider to remove at a later stage.
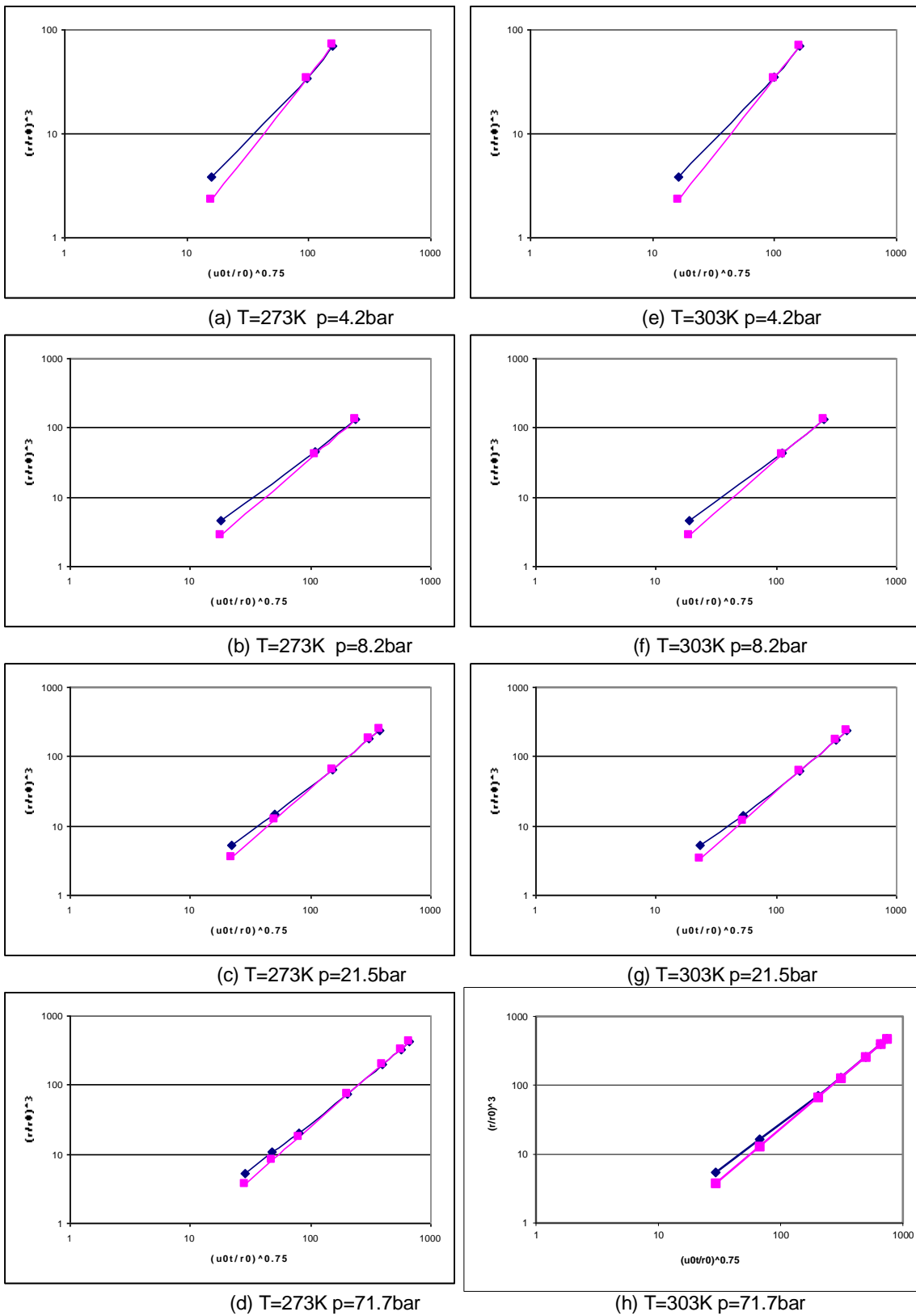
(a) T=273K  p=4.2bar

(e) T=303K  p=4.2bar

(b) T=273K  p=8.2bar

(f) T=303K  p=8.2bar

(c) T=273K  p=21.5bar

(g) T=303K  p=21.5bar

(d) T=273K  p=71.7bar

(h) T=303K  p=71.7bar

**Figure 8.** **Landis N$_2$ experiments - Old INEX verification of cloud volume versus time**
The graphs plot scaled cloud volume $(r/r_o)^3$ versus scaled time $(u_ot/r_o)^{0.75}$. The graphs verify UDM results (blue curve) against the 3/8 UDM power law (pink curve).
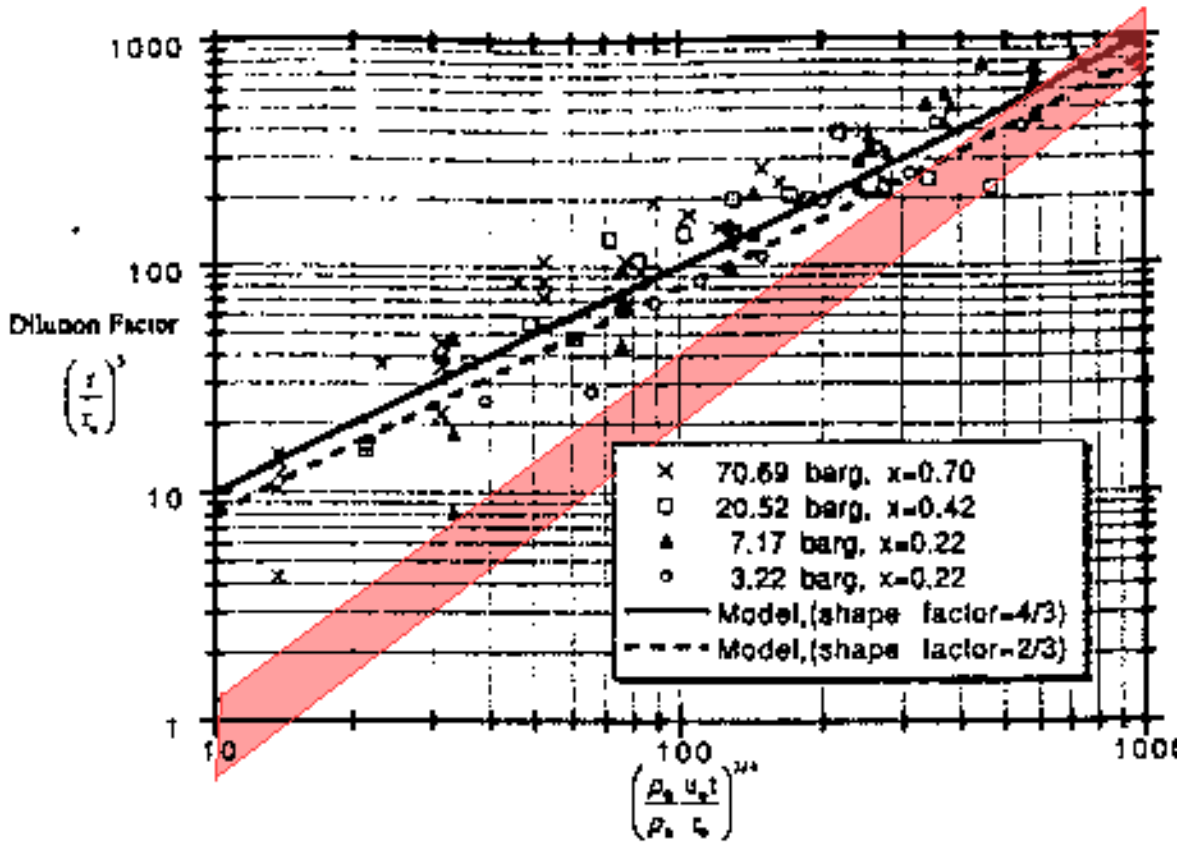
**Figure 9.** **Landis N₂ experiments - Old INEX validation of cloud volume versus time**
The graph plots the scaled cloud volume $(r/r_o)^3$ versus scaled time $[\rho_0 u_0 t/(\rho_a t_o)]^{3/4}$. The graph validates old UDM results (given by red region) against experimental data (approximated by black trend line).

## 6.1.3 Experiments by Maurer et al. (flashing propylene liquid)

Description of experiments

Maurer et al[x,xi] released various quantities of heated propylene instantaneously from cylindrical tanks. The initial state is liquid at a pressure of 60barg and in the temperature range 323K to 353K.

Reid and Prausnitz[xii] give the properties of propylene as:

Molecular weight: $M_w$ = 42.08 g/mol
Boiling point: $T_b$ = 225.5K (-47.7C)
Critical point: $T_c$=364.9K, $p_c$=46.0bar, $v_c$=181 cm$^3$/mol.

Thus the release temperature is well above the normal boiling point, and in fact the release pressure is well above the saturated vapour pressure at the release temperature. The above data $M_w$, $T_b$, $T_c$, $p_c$ are identical to those reported by the DIPPR database in Phast. The critical specific volume at $T_c$, $p_c$ is reported by Phast as 216 cm$^3$/mol.

Let M be the propylene mass in the tank which forms a hemispherical vapour cloud; 2M is the mass in the equivalent full spherical cloud.

The most relevant output for comparison is a graph of expansion velocity dR/dt against (normalised) time. The expansion velocity is that of the visible edge of the cloud due to droplet condensation. The normalised time used is $t/L_G$ (s/m) where $L_G$ is the cube root of the volume ($V_G$) of twice the released mass (2M) of propylene in the gaseous phase at 0 Celsius and 1bar, i.e.

$$L_G = V_G^{1/3} = \left\{ \frac{2M}{\rho_{vap}(1bara,0C)} \right\}^{1/3}$$

**( 64 )**

Table 3 includes for each of the 6 different size tanks, the associated values of the tank dimensions, the propylene mass $M_G$, the propylene volume $V_G$ and the scale factor $L_G$. As indicated by the table, for four of these tank sizes INEX simulations have been carried at each of the two different initial temperatures 323K and 353K spanning the temperature range quoted.

| Tank diameter D (mm) | Tank length L (mm) | Wall thickness t (mm) | Tank volume (litre) | Propylene mass M (kg) | 2M (kg) | $V_G$=M/ρ (m3) | $L_G$=$V_G^{1/3}$ (m) | INEX run? |
|---|---|---|---|---|---|---|---|---|
| 40 | 180 | 0.3 | 0.23 | 0.124 | 0.248 | 0.131 | 0.509 | X |
| 60 | 270 | 0.5 | 0.76 | 0.42 | 0.84 | 0.445 | 0.764 | |
| 100 | 450 | 0.75 | 3.53 | 1.95 | 3.9 | 2.068 | 1.274 | X |
| 150 | 675 | 1.25 | 11.93 | 6.55 | 13.1 | 6.946 | 1.908 | |
| 200 | 900 | 1.5 | 28.27 | 15.6 | 31.2 | 16.543 | 2.548 | X |
| 700 | 2800 | 5 | 1077.57 | 452 | 904 | 479.321 | 7.826 | X |

**Table 3.** **Maurer experiments – tank dimensions, propylene mass and volume**

Evaluation of expansion energy and initial expansion velocity

Table 4 includes results of evaluation of expansion energy and initial expansion velocity:

- yellow cells indicate spreadsheet input data: stagnation temperature $T_{st}$, stagnation pressure $P_{st}$, ambient pressure $P_a$
- orange cells indicate results from Phast property calculations: stagnation vapour density $\rho(P_{st},T_{st})$, specific stagnation vapour enthalpy $h(P_{st},T_{st})$, specific vapour and liquid enthalpy at final pressure $P_a$ and final temperature $T_f$, vessel mass M
- blue cells indicate results from the Phast discharge model DISC (always based on Phast property calculations): post-expansion temperature $T_f$ and liquid fraction $\eta_{Lf}$, old value of expansion energy $E_{exp}^{old}$ = $h(P_{st},T_{st})$ - $h(P_a,T_f; \eta_{Lf})$ – $(P_{st}-P_a)/ \rho(P_{st},T_{st})$
- white cells indicate results from the Excel spreadsheet: value of old expansion energy, values of new expansion energy $E_{exp}^{new}$ =$f_{kinetic}$ [$h(P_{st},T_{st})$ - $h(P_a,T_f)$], old and new values of initial INEX velocity $u_o$ = U(t=0) = (2 $E_{exp}$)$^{0.5}$. These results were verified to exactly match those values obtained from the numerical DISC and UDM INEX codes.

| RHO(0C,1bara) | 1.886 | kg/m3 [propylene vapour density from Phast at 0C,1bara] | | | Yellow cell - input data (user) |
|---|---|---|---|---|---|
| f_kinetic | 0.04 | | | | Orange cell - from PROP spreadsheet |
| | | | | | Blue cell - from DISC spreadsheet |

| Stagnation data | | | | Final Data | | | Enthalpies | | | | | Old UDM - exp. energy | | | New exp.en. | Initial velocity | |
|---|---|---|---|---|---|---|---|---|---|---|---|---|---|---|---|---|---|
| $T_{st}$ (K) | $P_{st}$ (bara) | liquid $\rho_{st}$ (kg/m³) | Mass M (kg) | $T_f$ (K) | final liq.fr. | $P_a$ (bara) | liquid h(Pst,Tst) (J/kg) | liquid h(Pa,Tf) (J/kg) | vapour h(Pa,Tf) (J/kg) | final h_f at Pa, Tf,liq.fr (J/kg) | h_st-h_f (J/kg) | (Pst-Pa)/ρst | Eexp UDM old | From DISC (UDMold) | fkin (hst-hf) | old DISC uo_old (m/s) | new INEX Uo_new (m/s) |
| 323 | 61.0133 | 454.1 | 0.124 | 225.5 | 0.57 | 1.0133 | -304658 | -548028 | -104949 | -357030 | 52371 | 13214 | 39157 | 39157 | 2095 | 279.8 | 64.7 |
| 323 | 61.0133 | 454.1 | 1.95 | 225.5 | 0.57 | 1.0133 | -304658 | -548028 | -104949 | -357030 | 52371 | 13214 | 39157 | 39157 | 2095 | 279.8 | 64.7 |
| 323 | 61.0133 | 454.1 | 15.6 | 225.5 | 0.57 | 1.0133 | -304658 | -548028 | -104949 | -357030 | 52371 | 13214 | 39157 | 39157 | 2095 | 279.8 | 64.7 |
| 323 | 61.0133 | 454.1 | 452 | 225.5 | 0.57 | 1.0133 | -304658 | -548028 | -104949 | -357030 | 52371 | 13214 | 39157 | 39157 | 2095 | 279.8 | 64.7 |
| 353 | 61.0133 | 367.1 | 0.124 | 225.5 | 0.42 | 1.0133 | -205919 | -548028 | -104949 | -291212 | 85292 | 16344 | 68948 | 68948 | 3412 | 371.3 | 82.6 |
| 353 | 61.0133 | 367.1 | 1.95 | 225.5 | 0.42 | 1.0133 | -205919 | -548028 | -104949 | -291212 | 85292 | 16344 | 68948 | 68948 | 3412 | 371.3 | 82.6 |
| 353 | 61.0133 | 367.1 | 15.6 | 225.5 | 0.42 | 1.0133 | -205919 | -548028 | -104949 | -291212 | 85292 | 16344 | 68948 | 68948 | 3412 | 371.3 | 82.6 |
| 353 | 61.0133 | 367.1 | 452 | 225.5 | 0.42 | 1.0133 | -205919 | -548028 | -104949 | -291212 | 85292 | 16344 | 68948 | 68948 | 3412 | 371.3 | 82.6 |

**Table 4.        Maurer experiments – expansion energy and initial velocity**

Cloud speed versus time – verification of INEX numerical against INEX analytical predictions; validation against experimental data

Figure 13 includes results of experimental data of the cloud expansion speed U (m/s) versus the dimensionless time $t/L_G$, obtained from the paper by Maurer. Likewise, Figure 10 plots U versus $t/L_G$ and includes the following results:

- Experimental data given by the markers. The INEX model starts from time t=0 after the initial ATEX isentropic expansion to atmospheric pressure, and (by comparing experimental radii with initial INEX radius) this is approximately 0.04s after the start of the release. Therefore, we have shown in the plot experimental data both with and without a time shift of 0.04s.
- Numerical predictions from the old INEX model
- Numerical predictions from the new INEX model, corresponding to the value $f_{kinetic}=0.04$ (recommended by Pattison)

The following is concluded from Figure 10:

- Predictions from both the old and new INEX models lie within the range of experimental data.
- The plots of U versus scaled time, is very similar for all the different type of releases.
- The recommended value $f_{kinetic}=0.04$ results in good agreement for the new INEX predictions. A further reduction of this value would further improve the performance for the new model. It was also reconfirmed that for $R>>r_o$ the numerical INEX predictions for U are indeed proportional to $f_{kin}^{1/8}$.
- The value of K does not affect the results significantly. Only for relative very large values of K (e.g. K=10) is there a slight noticeable decay of radial momentum during the INEX phase. Thus Figure 10a,d show virtual identical results between the $U_D=0$ and $U_D>0$ new INEX formulations.
- The value of $K_D$ is not relevant, since immediate rainout applies only during the INEX phase (ground-level release)

For the case of released mass M=452kg and initial temperature of 323K, Figure 10d also includes results from the analytical equation according to Equation ( 60 )/( 58 ), which is confirmed to very closely match the numerical INEX solution for all times.  Thus this verifies that the numerical INEX model correctly solves the INEX differential equations.
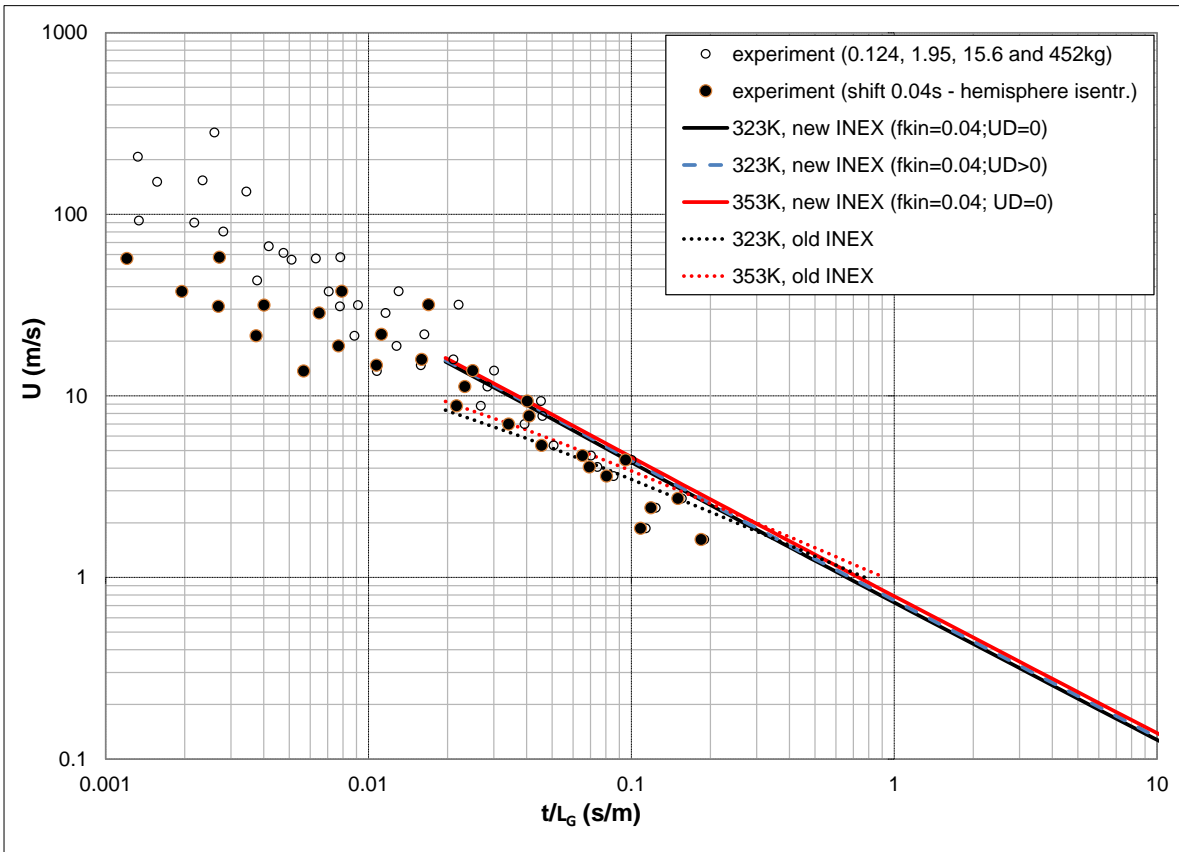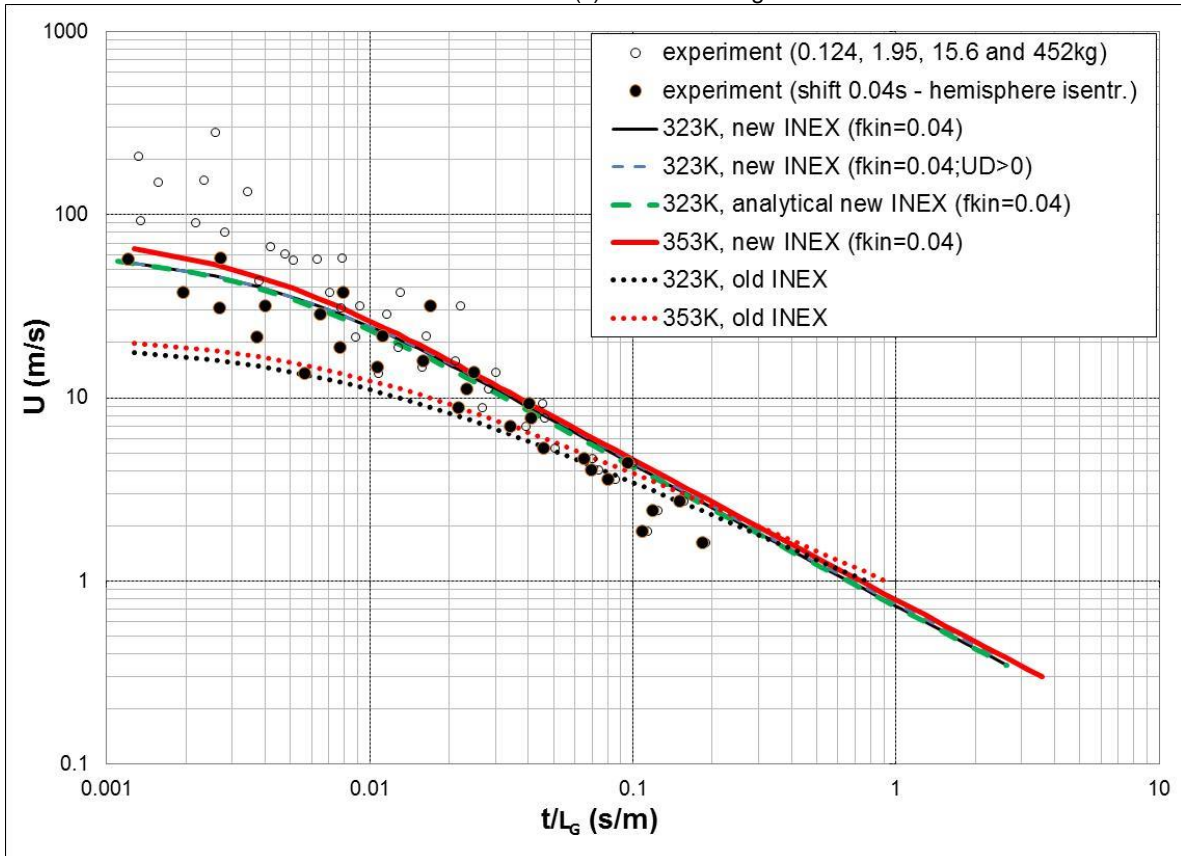
(a)  Mass 0.124 kg
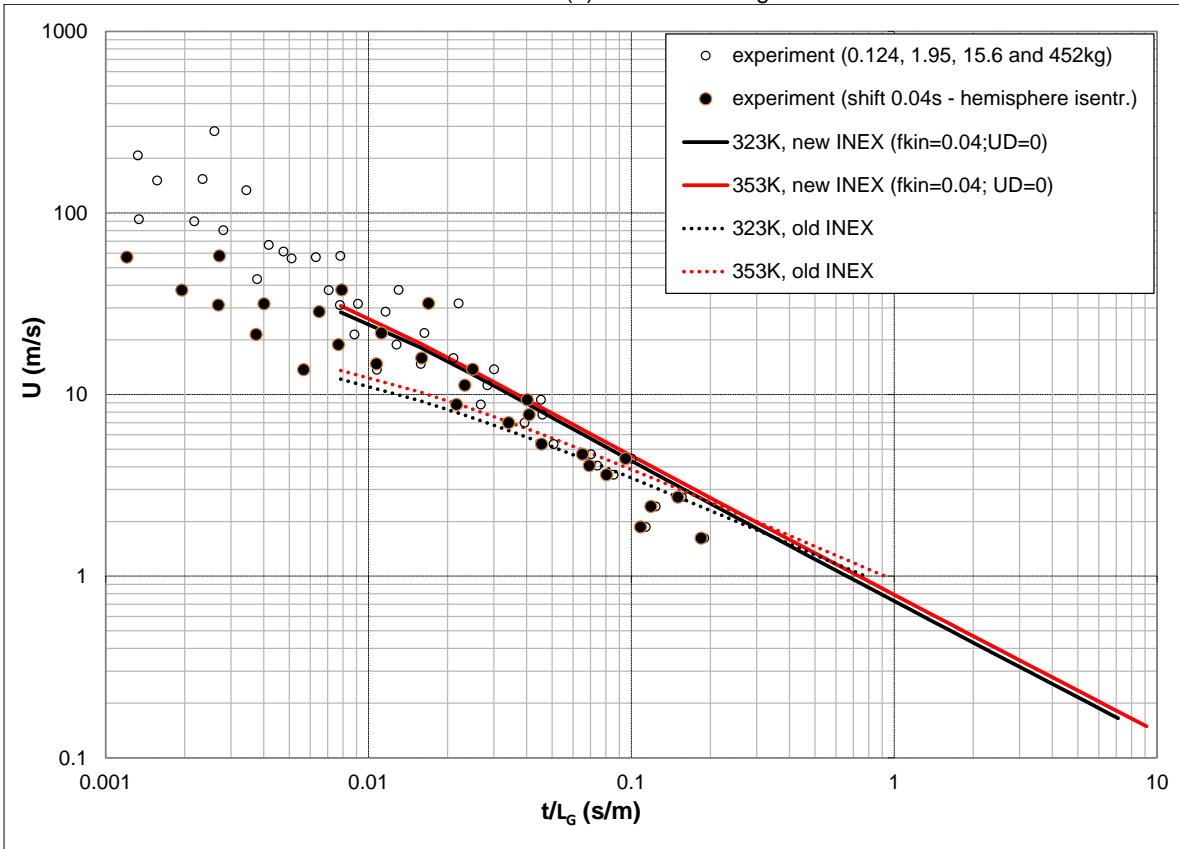


(b)  Mass 1.95 kg
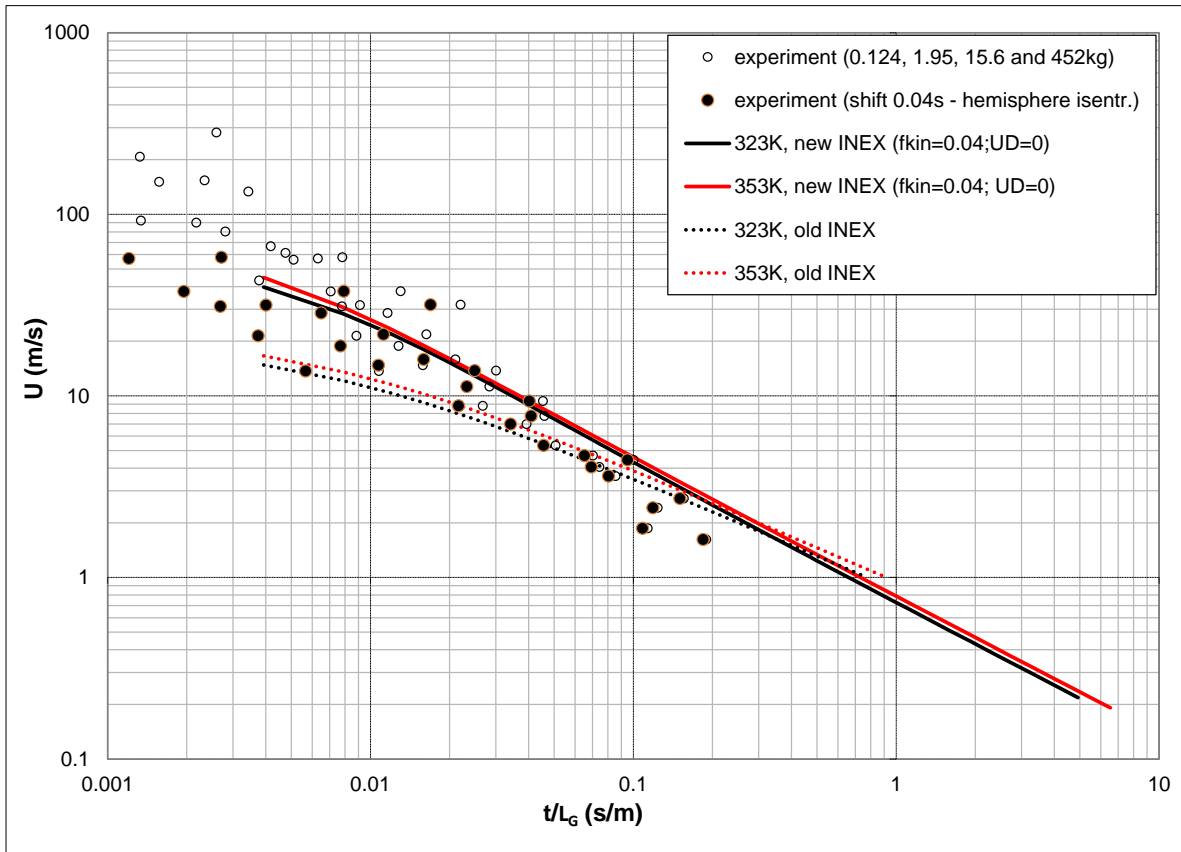
(c)  Mass 15.6 kg



(d)  Mass 452 kg

**Figure 10.**     **Maurer experiments - INEX validation of cloud speed versus time**
The figure plots cloud expansion speed U versus dimensionless time $t/L_g$.

Cloud radius versus time –validation against experimental data (M = 452kg, 323K or 353K)

Figure 11 includes results of validation of the new INEX model against experimental data (both before and after time shifting, with time shift of 0.04s as above) of cloud radius versus time for the case of M = 452kg. Figure 11a includes experimental data up to the ignition time of 0.5s (323K or 353K), and it indicates a linear logarithmic fit to the cloud radius versus time. Figure 11b compares results of model predictions by the new INEX model ($f_{kin}$=0.04) and old INEX model against the experimental data. It is seen that using $f_{kin}$=0.04 the new model slightly over-predicts the cloud radius, while the old model slightly under-predicts the cloud radius. Note that this comparison was also carried out by Coldrick[xiii] using the ACE instantaneous model, where the over-prediction by ACE was larger compared to the new INEX model.
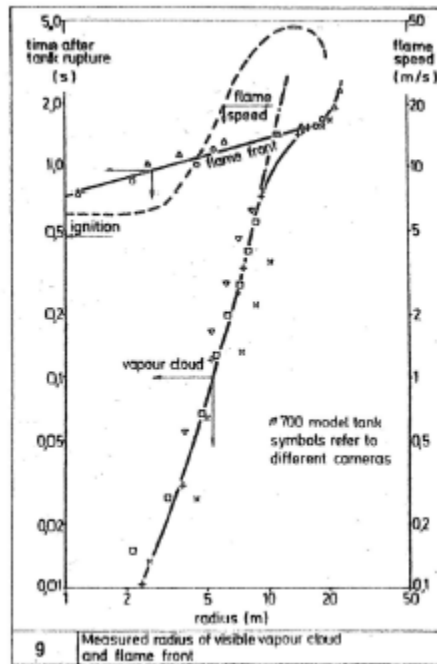


(a) Experimental data for cloud radius based on visible cloud (Figure 9 in Maurer et al.[xi])
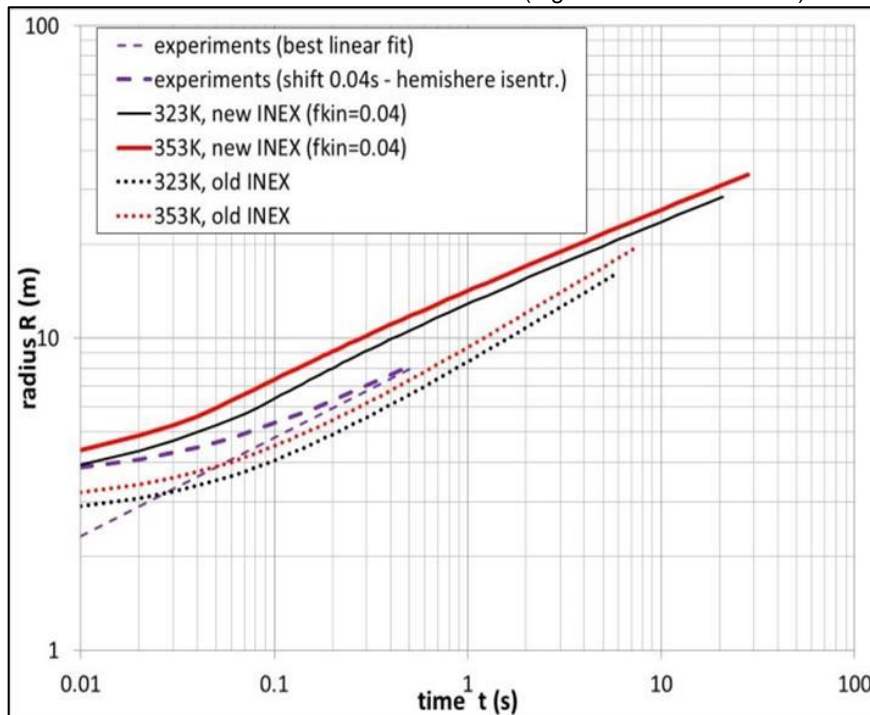


(b) Validation of new INEX model against experimental data

**Figure 11.        Maurer experiments (M=452kg) - INEX validation of cloud radius versus time**

Old UDM model[28]

---

[28] DOC. Description of old UDM model retained for now. Consider to remove at a later stage.

The $R_z$ radius was plotted against $t/L_G$ and checked against the 3/8 power law adopted by the UDM. In fact, the strict square root law is verified in the output during the pressurised expansion phase, except for very small time (where a displacement in the zero of time is used to allow for a finite initial radius).

We can write the behaviour (after the very short initial time) with a proportionality constant K as

$$R/L_G = K.(t/L_G)^{3/8}$$

or in a somewhat more dimensionally meaningful way as

$$R/L_G = (Ut/L_G)^{3/8}$$

where $U = K^{8/3}$ is a constant velocity which we extract from the UDM results. While this law holds, the expansion velocity is

$$W = dR_z/dt = 3/8\ K\ (t/L_G)^{-5/8} = 3/8\ U\ (Ut/L_G)^{-5/8}$$

Figure 12 depicts the graphs of $R/L_G$ against $(t/L_G)^{3/8}$ for the 8 runs performed.

The 3/8 power law gives $U=13.4$ m/s ( or $K=2.65$ $(m/s)^{3/8}$ ) for all the runs at 323K and $U=15.6$ m/s ( or $K=2.80$ $(m/s)^{3/8}$ ) for all the runs at 353K.

Thus a preliminary conclusion is that the results scale with size using the parameter $L_G$ in exactly the way Maurer et al suggest of their data. The UDM results do indicate a dependence on release temperature but this is very small in the temperature band quoted by Maurer et al.

We can now compare W as a function of $t/L_G$ as obtained from the UDM power law with the quoted results of Maurer et al. Figure 13 includes the results (on the graph of Maurer et al scanned from a less than perfect copy):

- The UDM cloud (shown in the red line of shallower slope) lies close to the data. The trend doesn't look entirely convincing though: the UDM cloud starts at early time by spreading more slowly than the experiment measures, but its spreading rate decreases more slowly than the data.
- The blue line of steeper slope is drawn through the data to guide the eye and has a power law behaviour $W \sim (t/L_G)^{-1}$ which, perhaps interestingly, would imply $R \sim \ln(t/L_G)$.

Thus the following conclusions can be drawn:

- The old UDM results scale with size in the way indicated by the data of Maurer et al.

- The old UDM results agree in magnitude with the spreading rate observed by Maurer et al. (NB we are identifying the visible radius in the experiments with the radius $R_z=R_y$ in the model – but the model cloud is sharp-edged at this stage and so other radius parameters are not really an option.)

- The trend in the old UDM data looks wrong, leaving doubts about the physical correctness of the model.
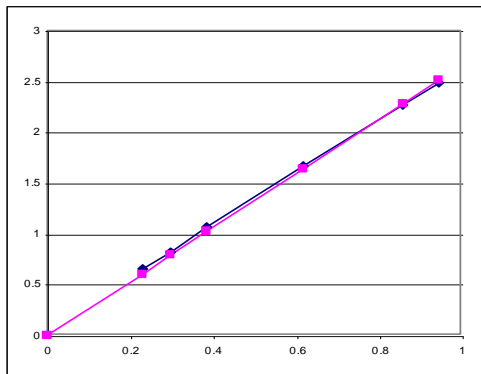
(a) 0.124kg at 323K
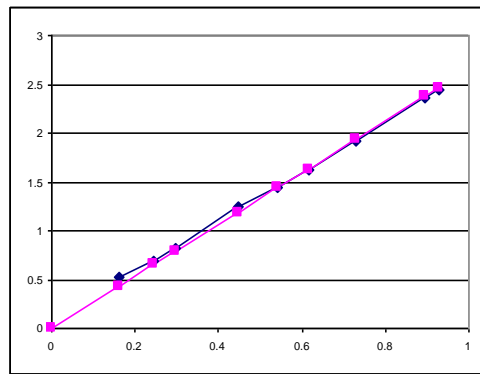
(b) 1.95kg at 323K
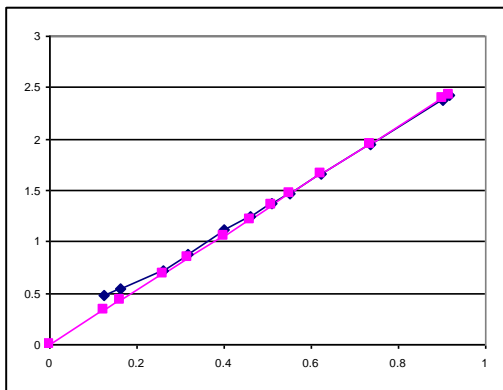
(c) 15.6 kg at 323K
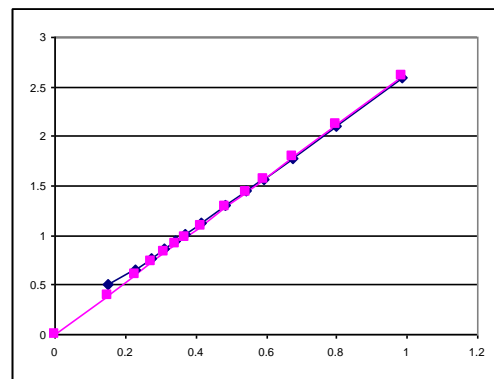
(d) 452kg at 323K
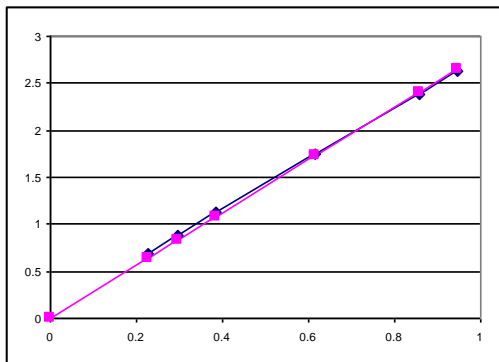
.124kg at 353K
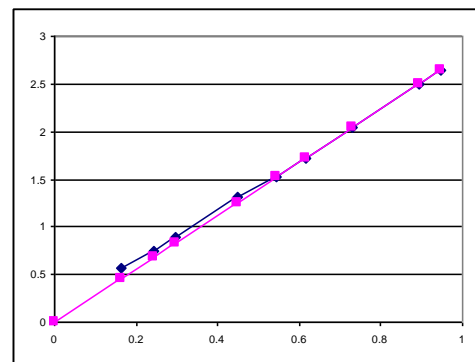
1.95kg at 353K
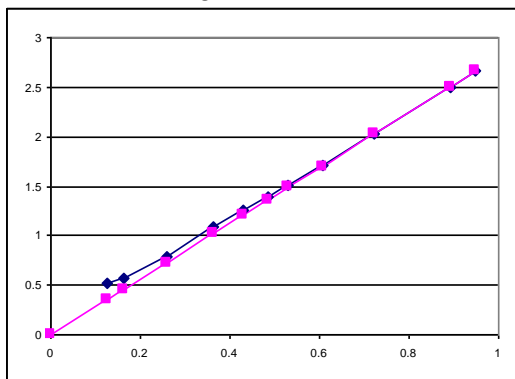
(e) 15.6 kg at 353K
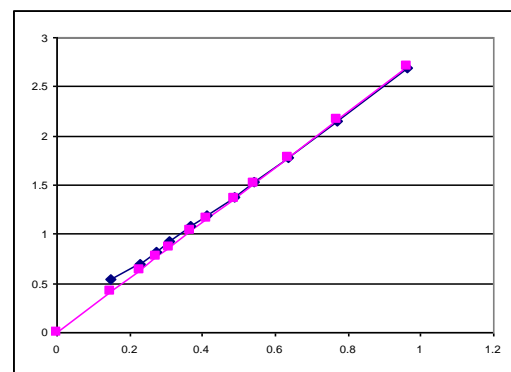
(f) 452kg at 353K

**Figure 12.** **Maurer experiments - Old INEX verification of cloud radius versus time**
The graphs plot scaled cloud radius $R/L_G$ versus scaled time $(t/L_G)^{3/8}$. The graphs verify UDM results (blue curve) against the 3/8 power law (pink curve).

**Figure 13.**     **Maurer experiments - Old INEX validation of cloud expansion speed versus time[29]**
The graphs plot the cloud expansion speed W = dR/dt (m/s) versus scaled time $t/L_G$ (s/m). The graph validates UDM results (pink line) against experimental data (approximated by blue trend line).

---

[29] DOC. Ideally to obtain a better copy of this figure from the original paper

## 6.2 Elevated releases

### 6.2.1 Experiments by Pettitt (flashing Freon 11 liquid)

<u>Description of experiments</u>
PhD studies were carried out at South Bank University (London) involving experimental work for rupture of spherical flasks containing superheated refrigerant liquid (Freon). Initial work was carried out by Bettis (1987)[xiv,xv] and Hardy (1990)[xvi] using Freon-11. They used a spherical vessel of $3.2 \times 10^{-3}$ m$^3$ held together as two hemispheres under pressure. The vessel fill volume and internal pressure were varied. Catastrophic failure was simulated by pulling the hemispheres apart resulting in an almost planar radial jet, perpendicular to the direction of the movement of the vessel halves. Hardy[xvi] also carried out experiments using a smaller vessel (volume $0.4 \times 10^{-3}$ m$^3$) and using Freon-114 instead of Freon-11.

Subsequent work was carried out by Pettitt (1990)[xvii] using complete catastrophic failure. Two methods of vessel failure were employed, namely by mechanical impact (smaller fragments) and explosive dissemination (larger energy input, isentropic expansion). The flask fill volume, internal pressure and release substance (Freon-11, Freon 114 and Freon-113 – different boiling points and therefore superheat) were varied. A copper vapour laser photographic system was employed to measure the droplet sizes. The following main conclusions were drawn:

- The aerosol cloud increases in size as a 'sphere', with cloud size increasing with initial mass and initial pressure.
- The expansion speed reaches its maximum value instantaneously and subsequently rapidly reduces as the cloud expands. By increasing the internal pressure in a $10^{-3}$ m$^3$ vessel containing $0.5 \times 10^{-3}$ m$^3$ of Freon-11 from 206kPa to 410kPa, the exit speed of the aerosol cloud increased from 26 m/s to 66 m/s. The vessel fill level was found not to have a significant effect on the expansion speed.
- Droplet sizes follow a log-normal distribution, and a relationship for droplet size was established as function of initial internal pressure and liquid surface tension [droplet size increasing with lower pressures (superheats)]
- Droplet speeds were shown to be independent of droplet size immediately following the release and dependent on the droplet size in the later stages of the release (almost increasing linearly with droplet size).
- Droplets are initially propelled radially in straight trajectories in all directions away from the vessel. Turbulent effects from air entrainment become soon apparent causing the droplets to swirl. The smaller droplets are affected more than the larger ones, because they have a large surface area to mass ratio.
- As the internal pressure is increased, the amount of residual liquid rained out below the vessel decreases, until all the liquid is entrained in the aerosol cloud. For a 50% fill-level of Freon-11 in a $10^{-3}$ m$^3$ vessel, the point at which all the liquid was entrained into the aerosol cloud corresponded to a superheat of about 45C, when the initial flash fraction was about 20%. For the laboratory work, the fill level was varied at a high pressure so that no residual liquid was produced.
- For non-full spherical glass vessels it was observed that following mechanical impact initial vessel failure was from the part of the vessels surrounding the vapour phase. This resulted at higher initial pressure in a larger proportion of the release being directed upwards and the cloud moved at higher speeds vertically than horizontally outwards.

An overview of the above PhD work (including key results) is given by Nolan et al. (1991)[xviii].

<u>DISC Verification and validation for post-expansion velocity (50% fill level)</u>
Table 5 includes data for experiments by Pettitt for saturated Freon-11[30] liquid spherical releases from a $10^{-3}$ m$^3$ vessel (50% fill) for 9 different internal pressures $P_o$. The left part of the table is taken directly from Table 1 in a paper by Melhem et al[xix] , while the right part includes added DISC predictions.

According to Nolan's paper, the values of the pressure $P_o$ in Table 5 appear to correspond with gauge pressures. However Melhem[xix] appear to have accidentally assumed that they are absolute instead of gauge pressures, and therefore accordingly also adopts a too low value for the saturated temperature $T_o$. Therefore the theoretical value $u_{theory}$ reported by him are higher, and they were confirmed to be consistent with DISC 6.54 predictions [using incorrect absolute values for $P_o$ and $T_o$; labelled by $u_{f,N}$ in table below]. Other date reported by Melhem in the table below are: $\rho_{v,o}$, $\rho_{l,o}$ stagnation vapour and liquid densities; $Y_{S,o}$, $Y_{S,1}$ are the vapour mole fraction in the surrounding medium before and after expansion to $P_a$??

Table 5 shows that the DISC 6.54 (=DISC 7.1) post-expansion speed [indicated by $u_{f,N}$ in the table] associated with the correct 'gauge' value of $P_o$ and corresponding saturated temperature $T_{oN}$ was found to be close to the theoretical value $u_{Nolan}$ reported by Nolan et al[xviii].

It was found by Melhem that using his predictions only an average fraction of 62% was converted into kinetic energy. Using the 'corrected' DISC 6.54 predictions (based on saturated liquid) is found that an average fraction of 36% was converted into kinetic energy and therefore the UDM value of $U_f$ leads to an average of 73% overestimate of the velocity term; see Table 5. The boiling temperature of Freon-11 equals 297K, thus superheats in Table 5 (based on correct saturated liquid temperature) vary between 27°C and 67.1°C (superheated).

---

[30]Freon-11 is labelled as trichlorofluoromethane in DIPPR

| $T_0$ (K) | $P_0$ (kPa) | $\rho_{v,0}$ (kg/m³) | $\rho_{l,0}$ (kg/m³) | $Y_{S,0}$ | $u_{actual}$ (m/s) | $A_E$ (J/kg) | $Y_{S,1}$ | $u_{theory}$ (m/s) | DISC 6.54 predictions | | | |
|---|---|---|---|---|---|---|---|---|---|---|---|---|
| | | | | | | | | | $u_{fM}$ (m/s) | $T_{oN}$ (K) | $u_{fN}$ (m/s) | $u_{Nolan}$ (m/s) |
| 306.0 | 140 | 7.87 | 1458 | 0.0054 | 11 | 132 | 0.050 | 16.2 | 15.7 | 324.0 | 45.2 | 42.0 |
| 312.5 | 172 | 9.59 | 1442 | 0.0066 | 19 | 378 | 0.082 | 27.4 | 26.5 | 328.3 | 52.5 | 50.6 |
| 318.3 | 206 | 11.35 | 1428 | 0.0078 | 26 | 703 | 0.110 | 37.4 | 36.4 | 332.6 | 59.5 | 60.6 |
| 326.7 | 264 | 14.32 | 1407 | 0.0100 | 44 | 1347 | 0.151 | 51.9 | 50.5 | 339.0 | 70.1 | 71.8 |
| 330.8 | 296 | 15.97 | 1396 | 0.0113 | 51 | 1734 | 0.171 | 58.9 | 57.3 | 342.3 | 75.5 | 78.9 |
| 336.4 | 345 | 18.47 | 1381 | 0.0131 | 60 | 2343 | 0.197 | 68.0 | 66.6 | 346.9 | 83.0 | 86.7 |
| 343.0 | 410 | 21.80 | 1364 | 0.0157 | 66 | 3175 | 0.230 | 79.0 | 77.5 | 352.4 | 92.1 | 96.7 |
| 348.5 | 471 | 24.90 | 1349 | 0.0180 | 72 | 3961 | 0.255 | 89.0 | 85.6 | 357.2 | 99.9 | 104.3 |
| 356.5 | 570 | 30.04 | 1326 | 0.0220 | 78 | 5260 | 0.293 | 102.5 | 98.7 | 364.1 | 111.1 | 111.2 |

**Table 5. Pettitt experiments - expansion velocities (from Melhem and old DISC)**
Data correspond to 9 experiments by Nolan et al. This left part of this table is taken directly from Table 1 in the paper by Melhem et al, while the right part includes added DISC predictions (old expansion energy).

Table 6 includes results of evaluation of expansion energy and initial expansion velocity:

- Yellow cells indicate spreadsheet input data: flask volume, fill level, stagnation stagnation pressure $P_{st}$
- Orange cells indicate results from Phast property calculations: stagnation liquid density $\rho(P_{st},T_{st})$, specific stagnation liquid enthalpy $h(P_{st},T_{st})$, specific vapour and liquid enthalpy at final pressure $P_a$ and final temperature $T_f$
- Blue cells indicate results from the Phast discharge model DISC (based on Phast property calculations): post-expansion temperature $T_f$ and liquid fraction $\eta_{Lf}$, old value of expansion energy $E_{exp}^{old} = h(P_{st},T_{st}) - h(P_a,T_f; \eta_{Lf}) - (P_{st}-P_a)/\rho(P_{st},T_{st})$
- White cells indicate results from the Excel spreadsheet: value of old expansion energy, values of new expansion energy $E_{exp}^{new} = f_{kinetic} [h(P_{st},T_{st}) - h(P_a,T_f)]$, old and new values of initial INEX velocity $u_o = U(t=0) = (2 E_{exp})^{0.5}$. These results were verified to exactly match those values obtained from the numerical DISC and UDM INEX codes. According to the theory for the old INEX model, at the initial time t=0, $U(t=0) = (3/8)*R(t=0)/t_o$ which is significantly smaller than the value $(2E_{exp}^{old})^{0.5}$ reported by DISC! On the other hand, for the new INEX model, $U(t=0) = (2E_{exp}^{new})^{0.5}$. This results in initial smaller rather than larger velocities for the old INEX model versus the new INEX model!
- The table also includes the observed exit speed. This speed was not directly measured but determined by Pettitt by extrapolation back on the graphs of aerosol cloud front speed versus distance from the vessel. It is seen that this exit speed is smaller than the old INEX speed and larger than the new INEX speed (based on $f_{kinetic}$=0.05). For the experimental exit speed, it is seen that in fact $f_{kinetic}$ appears to increase with pressure from 0.05 at 11m/s till around 0.45 at larger pressures. Pettitt points out that the observed exit speed by earlier Bettis results were about 7m/s at 310kPag, which is significantly lower than the speed of 51m/s observed by Pettitt at 296kPag. He also points out that the speed depended on the fill level, with a maximum initial speed at 50 percent fill level. The DISC old velocity over-predicts the experimental exit speed with about 30 m/s. Note that Pettitt adopts the old DISC formula for expansion energy to derive the theoretical velocity, while Schmidli adopts the new formula.

| | | | | | | |
|---|---|---|---|---|---|---|
| volume flask | 0.001 | m3 | | Yellow cell - input data (user) | | |
| fill level | 0.5 | fraction | | Orange cell - from PROP spreadsheet | | |
| f_kinetic | 0.04 | fraction | | Blue cell - from DISC spreadsheet | | |

| Stagnation data | | | | Final Data | | Enthalpies | | | | | Old UDM - expansion energy | | | New exp.en. | Initial velocity | | Experiment | |
|---|---|---|---|---|---|---|---|---|---|---|---|---|---|---|---|---|---|---|
| $T_{st}$ (K) = Tsat | $P_{st}$ (barg) | $\rho_{st}$ (kg/m³; liquid) | Mass M (kg) [ignore vapour] | $T_f$ (K) | final liq.fr. | $h(P_{st},T_{st})$ (J/kg; liquid) | liquid $h(P_a,T_f)$ (J/kg) | vapour $h(P_a,T_f)$ (J/kg) | final $h_f$ at $P_a$, $T_f$,liq.fr (J/kg) | $h_{st}-h_f$ (J/kg) | (Pst-Pa)/ρst | Eexp UDM old | From DISC (UDM old) | fkin (hst-hf) | uo_old from DISC (m/s) | Uo_new from INEX (m/s) | exit speed (m/s) | fraction of enthalpy change (h_st-h_f) |
| 324.0 | 1.40 | 1414 | 0.707 | 296.8 | 0.874 | -161761 | -185951 | -2257 | -162882 | 1121 | 99.0 | 1022.33 | 1022.3 | 44.855 | 45.2 | 9.5 | 11 | 0.054 |
| 328.3 | 1.72 | 1402 | 0.701 | 296.8 | 0.855 | -157757 | -185951 | -2257 | -159256 | 1499 | 122.7 | 1376.38 | 1376.4 | 59.9616 | 52.5 | 11.0 | 19 | 0.120 |
| 332.6 | 2.06 | 1391 | 0.696 | 296.8 | 0.836 | -153843 | -185951 | -2257 | -155760 | 1916 | 148.1 | 1768.31 | 1768.3 | 76.6559 | 59.5 | 12.4 | 26 | 0.176 |
| 339.0 | 2.64 | 1374 | 0.687 | 296.8 | 0.807 | -147800 | -185951 | -2257 | -150341 | 2651 | 192.2 | 2458.79 | 2458.8 | 106.038 | 70.1 | 14.6 | 44 | 0.365 |
| 342.3 | 2.96 | 1365 | 0.682 | 296.8 | 0.792 | -144741 | -185951 | -2257 | -147804 | 3063 | 216.9 | 2846.31 | 2846.3 | 122.527 | 75.4 | 15.7 | 51 | 0.425 |
| 346.9 | 3.45 | 1352 | 0.676 | 296.8 | 0.772 | -140361 | -185951 | -2257 | -144059 | 3699 | 255.1 | 3443.77 | 3443.8 | 147.956 | 83.0 | 17.2 | 60 | 0.487 |
| 352.4 | 4.10 | 1337 | 0.668 | 296.8 | 0.747 | -135016 | -185951 | -2257 | -139561 | 4545 | 306.7 | 4238.12 | 4238.1 | 181.795 | 92.1 | 19.1 | 66 | 0.479 |
| 357.2 | 4.71 | 1323 | 0.661 | 296.8 | 0.727 | -130392 | -185951 | -2257 | -135729 | 5337 | 356.0 | 4981.11 | 4981.1 | 213.485 | 99.8 | 20.7 | 72 | 0.486 |
| 364.1 | 5.70 | 1303 | 0.651 | 296.8 | 0.696 | -123520 | -185951 | -2257 | -130133 | 6613 | 437.6 | 6175.74 | 6175.7 | 264.534 | 111.1 | 23.0 | 78 | 0.460 |

**Table 6.          Pettitt experiments (1 litre, 50% fill, Freon11) – expansion energy and initial velocity**

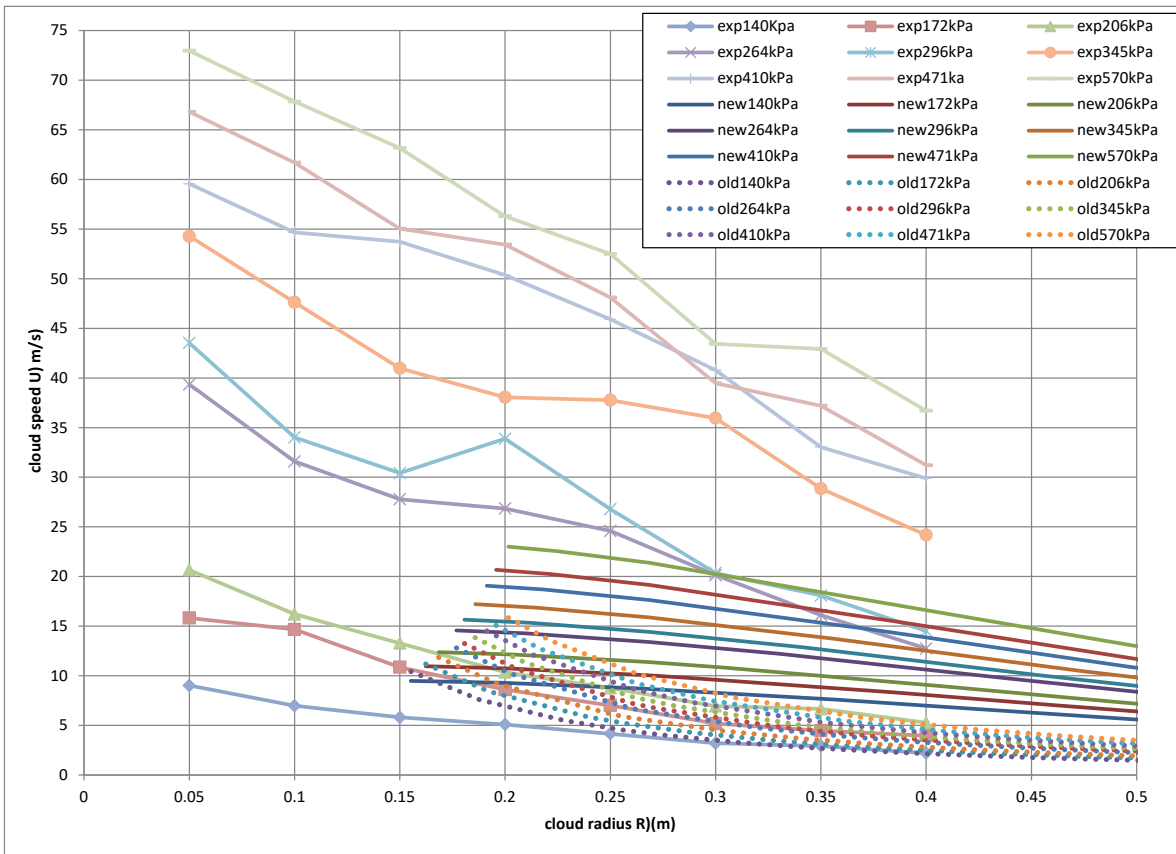INEX validation of expansion speed U (50% fill level)

Figure 14a plots observed mean aerosol cloud front speed versus distance from the vessel for each of the different stagnation pressures. Here it was not specified by Pettitt whether the 'distance from the vessel', refers to the distance s from the vessel wall or the distance R (cloud radius) from the centre of the vessel; note that s=R-0.062m. It is assumed that the plotted distance refers to the cloud radius R. Furthermore the initial value of the cloud radius R corresponds to the post-expansion volume = M / $\rho(T_f,P_a; \eta_{Lf})$, which will increase with the stagnation pressure.

Figure 14b includes old INEX predictions and predictions using the new INEX model ($U_D=0$ and $U_D>0$ produce very close results; $U_D=0$ plotted) presuming $f_{kin}=0.04$. The experimental cloud speeds are larger than those predicted by both the old and new INEX (except for the lower pressures) with the new INEX results considerably closer to the experimental data. More close agreement with the experimental data would be obtained by increasing $f_{kin}$ such that the initial radius $R(t=0)$ equals the experimental observed speed.
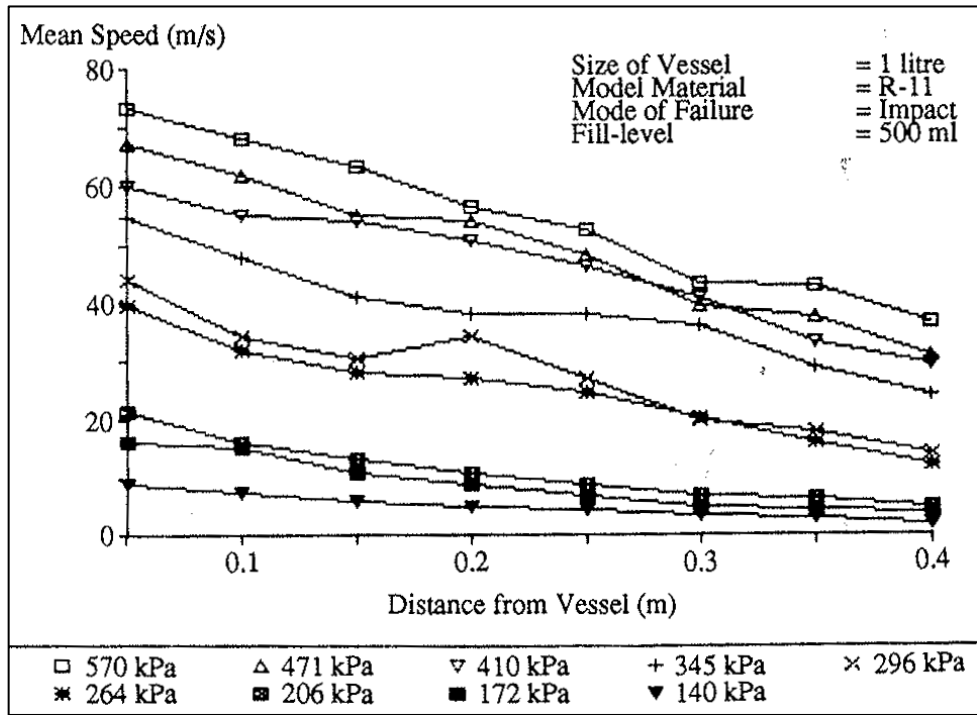
(a) Measured cloud speed (Figure taken from Figure 6.4 in Phd by Pettitt[xvii])



(b) experimental data, new INEX (fkin=0.04) and old INEX predictions

**Figure 14.** **Pettitt experiments (Freon 11, 50% fill) - INEX cloud speed validation**

INEX validation of cloud radius R and expansion speed U (100% fill level)

The case is considered of a 1 liter vessel with a 100% fill level and a stagnation pressure of 4.1 barg (410kPa).

Figure 15a plots the observed aerosol cloud front speed (minimum, mean and maximum values) versus distance from the vessel (figure taken from Figure V.16 in Phd of Pettitt). Again it is presumed that this distance equals the radius R of the vessel.

Figure 15b plots the cloud speed U versus the cloud radius R. The initial INEX value of the cloud radius R (after isentropic expansion to atmospheric pressure) corresponds to the post-expansion volume = $M / \rho(T_f, P_a; \eta_{Lf})$, where M is the vessel mass, $\rho$ the material density, $T_f$ the post-expansion temperature, $P_a$ the ambient pressure, and $\eta_{Lf}$ the post-expansion liquid fraction.

Figure 15b includes old INEX predictions and predictions using the new INEX model presuming either $f_{kin}$=0.04 or $f_{kin}$=0.15, where the latter value results in the initial INEX speed approximately to be equal of the observed mean exit speed at the initial post-expansion radius. It is seen that the old INEX model significantly under-predicts, while the new INEX model ($f_{kin}$=0.04) slightly under-predicts. It is seen than $f_{kin}$=0.15 results in improved agreement against the experimental data.
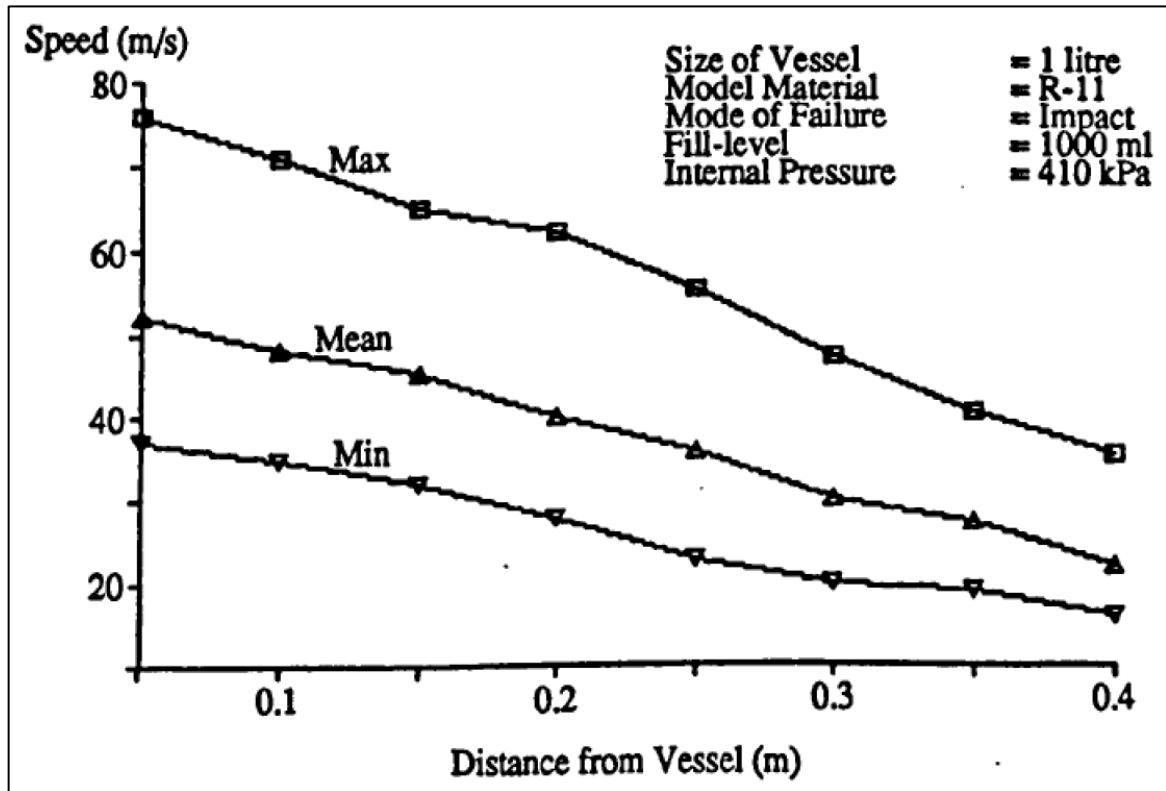
(a) Observed aerosol cloud speed versus distance from vessel wall (min., mean and max.)
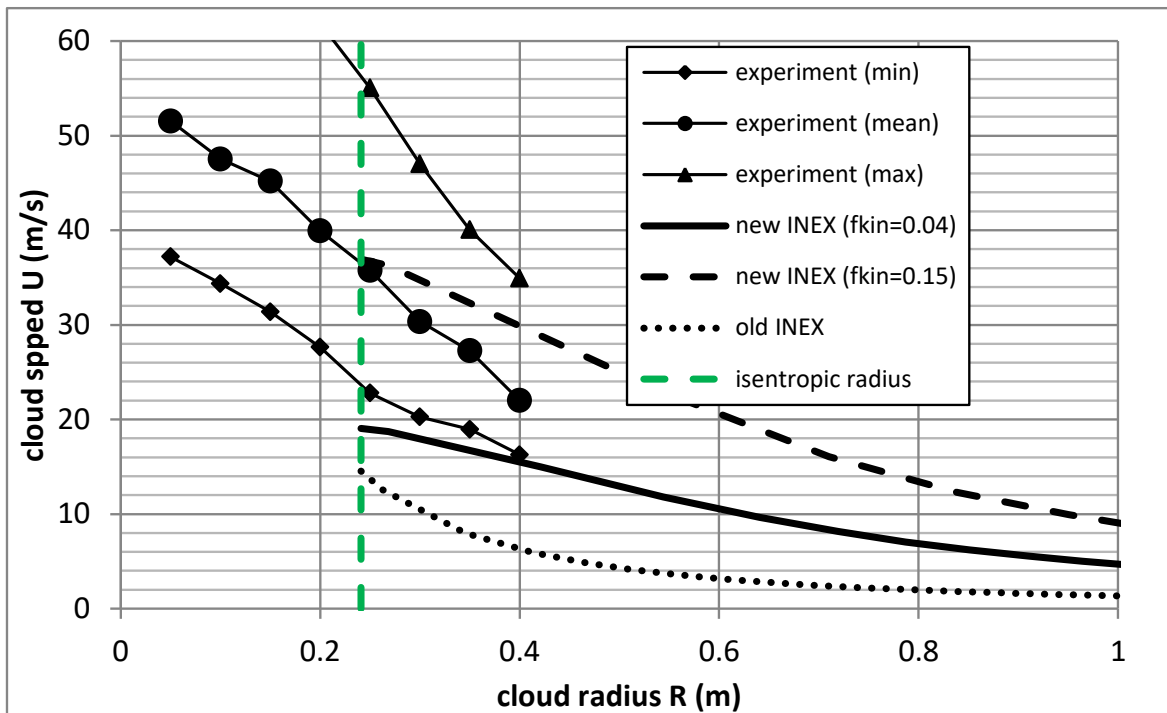


(b) INEX speed U versus cloud radius R [old model; new model ($f_{kin}$=0.05, and $f_{fin}$=0.30)]

**Figure 15.** Pettitt experiment (Freon 11, 100% fill, 410kPa) - INEX cloud speed validation[31]

---

[31] DOC. For clarity digitize data from Figure 15a and include these data in Figure 15b

DISC validation for post-expansion velocity and SMD

For internal pressure of 4.60 barg, DISC6.54 predicts a SMD of 210 μm using the CCPS droplet-size correlation. Figure 16 (taken from Nolan's paper) shows a measured SMD of 225 μm closest to the vessel and a subsequent decay of droplet size with distance from the vessel. Thus for this pressure Phast appears to over predict the initial cloud speed with about 39% and to under-predict the SMD with about 7%. Thus the SMD is in very close agreement.
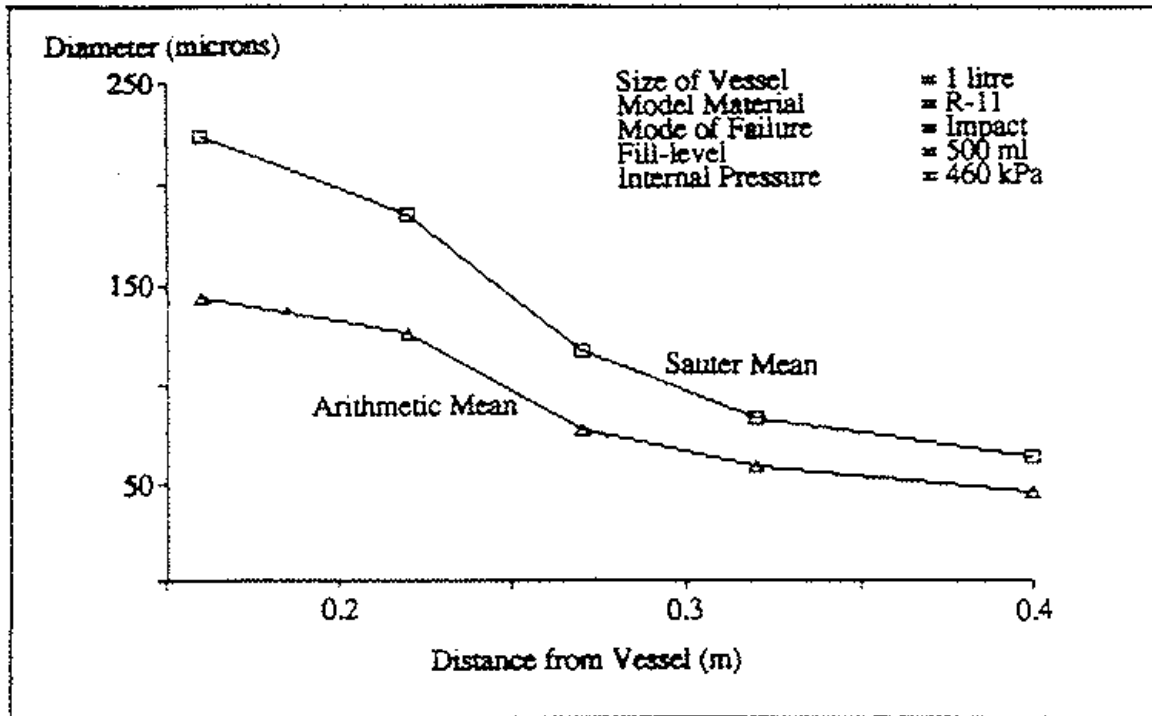


**Figure 16.** **Pettitt experiment (Freon 11, 50% fill, 460kPa) - Measured SMD versus distance**
[Figure taken from Figure 13 in the paper by Nolan et al[xviii]]

Nolan's paper includes figures of droplet size versus distance, fill rate and pressure, and also droplet speed versus time (for different downwind distances, fill levels and pressures). Finally it plots droplet speed versus droplet diameter illustrating a linear increase of droplet speed with droplet diameter. [32]

---

[32] FUTURE. These figures could be used for further droplet size validation.

## 6.2.2 Experiments by Schmidli (Freon 12, propane or butane flashing liquid with rainout)

Description of experiments (experimental setup I)
In the above experiments by South Bank University all the liquid appeared to be caught in the cloud and vaporised. However, at lower flash fractions and for liquids with different thermodynamic properties (such as higher surface tension) some portions of the liquid may be expected to fall to the ground and form a pool.

As a result, Schmidli et al.[xx] (Institute of Energy Technology, Switzerland) carried out experiments in early 1989 on vapour/aerosol and pool formation on rupture of spherical glass vessels containing superheated Freon 114 liquid [also known as 1,2-dichlorotetrafluoroethane; CASID 76142]. Parameters varied in the experiments were flask size (50 or 100 ml), release height (ground or 5 diameters elevation), flask filling degree (full or half full) and superheat (6.5C, 14.5C or 21.5C)[33]. It was confirmed that spherical clouds were obtained for elevated releases and hemispherical clouds for ground-level releases.



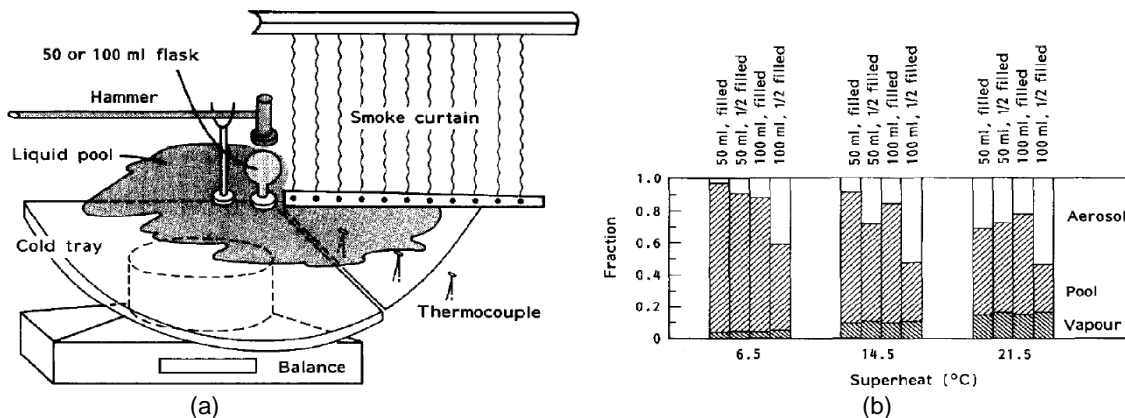(a)                                    (b)

**Figure 17.    Schmidli experiments (setup I - R-114)**
[Figure taken from Figures 1 and 3 in paper by Schmidli et al[xx]] Figure (a) is a schematic figure of the experimental setup; figure (b) includes post-exansion vapour fraction based on isentropic expansion, the measured rain-out liquid fraction in the pool and the remaining evaporating liquid in the aerosol.

The vapour-cloud formed, the release expansion velocities and the droplet sizes were measured with high-speed videos. The vapour cloud front was made visible using a smoke curtain. Pool formation was measured by collecting the liquid on a cold tray (to slow down evaporation and allow good measurement of amount of rainout). See Figure 17 for a schematic of the experimental apparatus.

The following was observed/concluded by Schmidli et al.:

1. Droplets appear to form when the volume fraction is about 50%. Sizes of the largest droplets are predicted by a Weber number $u_d^2 d_d \rho / \sigma \approx 20$, with observed values in the range 15-30. Measured droplet sizes were in the range 2800-3500 μm.
2. Initial velocities were similar for all droplet sizes. Like for the experiments by Nolan et al.[xviii], the expansion droplet speed measured (2.8-3.6 m/s) was found to be lower than predicted by isentropic expansion (Old TNO Yellow Book model 11.9-42.7m/s). It was suggested that the expansion speed is probably lowered due to conduction/convection processes during bubble growth. If it is assumed that flashing and isentropic expansion occurs to 30% void fraction predicted values were 4.4-8.3m/s (closer but still too high).
3. From the videos, the droplets appear to fly ahead of the expanding vapour. The mass fraction raining out was observed to reduce with superheat; see Figure 17b. It is not fully clear that Figure 17 (b) corresponds to the ground-level or elevated releases. For the ground-level release the pool was found to form extremely quickly, while for elevated releases the pool the pool had an annular shape (since droplets impinging at the centre were of lower concentration)

Description of experiments (experimental setup II and III)
Following on from the above experiments for Freon-114, experiments were carried out for propane, butane and Freon-12. Results of these are reported in the PhD thesis by Schmidli[xxi]. These additional experiments involved two different experimental setups II and III:

- Experiment setup II involved indoor experiments for R114 and R12 releases carried out at ENEA, Cassacia, Italy (summer 1989). These experiments included high speed video measurement of the cloud front velocity.

---

[33] UPDATE. Table 5 in Schmidli et al. (1990)[xx] includes results of cloud radius versus time for the case of Freon 114, 27C superheat, elevated at 5D, 100% fill, 50ml or 100ml flask. To consider to add these to INEX validation dataset?

- Experimental setup III involved outdoor experiments for propane and butane releases at the Paul Scherren Institute, Würenlingen, Switzerland. Here the substrate was chosen such as to minimise evaporation.

Schmidli's PhD thesis reports most extensive data for elevated releases and 100% fill of the data; see Table 7 for an overview of key input and key results for these experiments. As shown in the table, the PhD thesis reports results of cloud radius R versus time t for a number of limited experiments only. These tests have been selected for INEX simulation, i.e. the 1 liter R-12 and butane tests, and the 2 liter propane tests.

| Fluid | temperature /SH (C) | elevation (m) | initial expansion speed (m/s) | | | % rainout | | | R(t) plot given? | | |
|---|---|---|---|---|---|---|---|---|---|---|---|
| | | | 100ml | 1 ltr | 2 ltr | 100ml | 1 ltr | 2 ltr | 100ml | 1 ltr | 2 ltr |
| R-114 | 30/26.6 | 5D | Small | small | | 52+8 | | | | | |
| | 40/36.6 | 5D | Small | small | | 50+3 | | | | | |
| | 50/46.6 | 5D | 12.7+3.9 | 11.7+4.2 | | 24+5 | | | | | |
| R-12 | 22/52.1 | 5D | 14.7+1.5 | 13.9+0.4 | | 24+4 | | | | x | |
| Propane | 5/47.4 | 1 | | 17.4+1.7 | 19.4+0.9 | | 26+6 | 30+9 | | | x |
| | 12/54.4 | 1 | | 31.0+1.6 | 26.0+3.0 | | 13+2 | 26+17 | | | |
| | 18/60.4 | 1 | | 38.0+4.5 | 41.3+1.5 | | 16+3 | 25+5 | | | x |
| Butane | 42/42.6 | 1 | | 21.6+3.4 | | | | | | x | |
| | 52/52.6 | 1 | | 33.0+2.6 | | | | | | x | |

**Table 7.        List of Schmidli experiments (setup II&III, elevated release, 100% fill)**

DISC verification and validation for post-expansion velocity
Table 8 includes results for the selected Schmidli experiments of initial velocities:

- Prediction of the new INEX initial velocity and new INEX flash fraction ($f_{kin}=1$, $0.5u_f^2=h_{st}-h_f$) were confirmed to be virtually identical with the values reported in the PhD by Schmidli (presuming isentropic expansion).
- Schmidli produced the following formula to fit the data for observed exit speed: $U(t=0) = \max [0, 0.28u_f – 14.8$ m/s], and the predictions of this formula have also been included in the table.
- Pattison[vii] states that a value of $f_{kin}=0.04$ (corresponding to a reduction of initial velocity with a factor of 5) produces the best fit with experimental data, and therefore this value has been selected for the INEX runs.

| material | flask size / location | | | Stagnation data | | | | Initial velocity | | Experiment | | Schmidli formula | |
|---|---|---|---|---|---|---|---|---|---|---|---|---|---|
| | volume flask (m3) | Flask diameter D (m) | Elevation (m) | T_st (K) = Tsat | P_st (abs.,Pa) | Mass M (kg) [ignore vapour] | final liq.fr. | uo_old from DISC (m/s) | Uo_new from INEX fkin=0.04 (m/s) | exit speed (m/s) | fraction of enthalpy change (h_st-h_f) | formula schmidli speed u=u(fm) | fkin for schmidli formula |
| R12 | 0.001 | 0.124 | 0.62 | 295.15 | 6.00E+05 | 1.320 | 0.740 | 95.7 | 19.9 | 14.4 | 0.021 | 13.1 | 0.017 |
| Propane | 0.002 | 0.156 | 1.00 | 278.15 | 5.52E+05 | 1.043 | 0.762 | 143.7 | 29.9 | 18.4 | 0.015 | 27.1 | 0.033 |
| Propane | 0.002 | 0.156 | 1.00 | 285.15 | 6.74E+05 | 1.022 | 0.727 | 165.1 | 34.3 | 28.5 | 0.028 | 33.3 | 0.038 |
| Propane | 0.002 | 0.156 | 1.00 | 291.15 | 7.94E+05 | 1.004 | 0.697 | 183.4 | 38.2 | 39.6 | 0.043 | 38.6 | 0.041 |
| Butane | 0.001 | 0.124 | 1.00 | 315.15 | 4.01E+05 | 0.552 | 0.753 | 122.0 | 25.3 | 21.6 | 0.029 | 20.6 | 0.027 |
| Butane | 0.001 | 0.124 | 1.00 | 325.15 | 5.23E+05 | 0.539 | 0.696 | 150.7 | 31.2 | 33 | 0.045 | 28.8 | 0.034 |
| | | | | | | | | | | Average: | 0.030124 | | 0.032 |

**Table 8.        Schmidli experiments – initial expansion velocity**

INEX validation of cloud radius
Table 9 includes the UDM input data corresponding to the above selected experiments (new INEX runs with $f_{kinetic} = 4\%$). Since no information is given of the ambient data in Schmidli's thesis, a surface roughness of 0.1m, a temperature of 20C, and very small wind speed is presumed (minimum UDM value, D0.1). These values are expected to be appropriate for indoor conditions (applicable for Freon 12). For the outdoor conditions (applicable for propane and butane), these assumptions are also expected not to affect the predictions of INEX cloud radius, INEX cloud speed and rainout at the earlier times. However, at later times (particularly during the post-INEX stage) dispersion results will be significantly affected by these assumptions.

| Description | Units | R12T22 | PROT5 | PROT12 | PROT18 | BUTT42 | BUTT52 | Notes |
|---|---|---|---|---|---|---|---|---|
| **RELEASE DATA** | | | | | | | | |
| Released material name (from material database) | | Freon12 | Propane | Propane | Propane | n-butane | n-butane | Materials from Setup II and III (excl. R-114) |
| State flag (1 - temperature, 6 = liquid fraction) | | 6 | | | | | | 2-phase at boiling point |
| Temperature of release component | K | 243.3779 | 231.08 | 231.08 | 231.08 | 272.6174 | 272.6174 | not used |
| Liquid mass fraction of release component | kg/kg | 0.73993 | 0.76214 | 0.72707 | 0.69689 | 0.753347 | 0.695858 | from DISC |
| Droplet diameter (SMD) | m | 1.86E-05 | 7.79E-06 | 5.91E-06 | 4.78E-06 | 1.05E-05 | 6.85E-06 | droplet size from DISC (affecs rainout but not INEX R,U) |
| release mass (instantaneous only) | kg | 1.319724 | 1.04266 | 1.02223 | 1.0041 | 0.552311 | 0.539299 | = (fill fraction)*(vessel volume)*(liquid st. density) |
| Expansion energy (instantaneous only; = f_kinetic*exp.energy) | (J/kg) | 198.0912 | 447.492 | 589.673 | 728.089 | 319.5295 | 485.6635 | New INEX (4% of expansion energy) |
| Release height | m | 0.62035 | 1 | 1 | 1 | 1 | 1 | at 5D for Freon 12 (= distance flask- centre to ground/tray) |
| | | | | | | | | |
| **AMBIENT DATA** | | | | | | | | |
| Pasquill stability class (1-A,2-A/B,3-B,4-B/C,5-C,6-C/D,7-D,8-E,9-F,10-G); 0 = use | - | | | | | | | |
| Monin-Obukhov length | | 7 | | | | | | Presumed D0.1 (no wind) |
| Wind speed at reference height | m/s | 0.1 | | | | | | Presumed D0.1 (no wind) |
| Reference height for windspeed | m | 10 | | | | | | |
| Temperature at reference height | K | 293.15 | | | | | | Presumed (will affect liquid evaporation) |
| Pressure at reference height | N/m2 | 101325 | | | | | | Presumed |
| Reference height for temperature and pressure | m | 0 | | | | | | |
| Atmospheric humidity (fraction) | - | 0.7 | | | | | | Presumed |
| | | | | | | | | |
| **SUBSTRATE DATA** | | | | | | | | |
| Surface roughness length | m | 0.1 | | | | | | Presumed |
| Dispersing surface type (1-land,2-water) | | 1 | | | | | | |
| Temperature of dispersing surface | K | 293.15 | | | | | | Presumed |
| | | | | | | | | |
| **POOL DATA** | | | | | | | | |
| Pool surface type (1-wet soil, 2-dry soil, 3 - concrete, 4 - insulated concrete, 5 - dee | | 3 | | | | | | Presumed |
| Temperature of pool surface | K | 293.15 | | | | | | Presumed |
| Bund diameter (<=0: no bund) | m | 0 | | | | | | |
| | | | | | | | | |
| **AVERAGING TIME** | | | | | | | | |
| Averaging time | s | 18.75 | | | | | | Not relevant, only affects passive dispersion |

**Table 9.        UDM input data for selected Schmidli experiments (elevated, 100% fill)**

Figure 18, Figure 19 and Figure 20 include results of cloud radius versus time, where the time for the experiments has been modified such that the time t=0 corresponds to the end of isentropic expansion in line with the INEX assumption:

- Figure 18 includes experimental results for the R12 experiment (30C corresponding to 26.6C superheat) for two different humidities of 38% and 83%. Note that the effect of humidity is negligible in INEX, while for the experiment the increased humidity (and therefor increased liquid fog formation) results in slightly large visible cloud at larger times. It is seen that the old INEX is under predicting. The new INEX based on $f_{kin} = 0.04$, produces more accurate results than a value of $f_{kin}$ chosen such as to match the Schmidli formula.
- Figure 19 includes results for two propane experiments (5C and 18C corresponding to superheats of 47.4C and 60.4C). Again it is seen that the old INEX is under predicting, with the new INEX producing more close results. The values of $f_{kin}$ chosen such as to match the Schmidli formula happen to be very close to $f_{kin}=0.04$, and therefore the new INEX curves are almost overlapping. The effect of superheat appears to be more pronounced for the experiments than for the INEX runs. However, this may be caused by added visibility of the cloud due to increased fog formation at increased superheat, while the actual difference in cloud speeds for the experimental data is expected to be smaller.
- Figure 20 includes results for butane experiments (42C and 52C corresponding to superheats of 42.6C and 52.6C). Note that there are only very limited experimental data available beyond isentropic expansion. Based on these very limited data, the old INEX appears to be more accurate than the new INEX.
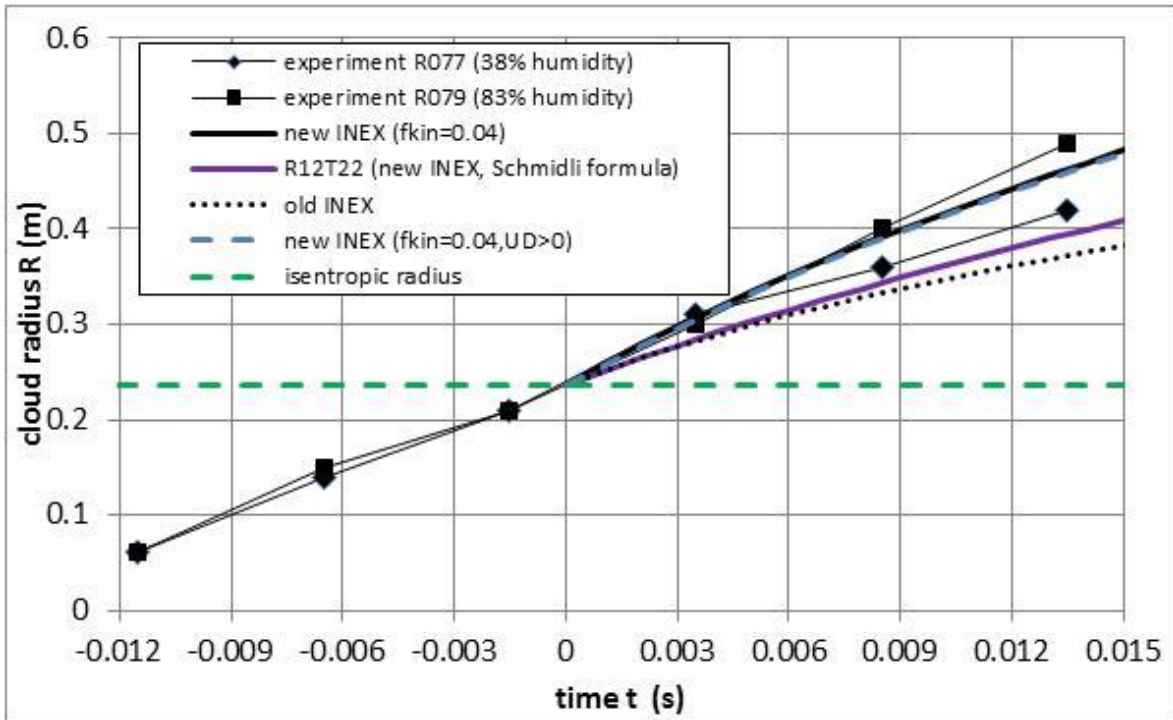
**Figure 18.** Schmidli experiment (R-12, 1ltr, 100% fill, 30C) - INEX cloud radius validation
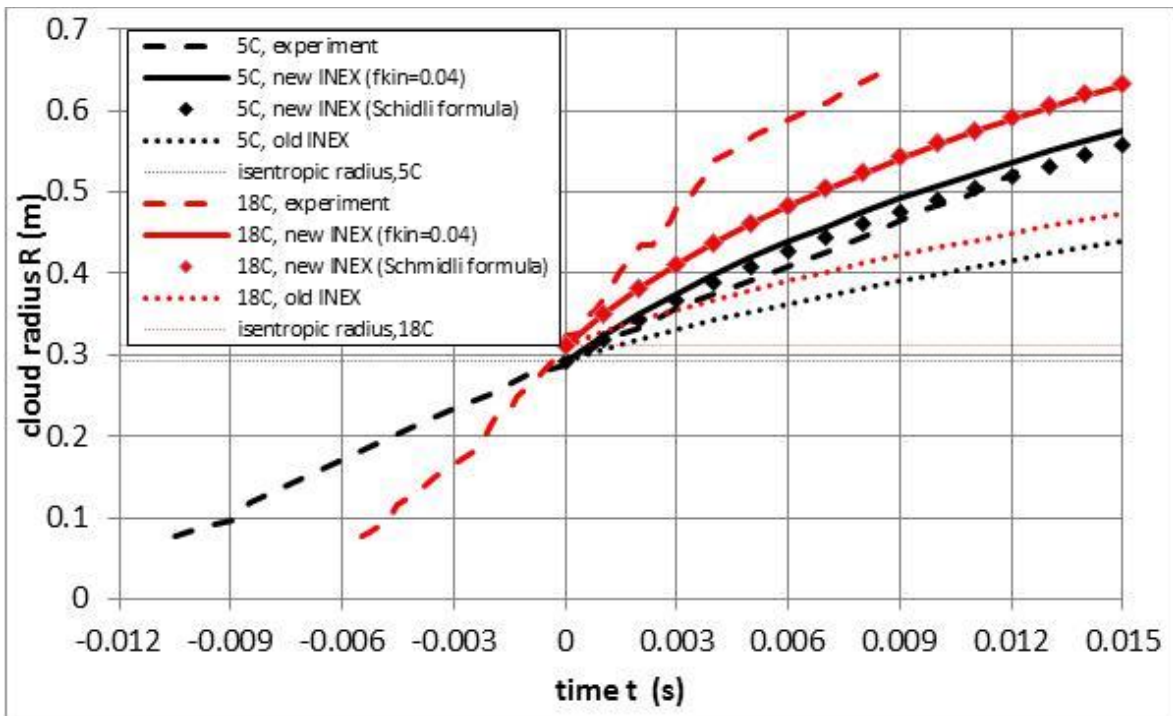


**Figure 19.** Schmidli experiment (propane, 2ltr, 100% fill, 5&18C) - INEX cloud radius validation
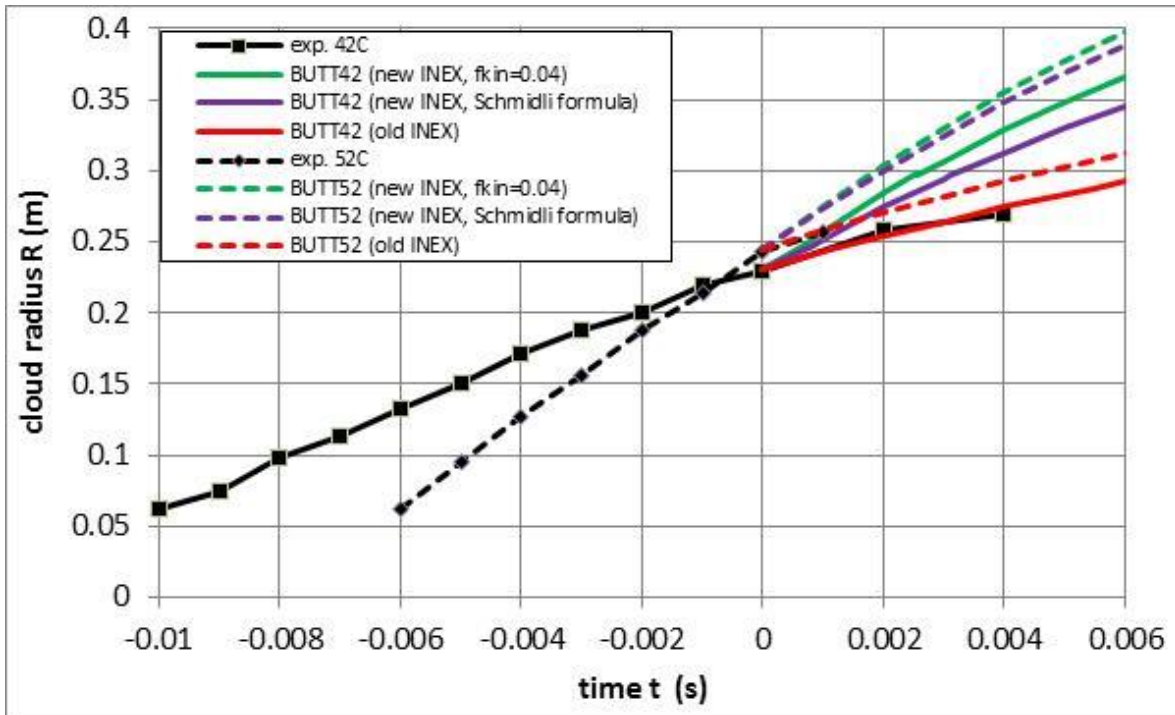
**Figure 20.** Schmidli experiment (butane, 2ltr, 100% fill, 42&52C) - INEX cloud radius validation

INEX validation of rainout

In Phast 7.2 the initial SMD droplet size for instantaneous releases is always based on the CCPS flashing correlation. On the other hand, Schmidli suggests to use a 'Weber' criterion based on the reduced post-expansion final velocity $u_f$ ($f_{kinetic}$=0.04). Table 10 includes results of SMD predictions. It is seen that the flashing SMD is about twice as small than the mechanical SMD for R-12, and very similar for propane.

| Fluid | temperature /SH (C) | elevation (m) | observed % rainout | | | FLASHING CORRELATION | | | MECHANICAL CORRELATION | | |
|---|---|---|---|---|---|---|---|---|---|---|---|
| | | | | | | SMD (μm) | predicted rainout | | SMD (μm) | predicted rainout | |
| | | | 100ml | 1 ltr | 2 ltr | | 1 ltr | 2 ltr | | 1 ltr | 2 ltr |
| R-12 | 22/52.1 | 5D | 24±4 | | | 214 | 20.7% | | 428 | 54.0% | |
| Propane | 5/47.4 | 1 | | 26±6 | 30±9 | 155 | | 5.1% | 180 | | 6.5% |
| | 12/54.4 | 1 | | 13±2 | 26±17 | 134 | | 4.3% | 136 | | 4.4% |
| | 18/60.4 | 1 | | 16±3 | 25±5 | 119 | | 3.6% | 110 | | 3.1% |
| Butane | 42/42.6 | 1 | | | | 179 | | | 244 | | |
| | 52/52.6 | 1 | | | | 148 | | | 160 | | |

**Table 10.** UDM predicted versus observed rainout (Schmidli experiments; elevated, 100% fill)

Figure 21 plots UDM liquid rainout (kg) versus time (s) for both the $U_D$=0 and $U_D$>0 INEX formulations. Figure 21a and Figure 21b include results for the flashing and mechanical SMD, respectively.

Figure 21 demonstrates the subsequence stages of (a) elevated INEX cloud (no rainout), (b) INEX cloud touching down (time-varying rainout), and (c) INEX/UDM grounded cloud (no rainout). For the case of R-12 (mechanical breakup) it shows also the final instantaneous rainout due to an INEX/UDM transition for a grounded plume.

It is seen that the significant smaller SMD in the case of flashing breakup for R-12 results in significant less rainout. Table 10 compares results of the thus predicted overall % liquid rainout ($U_D$=0). It is seen that for R-12 accurate results are obtained in case of flashing SMD, while results are over-predicted in case of mechanical SMD. For propane rainout is under-predicted.
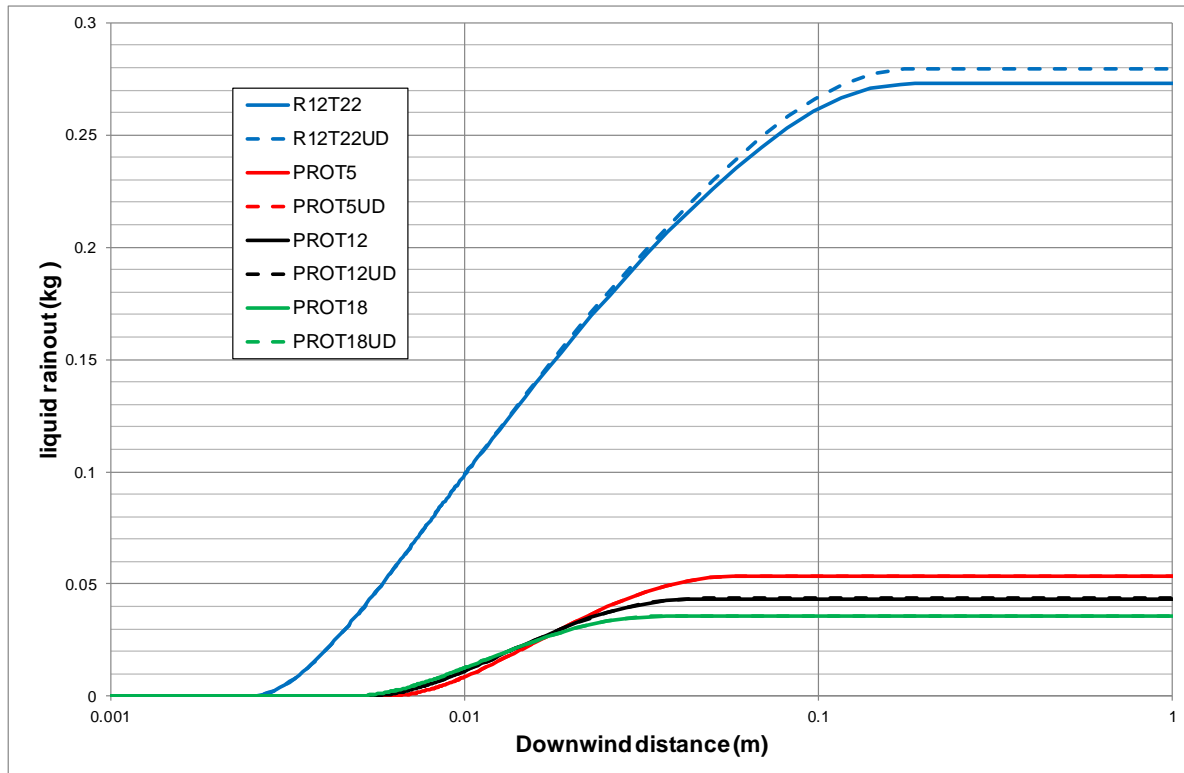
(a)  CCPS flashing SMD (Phast 7.2 default)
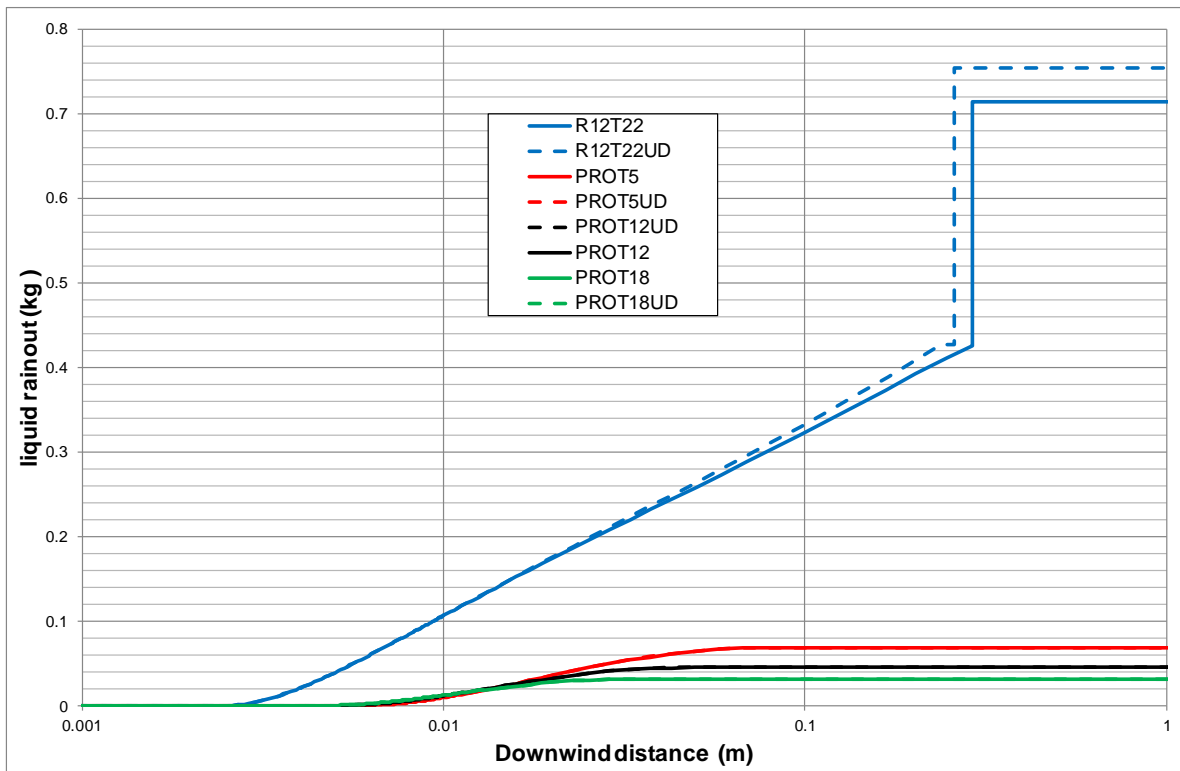


(b)  Mechanical SMD (Weber criterion based on reduced $u_f$)

**Figure 21.** **Rainout prediction for Schmidli experiments**

## 6.3 Analytical verification of rainout for non-evaporating liquid releases

This section considers the specific case of a pressurised release of a sub-cooled liquid, which does not evaporate during the dispersion stage. Selected input data correspond to a horizontal 1 kg/s release of nonane at 0.6 m height and expansion energy of 198.09 J/kg [initial expansion speed U(t=0) = 19.9 m/s]. The initial (post-expansion) data are 0C, 100% liquid and droplet size SMD = 160μm. The weather is chosen to be D0.1 with an ambient temperature of 0C.

Thus, since no evaporation of the nonane liquid occurs, isothermal mixing occurs between the nonane and the ambient moist air. From Equation ( 13 ) included in the UDM thermodynamics Section 3.1, it now follows that $v_{cld} = v_{vap} + v_{liq} = \eta_{wa}/\rho_{wa} + \eta_{cL}/\rho_{cL}$. Thus

$$V_{cld} = \frac{m_{cld}}{\rho_{cld}} = m_{cld}\, v_{cld} = \left(m_{wa} + m_{cL}\right)\left(\frac{\eta_{wa}}{\rho_{wa}} + \frac{\eta_{cL}}{\rho_{cL}}\right) = \frac{m_{wa}}{\rho_{wa}} + \frac{m_{cL}}{\rho_{cL}} \qquad (\ 65\ )$$

where $m_{wa}$ is the added mass of air in the cloud (kg/s), $m_{cL} = m_{cL}(t=0) - m_{ro}(t)$ the mass of liquid nonane in the cloud (kg/s), $\rho_{wa}$ the ambient moist air density, and $\rho_{cL}$ the liquid nonane density.

For a non-evaporating cloud, the rained out mass during the INEX stage is as follows:

$$m_{ro} = \left\{1 - \frac{V_{cld}}{(4/3)\pi R^3}\right\}m_{cR} \ , \ m_c = m_{cR} - m_{ro} = \frac{V_{cld}\, m_{cR}}{(4/3)\pi R^3} \qquad (\ 66\ )$$

Figure 22 depicts numerical INEX results against analytical results.

1. (Figure top left) The INEX variable A (area of cloud above ground) agrees against the analytical formula given by Equation ( 8 )
2. (Figure top right) Cloud volume $V_{cld}$ [the first 4 curves in figure overlay each other]
    a. The INEX variable $V_{cld}$ (cloud volume) agrees against the analytical formula given by Equation ( 8 ) as well as the analytical formula given by Equation ( 65 ). Furthermore, it was confirmed that the air entrainment equation was solved correctly, leading to $m_{wa} = \rho_{wa} (V_{cld} - V_o)$.
    b. $V_{cld}$ is determined in the spreadsheet by integrating he right-hand side of Equation ( 14 ) for $dV_{cld}/dt$ using the trapezoidal rule: $V_{cld,i} = V_{cld,i-1} + 0.5[ (rhs)_{i-1} + (rhs)_i] (t_i - t_{i-1})$. Using in this right-hand side the INEX values of U=dR/dt results in virtually exact matching of the INEX $V_{cld}$; the analytical values are very close
3. (Figure bottom right) Cloud speed
    a. dR/dt = (R/t) d ln(R)/d(ln(t) was derived by differentiating in two different methods. Here, for example, dR/dt was obtained as follows: $(dR/dt)_i = [ (R_i - R_{i-1})/ (t_i - t_{i-1}) + (R_{i+1} - R_i)/ (t_{i+1} - t_i)]/2$
    b. The speeds obtained from dR/dt or (R/t) d ln(R)/d(ln(t) were shown to be identical to the speed obtained from the differential equation for $dV_{cld}/dt$ (with $dV_{cld}/dt$ derived as above for dR/dt). It was also shown that dR/dt is identical to U.
4. (Figure bottom left) Here $m_{ro}$ was obtained in three different ways:
    a. From INEX output variable – produces 50% rainout and agrees with actual analytical result given by Equation ( 66 ).
    b. Rainout obtained by integration from rhs of d.e. for $dm_{ro}/dt$ and using INEX U results in matching above result.
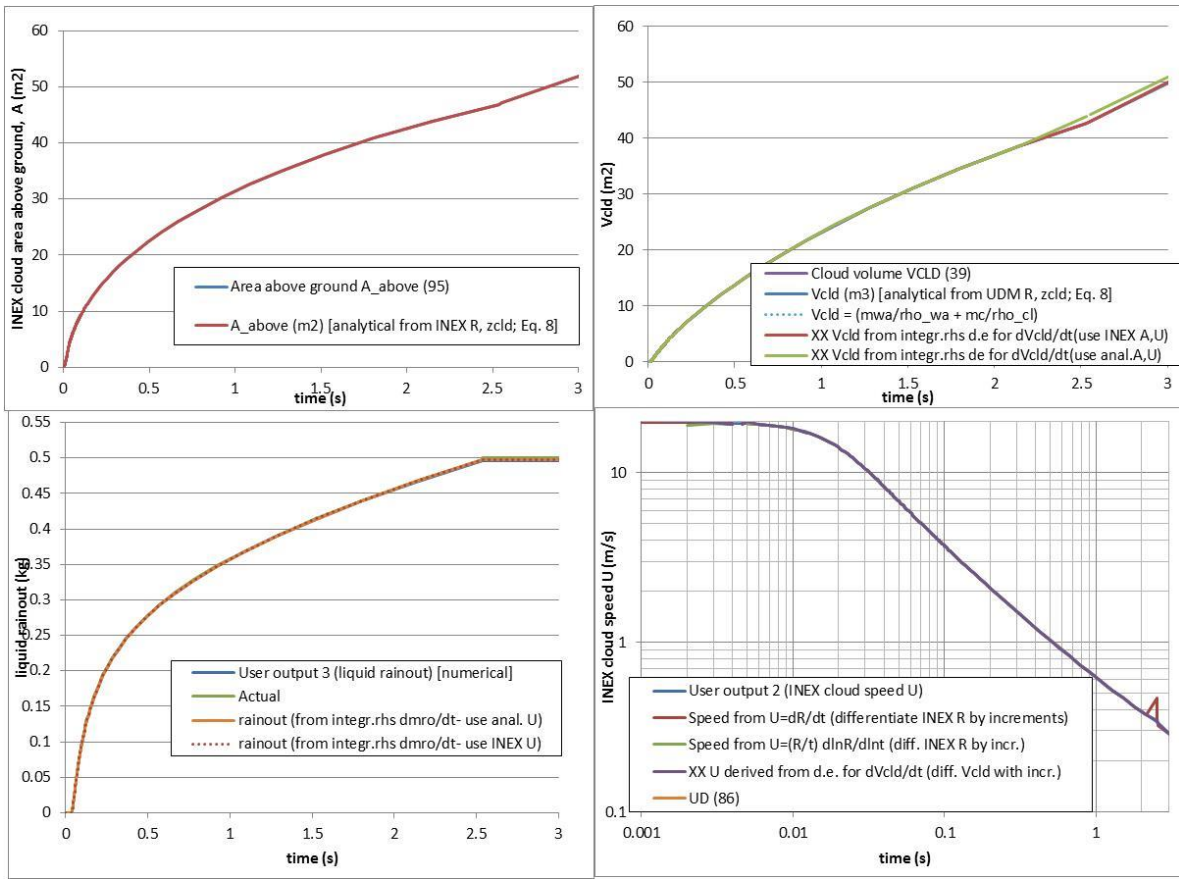    c. Rainout obtained by integration from rhs of d.e. for $dm_{ro}/dt$ and using analytical U=dR/dt matches results

**Figure 22.** **Non-evaporating liquid nonane – INEX verification against analytical results**

# Appendix A. Air entrainment

This section constitutes a summary of Section 3.4 of the UDM theory manual to include the equations for air entrainment in the case of an instantaneous release after the INEX stage. See the UDM theory manual for details and further justification.

Air entrainment into a plume may be caused by a range of mechanisms:

- 'jet' entrainment is caused by turbulence resulting from the difference between the jet speed and the ambient wind speed
- cross-wind entrainment in response to the deflection of the plume by the wind
- passive entrainment is caused by ambient turbulence
- heavy-gas entrainment is the reduced air entrainment included for a grounded heavy-gas plume

Thus the total air entrainment $E_{tot}$ (kg/s) is taken for an elevated 'jet' as[34]

$$
\begin{aligned}
E_{tot} \quad &= \quad E_{jet} + E_{cross} + E_{pas}^{nf}, & x < x_{tr}^{pas} \\
&= \quad f(x) \, [\, E_{jet} + E_{cross} + E_{pas}^{nf}] + [1-f(x)] \, E_{pas}^{ff}, & x_{tr}^{pas} < x < r_{tr}^{pas} \, x_{tr}^{pas} \\
&= \quad E_{pas}^{ff} & x > r_{tr}^{pas} \, x_{tr}^{pas}
\end{aligned}
$$

( 67 )

and for a grounded 'jet' as

$$
\begin{aligned}
E_{tot} \quad &= \quad \max\{E_{jet} + E_{cross}, E_{hvy}\} + E_{pas}^{nf}, & x < x_{tr}^{pas} \\
&= \quad f(x) \, [\max\{E_{jet} + E_{cross}, E_{hvy}\} + E_{pas}^{nf}] + [1-f(x)] \, E_{pas}^{ff}, & x_{tr}^{pas} < x < r_{tr}^{pas} \, x_{tr}^{pas} \\
&= \quad E_{pas}^{ff} & x > r_{tr}^{pas} \, x_{tr}^{pas}
\end{aligned}
$$

( 68 )

Here $E_{jet}$, $E_{cross}$, $E_{pas}^{nf}$, $E_{hvy}$, $E_{pas}^{ff}$, are respectively the jet entrainment, the cross-wind entrainment, the near-field passive entrainment, the heavy-gas entrainment[35] and the far-field passive entrainment.

Jet entrainment
The recommended formulation implemented in the new UDM for jet entrainment is a generalisation of the Morton-Taylor formulation for continuous clouds,

$$ E_{jet} = e_{jet} \; S_{above} \; \rho_a \; |u_{cld} - u_a \cos\theta| \quad \text{in} \quad \text{kg/s} \quad \text{(instantaneous)} $$

( 69 )

with $e_{jet} = 0.5 \, \pi^{-0.5} \, \alpha_1$, and $\alpha_1 = 0.17$.

Cross-wind entrainment
Cross-wind entrainment is associated with the formation in the wake of a rising or falling plume of trailing vortices in response to the deflection by the release plume of ambient air. The formulation is based on a generalisation of the continuous formulation by Morton et al.:

$$ E_{cross} = \alpha_2 \, \rho_a \, S_{above} |u_a \sin\theta| \quad \text{in kg/s} \quad \text{(instantaneous)} $$

( 70 )

with $\alpha_2 = 0.35$. In conjunction with this formulation the airborne drag coefficient is taken to be zero, $C_D = 0$.

Near-field passive entrainment

( 71 )

$$ E_{pas}^{nf} = \left[ 1 - \frac{W_{gnd}}{R_y} \right] \frac{4\pi}{3} \rho_a \, e_{pas} \, \varepsilon^{1/3} \left( l_x^{7/3} + l_y^{7/3} + l_z^{7/3} \right) \quad \text{in kg/s (instantaneous)} $$

---

[34] JUSTIFY. In the code the total entrainment is adjusted as $E_{tot} = E_{tot} *$ max(0.01, 1 - $\eta_{cL}$), if the cloud is 'slumping', i.e. if the cloud is instantaneous and the spreading

velocity $U_{spd} = \sqrt{\max( g \times H_{eff} (1 + h_d) \times \dfrac{\rho_{cld} - \rho_a(z_c)}{\rho_a(z_c)}, 0)}$ is larger than the expansion velocity $U_{exp} = (2E_{exp})^{0.5}$.

[35] For heavy-gas ground-level non-jet plumes, concentrations will be too high if the transition is too early (at which passive entrainment is larger than heavy), but in the far-field $E_{hvy}$ should approach $E_{pas}$ [provided cloud density is close to the ambient density]

For stability classes A,B,C,D $l_x=l_y=l_z$ and for sufficiently high cloud $W_{gnd}=0$, $l_x=l_y=l_z=R_y$ and $E_{pas}^{nf}$ reduces to the above expression $E_{pas}^{nf} = e_{pas}\rho_a [4\pi R_y^2] (\varepsilon R_y)^{1/3}$.

Here the coefficient $e_{pas} = 1$; the turbulent (transverse horizontal, vertical) eddy length scales $l_y$, $l_z$, and the dissipation rate of kinetic energy $\varepsilon$ are given by

$$l_y = \min\{R_y, 0.88(z_c+z_0)L_y(Z) \}, \quad l_z = \min\{R_y, 0.88(z_c+z_0)L_z(Z) \}$$
$$\varepsilon = E(Z) u_*^3/[\kappa(z_c+z_0)]$$

where $Z = (z_c+z_0)/L$, $z_c$ the centroid height, $z_0$ the surface roughness length, $L$ the Monin-Obukhov length, $u_*$ the friction velocity, and $\kappa$ the Von Karman constant. The functions $L_y(Z)$, $L_z(Z)$ and $E(Z)$ are defined as a function of stability class by

$$L_y(Z) = L_z(Z) = (1-7.4\kappa Z)/E(Z), \quad E(Z) = 1 - 5\kappa Z, \qquad \text{stability class = A,B,C}$$
$$L_y(Z) = L_z(Z) = E(Z) = 1 \qquad \text{stability class = D}$$
$$L_y(Z) = 1 / (1+0.1Z), \quad L_z(Z) = 1/ E(Z), \quad E(Z) = 1 + 4Z, \qquad \text{stability class = E,F}$$

Note that the near-field passive entrainment is phased out during touchdown.[36]

Heavy-gas entrainment

$$E_{hvy} = \left[\frac{W_{gnd}}{R_y}\right] \{u_{side} A_{side} + u_{top} A_{top}\} \rho_a \tag{72}$$

where $u_{side}$ is the horizontal air-entrainment velocity through the plume side-area $A_{side}$, $u_{top}$ is the vertical air-entrainment velocity through the plume top-area $A_{top}$. The side area $A_{side}$ and the top area $A_{top}$ correspond to an instantaneous plume of cylindrical shape with height $H_{eff}(1+h_d)$ and radius $W_{eff}$,

$$A_{side} = 2\pi W_{eff} H_{eff} (1+h_d) , \qquad A_{top} = \pi W_{eff}^2 \tag{73}$$

The term $[W_{gnd}/R_y]$ in Equation ( 72 ) ensures that the heavy-gas entrainment is not applied for an elevated plume, is phased in during touching down and phased out during lifting-off.

The side surface entrainment velocity is taken to be proportional to the spread rate or

$$u_{side} = \gamma \frac{dW_{eff}}{dt} \tag{74}$$

where $\gamma=0.3$ is an edge-entrainment coefficient.

To retain this form, the top-entrainment velocity $u_{top}$ is defined by:

$$u_{top} = \frac{\kappa u_*}{\Phi( Ri_* )} \tag{75}$$

where $\kappa=0.4$ is the Von Karman constant, and $\Phi$ the entrainment function of the Richardson number $Ri_*$[37]:

$$Ri_* = \frac{g \left[\rho_{cld} - \rho_a (z = z_{cld} )\right] H_{eff} (1+h_d )}{\rho_a u_*^2} \tag{76}$$

Far-field passive entrainment

Passive dispersion is represented by correlations for the ambient horizontal ($\sigma_{ya}$) and vertical ($\sigma_{za}$) dispersion coefficients. These correlations depend upon the stability class and distance from the release point. For $\sigma_{ya}$ it also depends on the averaging time $t_{av}$ and for $\sigma_{za}$ it also depends on the surface roughness length $z_0$. The entrainment rate by the far-field passive dispersion mechanism, $E_{pas}^{ff}$ (kg/s) is given by[38]:

---

[36] The passive-entrainment formula is taken to be compatible with those adopted by Ooms and HGSYSTEM (based on Disselhorst experiments). It may need to be further refined, in order to ensure full convergence to the passive formula in the far field automatically. This may involve considering the use of an alternative formula for the near-field and/or far-field passive entrainment.

[37] Note that HEGADAS uses the definition $Ri_* = g[\rho_{cld}-\rho_a(z=H_{eff})]H_{eff} / [\rho_a(z=0)u_T^2]$ with the friction velocity $u_T$ modified for heat transfer. In the old UDM $Ri_* = g[\rho_{cld}-\rho_a(z=z_c)]H_{eff} / [\rho_{cld}u_*^2]$

[38] JUSTIFY - In the above equations $d\sigma_{ya}/dx$ and $d\sigma_{za}/dx$ were originally evaluated at $x - x_0$ with $x_0$ a virtual source distance such that spread rate is continuous. However, the use of $x_0$ in code has been eliminated (why?), and instead the continuous spread rate is obtained via a more arbitrary smoothing algorithm. Note that strictly

$$E_{pas}{}^{ff} \quad = \quad V_{cld}(x)\left[\frac{2}{\sigma_y}\frac{d\sigma_{ya}}{dx} + \frac{1}{\sigma_z}\frac{d\sigma_{za}}{dx}\right]\rho_a(z = z_{cld}) \quad u_a(z = z_c) \tag{77}$$

---

speaking for continuous, $E_{pas} = \rho_a u_a [\partial A_{cld}/\partial x] = \rho_a u_a \ \partial/\partial x[4\Gamma(1+s^{-1}) \ \Gamma(1+m^{-1})(1+h_d)\sigma_y\sigma_z]$. This leads to Equation (180) ignoring downwind variations of $s,m,h_d$ and assuming $\partial\sigma_y/\partial x = \partial\sigma_{ya}/\partial x$, $\partial\sigma_z/\partial x = \partial\sigma_{za}/\partial x$. Likewise for instantaneous: $E_{pas} = \rho_a u_a [\partial V_{cld}/\partial x] = \rho_a u_a \ \partial/\partial x[\pi\Gamma(1+s^{-1}) \ \Gamma(1+2m^{-1}) \ \sigma_y{}^2\sigma_z]$.

# Appendix B. Evaluation of $dR_y/dt$ during INEX stage

An expression of the spread rate $dR_y/dt$ is required for the UDM/INEX transition criterion. During the INEX phase, it is assumed for the UDM geometry that $R_x = R_y = R_z$. Thus (see Section 2.1):

$$
\begin{aligned}
V_{cld} &= \pi W_{eff}^2 \; H_{eff}(1+h_d) \\
&= \pi \left\{ C_m R_y \right\}^2 \left\{ C_n R_z \right\}(1+h_d) \\
&= \pi C_m^2 C_n(1+h_d) R_y^3
\end{aligned}
\tag{78}
$$

Where

$$
C_n = \Gamma\left(1+\frac{1}{n}\right), \; with \; n \; function \; of \; H_{eff} = C_n R_z
\tag{79}
$$

$$
C_m = \sqrt{\Gamma\left(1+\frac{2}{m}\right)}, \; with \; m \; function \; of \; r = \frac{\rho_{cld} - \rho_a}{\rho_a}
\tag{80}
$$

$$
h_d = P\left[\frac{1}{n}, \left(\frac{z_{cld}}{R_z}\right)^n\right], \; with \; P(a,b) = \frac{1}{\Gamma(a)}\int_0^b t^{a-1} e^{-t} \, dt
\tag{81}
$$

At the time of the UDM/INEX transition, one would normally expect already a significant amount of entrainment, implying approximately a Gaussian profile (m and n approximately equal to 2) and therefore $C_m$ and $C_n$ are approximately constant. Thus ignoring $dC_m/dt$ and $dC_n/dt$, one can derive:

$$
\begin{aligned}
\frac{dh_d}{dt} &= \frac{1}{\Gamma(1/n)} \left(\frac{z_{cld}}{R_y}\right)^{1-n} e^{-(z_{cld}/R_y)^n} n\left(\frac{z_{cld}}{R_y}\right)^{n-1} \left\{\frac{1}{R_y}\frac{dz_{cld}}{dt} - \frac{z_{cld}}{R_y^2}\frac{dR_y}{dt}\right\} \\
&= \frac{1}{C_n} e^{-(z_{cld}/R_y)^n} \left\{\frac{1}{R_y}\frac{dz_{cld}}{dt} - \frac{z_{cld}}{R_y^2}\frac{dR_y}{dt}\right\}
\end{aligned}
\tag{82}
$$

and

$$
\begin{aligned}
\frac{dV_{cld}}{dt} &= \pi C_m^2 C_n \left\{(1+h_d)3R_y^2\frac{dR_y}{dt} + R_y^3\frac{dh_d}{dt}\right\} \\
&= \pi C_m^2 R_y^2 \left\{3C_n(1+h_d)\frac{dR_y}{dt} + e^{-(z_{cld}/R_z)^n}\left\{\frac{dz_{cld}}{dt} - \frac{z_{cld}}{R_y}\frac{dR_y}{dt}\right\}\right\} \\
&= \pi C_m^2 R_y^2 \left\{\left[3C_n(1+h_d) - \frac{z_{cld}}{R_y}e^{-(z_{cld}/R_z)^n}\right]\frac{dR_y}{dt} + e^{-(z_{cld}/R_z)^n}\frac{dz_{cld}}{dt}\right\}
\end{aligned}
\tag{83}
$$

The above equation can be solved for of $dR_y/dt$:

$$
\frac{dR_y}{dt} = \frac{\dfrac{1}{\pi C_m^2 R_y^2}\dfrac{dV_{cld}}{dt} - e^{-(z_{cld}/R_z)^n}\dfrac{dz_{cld}}{dt}}{3C_n(1+h_d) - \dfrac{z_{cld}}{R_y}e^{-(z_{cld}/R_z)^n}}
\tag{84}
$$

which for a fully grounded cloud ($z_{cld} = dz_{cld}/dt=0$) while using Equation ( 78 ) and ( 13 ) reduces to

$$
\frac{dR_y}{dt} = \frac{\dfrac{1}{\pi C_m^2 R_y^2}\dfrac{dV_{cld}}{dt}}{3C_n(1+h_d)} = \frac{R_y}{3V_{cld}}\frac{dV_{cld}}{dt} = \frac{R_y}{R}U = \frac{R_y}{R}\frac{dR}{dt}
\tag{85}
$$

Please note that the above equation is analogous to the INEX radius geometry equation during fully grounded: $V_{cld} = (2/3) \pi R^3 \rightarrow dR/dt = (R/3V_{cld}) \, dV_{cld}/dt$.

For an elevated cloud, the above equation provides an expression of $dR_y/dt$ as function of $dz_{cld}/dt$ and known secondary variables $dV_{cld}/dt$ [from Equation ( 14 )], $R_y$, n, $C_m$ and $C_n$. For a grounded cloud is a function of $dV_{cld}/dt$ and the known secondary variables $V_{cld}$ and $R_y$. This is the value of $dR_y/dt$ as derived from the INEX geometry. A transition is made to the UDM if this value reduces to below the value of the gravity spreading rate $dR_y/dt$ as given by either equation ( 51 ) or equation ( 53 ).[39]

---

[39] CODE. In the code currently a transition is only made AFTER the cloud is fully grounded.

# Appendix C.  Summary of equations for new INEX model

This appendix summarises the key equations applicable for the new UDM INEX model.

The following cloud geometry (sphere or truncated sphere; radius R, elevation height $z_{cld}$): volume $V_{cld}$, area above ground A, $A_{footprint} = \pi L^2$) is presumed (see Section 2.2 for details):

$$V_{cld} = \frac{4}{3}\pi R^3 \; , \; A = 4\pi R^2 \, , \, L = 0 \quad , \quad if \; z_{cld} \geq R \; (cloud\ elevated) \tag{86}$$

$$V_{cld} = \frac{1}{3}\pi (R + z_{cld})^2 (2R - z_{cld}), \, A = 2\pi R(R + z_{cld}), \, L = \sqrt{R^2 - z_{cld}^2} \; , \, if \; 0 < z_{cld} < R$$

$$V_{cld} = \frac{2}{3}\pi R^3 \, , \, A = 2\pi R^2, \, L = R \quad , \quad if \; z_{cld} = 0 \; (cloud\ grounded)$$

## *C.1*   Formulation including air-displacement velocity ($U_D > 0$)

1.   Set secondary variables: (a) Set speed U from $I_r = m_{cld}U$, (b) set $dV_{cld}/dt$, $U_E$, $U_D$ from equations below:

$$\frac{dV_{cld}}{dt} = AU \; , \qquad\qquad\quad if \; z_{cld} \geq R\,(cloud\ elevated) \; or \; if \; z_{cld} = 0 \;(cloud\ grounded) \tag{87}$$

$$= AU + A_{footprint}\frac{dz_{cld}}{dt} \; , \quad if \; 0 < z_{cld} < R \; (cloud\ touching\ down)$$

$$U_E \approx \frac{1}{A\rho_a \dfrac{\partial V_{cld}}{\partial m_{wa}}} \frac{dV_{cld}}{dt} - (A_{footprint}/A)\frac{dz_{cld}}{dt} \tag{88}[40]$$

$$U_D = U - U_E \tag{89}$$

2.   Three differential equations below for primary variables $m_{wa}$, $m_{ro}$ and $I_r$:

$$\frac{dm_{wa}}{dt} = \rho_a A U_E \; , if \; z_{cld} \geq R\,(cloud\ elevated)\ or\ if \; z_{cld} = 0 \;(cloud\ grounded) \tag{90}$$

$$= \rho_a \left\{ AU_E + A_{footprint}\frac{dz_{cld}}{dt} \right\} \; , \quad if \; 0 < z_{cld} < R \; (cloud\ touching\ down)$$

$$\frac{dm_{ro}(t)}{dt} = 0 \; , \; z_{cld} > R \; ('elevated'\ plume) \; or \; z_{cld} = 0 \;('grounded'\ plume) \tag{91}$$

$$= \max\left\{ K_D \frac{m_{cL}}{V_{cld}} A_{footprint}\left[ \frac{z_{cld}}{R}\frac{dR}{dt} - \frac{dz_{cld}}{dt} \right],0 \right\}, \; else$$

$$\frac{dI_r^{\,i}}{dt} = -K\rho_a A U_D^2 - \frac{dm_{ro}}{dt}U \tag{92}$$

Disadvantages
-   Needs approximate solution for $U_E$ via repetitive THRM calls
-   Needs drag parameter K
-   More complex
-   More numerical problems

Advantages: allows for displacement velocity

---

[40] IMPROVE CODE. The UDM INEX code currently erroneously omits the second term, which is only relevant during touchdown; see also footnote 2.

## C.2 Formulation excluding air-displacement velocity ($U_D=0$)

This includes the following modifications: $U_D=0$, $U=U_e$

1. Set secondary variables: (a) Set speed U from $I_r = m_{cld}U$, (b) set $dV_{cld}/dt$, $U_E$, $U_D$ from equations below:

$$\frac{dV_{cld}}{dt} = AU \; , \qquad\qquad if \; z_{cld} \geq R(cloud\;elevated) \; or \; if \; z_{cld} = 0 \; (cloud\;grounded) \qquad\qquad (93)$$

$$= AU + A_{footprint}\frac{dz_{cld}}{dt} \; , \quad if \; 0 < z_{cld} < R \; (cloud\;touching\;down)$$

$$U_D = 0, \; U_E = U \qquad\qquad\qquad (94)$$

2. Three differential equations below for primary variables $m_{wa}$, $m_{ro}$ and $I_r$:

$$\frac{dm_{wa}}{dt} = \rho_a \frac{dV_{cld}}{dt} \qquad\qquad\qquad (95)$$

$$\frac{dm_{ro}(t)}{dt} = 0 \; , \; z_{cld} > R \; ('elevated'\;plume) \; or \; z_{cld} = 0 \; ('grounded'\;plume) \qquad (96)$$

$$= \max\left\{K_D \frac{m_{cL}}{V_{cld}} A_{footprint}\left[\frac{z_{cld}}{R}\frac{dR}{dt} - \frac{dz_{cld}}{dt}\right],0\right\}, \; else$$

$$\frac{dI_r^{\,i}}{dt} \;\; = \;\; -\frac{dm_{ro}}{dt}U \qquad\qquad\qquad (97)$$

Advantages
- Avoids approximate solution for $U_E$ via repetitive THRM calls
- Eliminates drag parameter K
- More simplistic
- More consistent with non-instantaneous solution algorithm

## Appendix D.  INEX rainout logic accounting for bund walls

During the INEX phase, the liquid is presumed to be uniformly distributed along the INEX cloud, which is modelled as a sphere (before touching down), a capped sphere (during touching down) or a hemisphere (when fully grounded) with cloud centre height $z_{cld}$ and cloud radius R.

In the absence of a bund, immediate instantaneous rainout occurs at time t=0 when after the DISC expansion the cloud immediately hits the ground; see Equation ( 25 ). In addition, time-varying rainout occurs during the INEX phase (as long as liquid is present), while the cloud is touching down; see Equation ( 28 ). No rainout occurs during the INEX phase, while the cloud is elevated or fully grounded. In addition, instantaneous rainout of all remaining liquid occurs after the INEX phase, when the droplet height reduces to 0m (droplet hits the ground).

In the presence of a cylindrical bund (bund radius $R_{bund}$), it is currently simplistically assumed that immediate instantaneous rainout occurs of all remaining liquid when the cloud centre-line ($x_{cld}$, $z_{cld}$) hits the bund.  This assumption is consistent with the previous Phast 7.2 assumption, where it is assumed that all liquid rains out which either hits the ground or the bund walls. In addition, the vapour cloud is modelled to move 'freely' across the bund wall, while in reality the vapour cloud would be contained within the bund. This assumption is only valid when the cloud vapour height is considerably larger than the bund wall height.

Intersection of INEX cloud with cylindrical bund

However, based on the presumed bund geometry and INEX cloud geometry, and retaining the assumption of a uniform distribution of the liquid across the ENTIRE cloud with volume $V_{cld}$ and presuming all liquid which hits the bund rains out immediately, the following applies:

- Additional immediate rainout (at UDM INEX time t=0) may occur if after the DISC expansion the cloud hits the bund wall.

- Time-varying rainout will occur during the INEX phase (as long as liquid is present), while the INEX cloud passes through the bund wall. This will happen when

$$\left\{ z_{cld} \le H_{bund} \ \wedge \ R > |R_{bund} - x_{cld}| \right\} \ \ or$$
$$\left\{ z_{cld} > H_{bund} \ \wedge \ R^2 > (x_{cld} - R_{bund})^2 + (z_{cld} - H_{bund})^2 \right\} \tag{98}$$

In case Equation ( 98 ) is satisfied the INEX cloud intersects with the vertical bund wall for $z_{min} < z < z_{max}$, where (see Figure 23a)
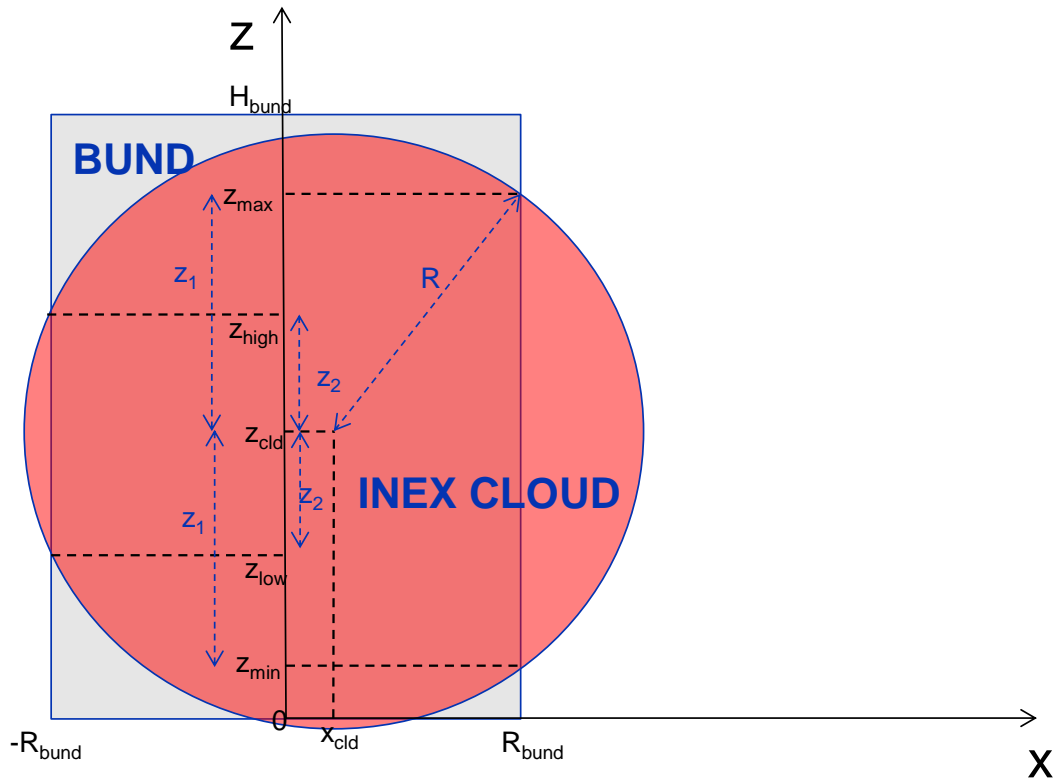
$$z_{min} = \max \left\{ 0, \min \left[ H_{bund}, z_{cld} - z_1 \right] \right\}, z_{max} = \min \left\{ H_{bund}, z_{cld} + z_1 \right\}, with \tag{99}$$
$$z_1 = \sqrt{R^2 - (R_{bund} - x_{cld})^2}$$

If $R < R_{bund} + x_{cld}$, the INEX cloud will not envelope the entire bund at any height z. Otherwise, at a given height z, the outer boundary of the INEX cloud lies completely outside the bund wall if $L(z) > R_{bund} + x_{cld}$, i.e. for $z_{low} < z < z_{high}$ where (see Figure 23a)

$$z_{low} = \max \left\{ z_{min}, z_{cld} - z_2 \right\}, z_{high} = \min \left\{ z_{max}, z_{cld} + z_2 \right\}, with \tag{100}$$
$$z_2 = \sqrt{R^2 - (R_{bund} + x_{cld})^2}$$

(a) Vertical cross-section of INEX cloud with bund (at y=0)
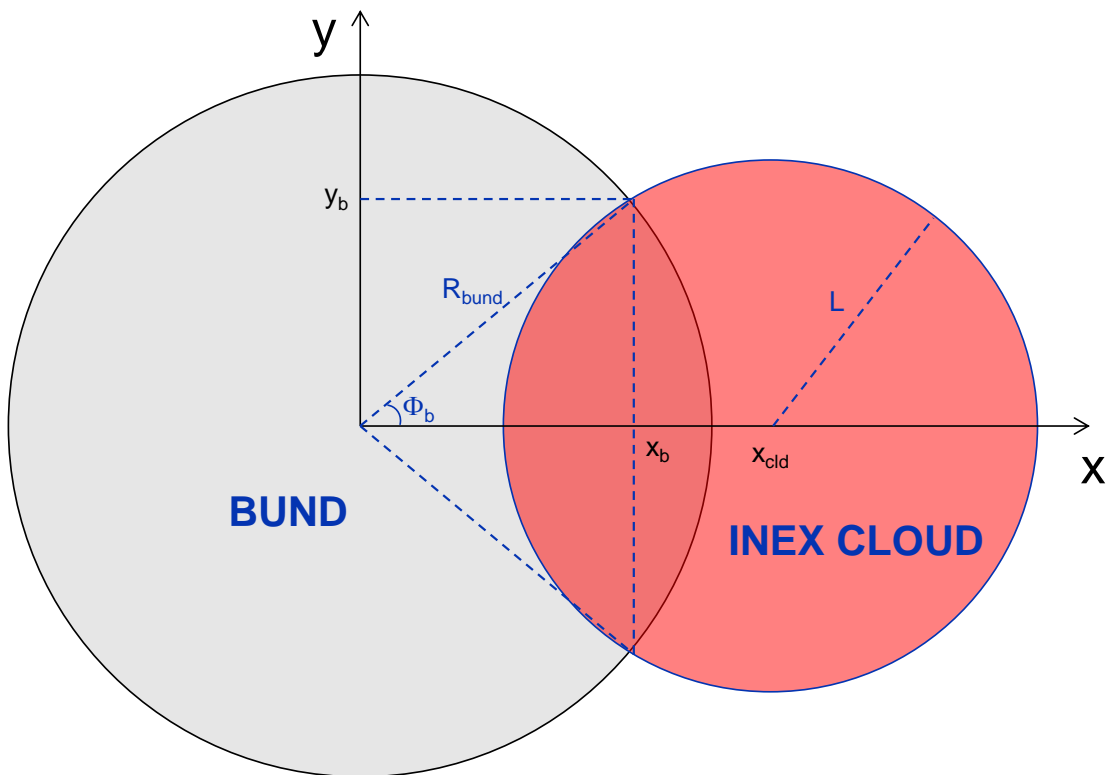


(b) Horizontal cross-section of INEX cloud with bund (at height z)

**Figure 23.      Intersection of INEX cloud with cylindrical bund**

Immediate rainout including added rainout due to bund wall

Let $V_{out}^{bund} = V_{out}(R, z_{cld}, R_{bund}, H_{bund})$ be the volume of the INEX sphere outside the bund (above the ground and below the bund wall height $H_{bund}$). In case Equation ( 98 ) is not satisfied at the initial time t=0 ($x_{cld}$=0), $V_{out}^{bund}$=0. Otherwise it is evaluated as

$$V_{out}^{bund} = \pi \int_{z_{min}}^{z_{max}} \{L^2 - R_{bund}^2\}dz = \pi \int_{z_{min}}^{z_{max}} \{R^2 - R_{bund}^2 - (z - z_{cld})^2\}dz \tag{101}$$

$$= \pi \left\{ (R^2 - R_{bund}^2)(z_{max} - z_{min}) - \frac{1}{3}\left[(z_{max} - z_{cld})^2 - (z_{max} - z_{cld})^2\right] \right\}$$

Equation ( 25 ) for immediate rainout is now replaced by[41]

$$\eta_{immediate\_rainout} = \frac{\frac{4}{3}\pi R_{pr}^3 - V_{cld}(R_{pr}, z_{cld}) + V_{out}^{bund}(R_{pr}, z_{cld}, R_{bund}, H_{bund})}{\frac{4}{3}\pi R_{pr}^3} \eta_{cLf} \tag{102}$$

Where the INEX cloud volume $V_{cld}(R, z_{cld})$ is defined by Equation ( 8 ).

Added time-varying rainout due to bund

The additional time-varying rainout rate while the INEX cloud is passing the bund can be expressed as [42]

$$\frac{dm_{ro}(t)}{dt} = K_D \frac{m_{cL}}{V_{cld}} F_{out} , \ with \ F_{out} = \iint_{bund\,wall\,S} \underline{v}_{INEX} \bullet \underline{n}_{bund} \, dS \tag{103}$$

In the above integrand $\underline{v}_{INEX} = U/R \ [R_{bund} \cos\varphi - x_{cld}, R_{bund} \sin \varphi, z - z_{cld}]^T$ is the INEX velocity vector at the bund wall pointing from the INEX cloud center $[x_{cld},0,z_{cld}]^T$ radially outwards. Here $\varphi$ is the anti-clockwise angle with the x-axis (-$\Phi_b<\varphi<\Phi_b$). For $z_{low}\leq z\leq z_{high}$, $\Phi_b = \pi$, i.e. the INEX cloud completely envelopes the bund. Otherwise the angle $\Phi_b$ = arcos ($x_b/R_{bund}$); see Figure 23b. Here the distance $x_b$ is derived from the bund wall equation $x_b^2 + y_b^2 = R_{bund}^2$ and the INEX cloud boundary equation $(x_b - x_{cld})^2 + y_b^2 = L^2$,

$$x_b = \frac{x_{cld}^2 + R_{bund}^2 - L^2}{2x_{cld}} = \frac{x_{cld}^2 + (z - z_{cld})^2 + R_{bund}^2 - R^2}{2x_{cld}} , \ for \ z_{min}<z<z_{low} \ or \ z_{high}<z<z_{max} \tag{104}$$

Furthermore in the above integrand $\underline{n}_{bund} = [\cos \varphi, \sin \varphi, 0]^T$ is the normal to the bund wall. Following the above the integral $F_{out}$ can be evaluated as follows:

$$F_{out} = \int_{z_{min}}^{z_{max}} \left\{ \int_{-\Phi_b}^{\Phi_b} \frac{U}{R} \begin{bmatrix} R_{bund}\cos\varphi - x_{cld} \\ R_{bund}\sin\varphi \\ z - z_{cld} \end{bmatrix} \bullet \begin{bmatrix} \cos\varphi \\ \sin\varphi \\ 0 \end{bmatrix} R_{bund}d\varphi \right\}dz \tag{105}$$

$$= U\frac{R_{bund}}{R} \int_{z_{min}}^{z_{max}} \left\{ \int_{-\Phi_b}^{\Phi_b} [R_{bund} - x_{cld}\cos\varphi]d\varphi \right\}dz = 2U\frac{R_{bund}}{R} \int_{z_{min}}^{z_{max}} [R_{bund}\,\Phi_b - x_{cld}\sin\Phi_b]dz$$

$$= 2U\frac{R_{bund}}{R} \left\{ R_{bund}\pi(z_{high} - z_{low}) + \int_{z_{min}}^{z_{low}} [R_{bund}\,\Phi_b - x_{cld}\sin\Phi_b]dz + \int_{z_{high}}^{z_{max}} [R_{bund}\,\Phi_b - x_{cld}\sin\Phi_b]dz \right\}$$

Current UDM INEX implementation of rainout modelling due to bunds

Equation ( 102 ) instead of ( 25 ) has been applied for immediate rainout.

---

[41] Please note that rainout factor $K_D$ could be considered to be applied to both immediate rainout and subsequent time-varying rainout. However not relevant as long as $K_D$=1 is presumed (current default value).

[42] JUSTIFY. Please note that the above equation assumes that the liquid is uniformly distributed across the entire volume $V_{cld}$, i.e. both inside and outside of the bund! In addition, the same rainout fraction $K_D$ is applied as for the droplets hitting the ground

Subsequently additional instantaneous rainout is applied in case the UDM INEX cloud centre-line hits the bund. For potential future implementation, the following options could be considered  for modelling additional time-varying rainout due to bunds

1.  Method above: add term given by Equations ( 103 ) and ( 105 ): disadvantages
    a.  need integral evaluation – more complex
    b.  use of $V_{cld}$ in Equation ( 103 ), while liquid possibly only contained inside bund (??) – note however possible effects of condensation etc. – this results in more conservative (lower) estimate of rainout

2.  Further refine method to use term $V_{cld}^{in}$ (volume of INEX cloud contained inside the bund ($z<H_{bund}$, $x^2+ y^2<R_{bund}^2$) instead of $V_{cld}$ in Equation ( 103 ). For a ground-level INEX cloud or a fully elevated cloud $V_{cld}^{in}$ with a fully effective bund ($H_{bund}$ sufficiently large) this can be evaluated using formula of Lamarche and Leroy (1990)[xxii]. Otherwise this may need to be extended in analogy with the derivation in the latter reference. Should result in either additional 1D integral or evaluation of complete elliptic integrals.

# Appendix E.  Evaluation of elevation height and pressure as input to INEX

In the DISC theory manual, it is indicated that the following pressure is input to DISC in case of a catastrophic rupture.[43]

$$P_i = P_{st} + \rho_L \big(P_{st}, T_{st}\big) g \, \frac{\Delta H_L}{2}$$
$$T_i = T_{st}$$

( 106 )

Here $P_i$ is considered to be the averaged vessel pressure inside the tank; $P_{st}$ equals the stagnation pressure at the top of the liquid, while $\Delta H_L$ is considered the total liquid height (labelled as 'tank head').

Future methodology (not yet implemented in product)

Section 2.3.1 in the TVDI 8.0 theory manual allows for four different geometries, i.e. rectangular tanks, horizontal and vertical cylindrical tanks and spherical tanks.

In the new methodology, the pressure is recommended to be evaluated at the liquid centroid height $Z_c$ above the bottom of the tank, i.e. it is given by the following formula

$$P_i = P_{st} + \rho_L \big(P_{st}, T_{st}\big) g (Z_L - Z_c)$$
$$T_i = T_{st}$$

( 107 )

Here $Z_L$ is the total liquid height above the bottom of the tank; see the TVDI manual for the evaluation of $Z_L$. The height $Z_c + Z_{tank}^{bottom}$ should be selected as the elevation height, where $Z_{tank}^{bottom}$ is the height of the bottom of the tank above the ground.

For rectangular tanks and vertical cylindrical tanks, the new methodology corresponds with the old methodology, since for these cases $Z_L - Z_c = \frac{1}{2}\,\Delta H_L$.  For the horizontal cylindrical tanks and spherical tanks, the centroid height $Z_c$ is evaluated as indicated below.

## E.1    Horizontal cylinder

This section describes an analytical derivation of the liquid centroid height method for a horizontal cylinder (length L, inner radius R, liquid height $Z_L$) with planar end caps (no spherical end caps).

The angle Φ as shown in Figure 24 is the angle from the negative z-axis to the top of the liquid, and is set from the equation below

$$Z_L = R[1 - \cos\Phi] \;\Rightarrow\; \Phi = \arccos\!\left(1 - \frac{Z_L}{R}\right)$$

( 108 )

Here $0 \le \Phi \le \pi$ with Φ=0 corresponding with $Z_L$=0 (no liquid present in vessel) and Φ=π with $Z_L$=2R (vessel fully filled with liquid). The area of the wedge (enclosing an angle 2Φ) and the triangle as shown in Figure 24 can now be determined as follows:

$$A_{wedge} = \int_0^R dr \int_{-\Phi}^{\Phi} r\, d\varphi = \left\{ \int_0^R r\, dr \right\} \left\{ \int_{-\Phi}^{\Phi} d\varphi \right\} = R^2 \Phi$$

( 109 )

$$A_{triangle} = \left| \left\{ R\cos\!\left(\frac{\pi}{2} - \Phi\right) \right\} \left\{ R\sin\!\left(\frac{\pi}{2} - \Phi\right) \right\} \right| = R^2 \left| \cos\Phi \sin\Phi \right| = R^2 \left| \frac{1}{2}\sin 2\Phi \right|$$

( 110 )

If Φ<π/2, the total liquid area $A_L$ equals the wedge area minus the triangle area, while for Φ>π/2 it is the sum of the areas. Thus

---

[43] In the DISC manual it is noted that this is applied in the model, but not in SAFETI (only option of input for atmospheric liquids – not pressurised or saturated; in 7.2 can always be specified – although – because of bug – not always on equipment level)

$$A_L = R^2 \left[ \Phi - \frac{1}{2} \sin 2\Phi \right]$$

<div align="right">( 111 )</div>

The liquid volume $V_L$ is now determined as follows:

$$V_{liquid} = L\,A_L = LR^2 \left[ \Phi - \frac{1}{2} \sin 2\Phi \right]$$

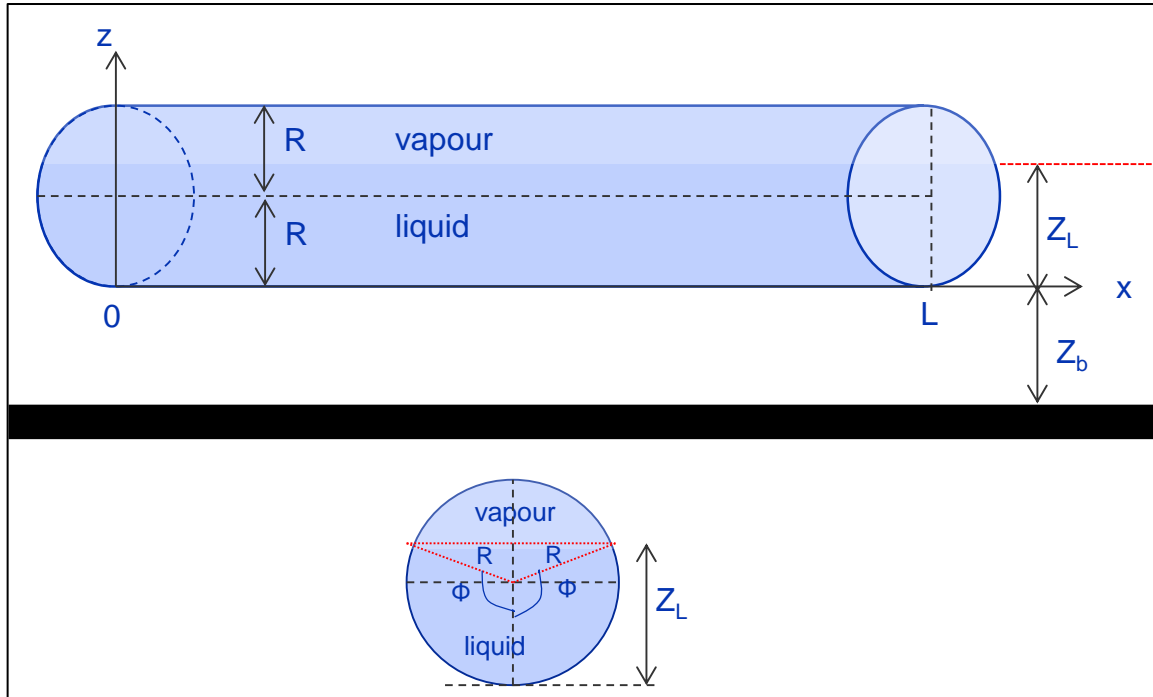<div align="right">( 112 )</div>



**Figure 24.** **Horizontal cylinder (no spherical caps)**

The upper figure depicts the horizontal cylinder (liquid height $Z_L$, height above ground $Z_b$). The lower figure depicts the vessel cross section with the liquid area $A_{liquid}$ split into an upper triangular area $A_{triangle}$ (enclosed by dotted red line) and a lower wedge-shaped area $A_{wedge}$ (enclosing an angle $2\Phi$)

The centroid height $Z_c$ is now set as follows

$$
\begin{aligned}
A_L Z_c = A_{wedge} &= \iint\limits_{A_{wedge}} z\,dA + \iint\limits_{A_{triangle}} z\,dA \\
&= 2\int_0^R dr \int_0^\Phi [R - r\cos\varphi]\,r\,d\varphi \;+\; 2\int_R^{Z_L} z\,(z - R)\tan(\pi - \Phi)\,dz \\
&= 2\int_0^R [R\Phi - r\cos\Phi]\,r\,dr \;-\; 2\tan(\Phi)\int_0^{Z_L - R}(s + R)\,s\,ds \\
&= R^3\left[\Phi - \frac{2}{3}\sin\Phi\right] - 2\tan(\Phi)\int_0^{-R\cos\Phi}(s + R)\,s\,ds \\
&= R^3\left\{\Phi - \frac{2}{3}\sin\Phi - \sin(\Phi)\cos\Phi\left[1 - \frac{2}{3}\cos\Phi\right]\right\}
\end{aligned}
$$

<div align="right">( 113 )</div>

Using **Error! Reference source not found.** into ( 113 ) it now follows that:

$$Z_c = R\left\{\frac{\Phi - \frac{2}{3}\sin\Phi \;-\; \sin(\Phi)\cos\Phi\left[1 - \frac{2}{3}\cos\Phi\right]}{\Phi - \sin(\Phi)\cos\Phi}\right\}$$

$$= R\left\{1 \;-\; \frac{2}{3}\left[\frac{\sin^3(\Phi)}{\Phi - \sin(\Phi)\cos\Phi}\right]\right\}$$

( 114 )

Note that $Z_c = 0$ for $\Phi=0$ (empty vessel) and $Z_c=R$ for $\Phi=\pi$ (full vessel).
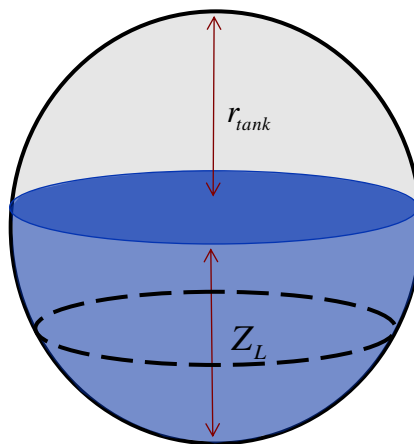
## E.2    Spherical vessel



**Figure 25.        Spherical vessel (radius $r_{tank}=R$, liquid height $Z_L$) )**

See http://mathworld.wolfram.com/SphericalCap.html for details of the derivation of the liquid volume and the centroid height:

$$V_L = \frac{1}{3}\pi Z_L{}^2(3R - Z_L), \;\; Z_c = R - \left\{\frac{3(2R - Z_L)^2}{4(3R - Z_L)}\right\}$$

( 115 )

Note that $Z_c = 0$ for $Z_L=0$ (empty vessel) and $Z_c=R$ for $Z_L =2R$ (full vessel).

## E.3    DISC and GUI implementation

Simplified methodology based on current GUI implementation

1.    Presume always rectangular tank or vertical cylinder in case of catastrophic rupture (using the specified tank head = maximum liquid height), i.e. $P_i = P_{st} + \frac{1}{2}\,\rho_L g\Delta H_L$

2.    User-specified elevation height (i.e. for Safeti-NL for a vessel resting above the ground)

    a.    leak and 10 minute scenarios: $Z_{release} = \max\{1m, Z_{tank}{}^{bottom}\}$

    b.    instantaneous: $Z_{release} = Z_{tank}{}^{bottom} + \frac{1}{2}\,\Delta H_L$

For catastrophic ruptures, a proportion of the hazardous material can get outside the bund, even if the bund capacity is larger than the tank storage capacity. The HSE[xxiii,xxiv] has carried out a number of experiments to determine what fraction may get outside the bund, where the percentage of overtopping varies between 20%-70% depending on the configuration. Thus based on these HSE results, the user is advised to use 1.5 the actual bund area for catastrophic

ruptures (parameter= bund area multiplier, default value 1.5) in order to account for bund overflow.  This value of 1.5 is prescribed for Safeti-NL calculations; see Module C of the BEVI risk assessment manual[xxv] (Section 4.2.1.2 and sub-section 4.2.1 inside Section 12.3).

<u>Future recommended methodology/implementation</u>

1.  User need to always specify type of vessel as currently for time-varying TVDI discharge model, with added input as for TVDI.

    GUI to evaluate centroid height $Z_c$ using logic as described in previous section.

2.  GUI to specify as input for catastrophic ruptures:

    a.  $P_i = P_{st} + \frac{1}{2} \rho_L g [Z_L - Z_c] = P_{st} + \frac{1}{2} \rho_L g [\Delta H_L - Z_c]$,  $T_i = T_{st}$

$Z_{release} = Z_{tank}^{bottom} + Z_c$

## About DNV

We are the independent expert in risk management and quality assurance. Driven by our purpose, to safeguard life, property and the environment, we empower our customers and their stakeholders with facts and reliable insights so that critical decisions can be made with confidence. As a trusted voice for many of the world's most successful organizations, we use our knowledge to advance safety and performance, set industry benchmarks, and inspire and invent solutions to tackle global transformations.

## Digital Solutions

DNV is a world-leading provider of digital solutions and software applications with focus on the energy, maritime and healthcare markets. Our solutions are used worldwide to manage risk and performance for wind turbines, electric grids, pipelines, processing plants, offshore structures, ships, and more. Supported by our domain knowledge and Veracity assurance platform, we enable companies to digitize and manage business critical activities in a sustainable, cost-efficient, safe and secure way.

# REFERENCES

[i] Witlox, H.W.M., "UDM Theory Document", Part of Phast 6.7 Technical Documentation, DNV, London (2011)

[ii] Witlox, H.W.M., "UDM Thermodynamics Theory Document", Part of Phast 6.7 Technical Documentation, DNV, London (2009)

[iii] Witlox, H.W.M., Fernandez, M., and Oke, A., "PVAP Theory Document", Part of Phast 7 Technical Documentation, DNV, London (2012)

[iv] Witlox, H.W.M, and Harper, M., "UDM theory manual", Part of Phast 8.0 Technical Documentation, DNV, London (2015)

[v] Witlox, H.W.M., "Modelling of initial phase of pressurised instantaneous expansion for catastrophic releases - Literature review and proposed SAFETI-NL improvement, Internal DNV document" (2010)

[vi] Webber, D., "Modelling of initial phase of pressurised instantaneous expansion for catastrophic releases", Contract 984B0008 for RIVM, July 2012 (2012)

[vii] Pattison, M.J., "E.C. Cloud Project – Initial stages of release", Draft note, Department of Chemical Engineering and Chemical Technology, Imperial College, London (1994)

[viii] Webber, D.M., "Comparison of the DNV instantaneous expansion model with experimental data", DNV (2000)

[ix] Landis, J.G., R.E. Linney, and Hanley, B.F., "Dispersion of instantaneous jets", Process Safety Progress, Volume 13, Issue 1, pp. 35-40 (1994)

[x] Maurer, B., H.Schneider, K.Hess and W.Leuckel, "Modellversuche zur flash-entspannung, atmosphärischen vermischung und deflagration von flüssigassen nach deren freisetzung bei behälterzerknall." International seminar on extreme load conditions and limit analysis procedures for structural reactor safeguards and containment structures (ELCALAP), Berlin, 8-11 September 1976

[xi] Maurer, B., Schneider, H., Hess, K. and Leuckel, W., "Modelling of vapour cloud dispersion and deflagration after bursting of tanks filled with liquefied Gas", Int. Loss Prevention Symposium, Heidelberg, 1977

[xii] Reid R.C., Prausnitz, J.M., and Poling, B.E., 1987, "The properties of gases and liquids", McGraw-Hill (1987)

[xiii] Coldrick, S., "Further validation of the ACE instantaneous source model", Research Report RR1028, HSE (2014)

[xiv] Bettis, R.J., "Two-phase releases following rapid vessel failure", PhD Thesis, South Bank Polytechnic, London (1987)

[xv] Bettis, R.J., Makhviladze, G.M. and Nolan, PF, "Expansion and evolution of heavy gas and particulate clouds", J. Haz. Mat. $\underline{14}$, pp. 212-232 (1987)

[xvi] Hardy, N.R., "Two-phase releases following catastrophic failure of pressurised storage vessels", PhD Thesis, South Bank Polytechnic, London (1990)

[xvii] Pettitt, G.N., "Characterisation of two-phase releases", PhD Thesis, South Bank Polytechnic, London (1990)

[xviii] Nolan, P.F., Hardy, N.R., and Pettitt, G.N., "The physical modelling of two phase releases following the sudden failure of pressurised vessels", pp. 125-146 in Proceedings of Int. Conf. and Workshop on Modeling and Mitigating the Consequences of Accidental Releases of Hazardous Materials, New Orleans (1991)

[xix] Melhem, G.A., Fisher, H.G., and Shaw, D.A., "An advanced method for the estimation of reaction kinetics, scaleup, and pressure relief design", Process Safety Progress (Vol.14, No1), pp.1-21 (1995)

[xx] Schmidli, J., Banerjee, S., and Yadigaroglu, G., "Effects of vapour/aerosol and pool formation on ruptures of vessels containing superheated liquid", J. Loss Prev. Ind. 3, pp. 104-111 (1990)

[xxi] Schmidli, J., "The initial phase of sudden releases of superheated liquid", Ph.D. Thesis, ETH, Zurich (1993)

[xxii] Lamarche, F. and Leroy, C., "Evaluation of the volume of intersection of a sphere with a cylinder by elliptic integrals", Computer Physics Communications $\underline{59}$, pp. 359-369 (1990)

[xxiii] Atherton, W.A., "An experimental investigation of bund wall overtopping and dynamic pressures on the bund wall following catastrophic failure of a storage vessel, Research Report 333, HSE (2005)

[xxiv] Thyer, A.M., Hirst, I.L., and Jagger, S.F., "Bund overtopping – the consequences of catastrophic tank failure, J. Loss Prevention in the Process Industries $\underline{15}$, pp. 357-363 (2002)

[xxv] RIVM, "Reference Manual BEVI Risk Assessments", Version 3.2, RIVM, Bilthoven, The Netherlands (2009)